Optimization of cathode performance of microbial fuel cells for wastewater treatment and electrochemical power evaluation

Doctoral Thesis

To be awarded the degree
Doctor of Engineering (Dr.-Ing.)

Submitted by

M. Sc. Bolong Jiang
From Daqing, China

Approved by the
Faculty of Mathematics/Computer Science and Mechanical Engineering,
Clausthal University of Technology, Germany

Date of oral examination
27.07.2018

Abstract

The improvement of microbial fuel cell (MFC) performance in a real wastewater treatment plant requires the investigation of several aspects. Firstly, a suitable cell design and electrochemical test procedure has to be set up and operated. Secondly, it is necessary to identify which electrode is the limiting electrode. Thirdly, it requires developing catalysts for the performance determining electrode. Fourthly, a method needs to be developed for the attachment of solid catalysts to the surface of the electrode. Finally, all these steps need transfer to technical scale.

Based on a regular hydrogen/oxygen fuel cell design, different test cells for MFC evaluation were operated. To receive reliable data in a first step, artificial wastewater was used. Later real wastewater from a municipal treatment plant at Goslar was applied to get results more relevant to industrial situations. An automated computer based process control system based on National Instruments Labview platform was used to measure electrochemical performance of several test cells simultaneously.

From the literature is it well known that potassium ferricyanide ($K_3Fe(CN)_6$) solution is a good catholyte. Therefore solutions with different concentrations were used to improve the performance of the cathode. A reversible hydrogen electrode (RHE) was applied as reference electrode to measure the potentials of anode and cathode individually. The results revealed that the performance of the cathode became better with increasing the $K_3Fe(CN)_6$ concentration. The long term performance of optimal power density of MFCs with $K_3Fe(CN)_6$ was also studied. Results showed that the optimal power density can be improved by adding $K_3Fe(CN)_6$ continuously, which improved from 600 mW/m^2 at the 1^{st} day to 1050 mW/m^2 after one month. The effect of air sparging on power density of MFC with $K_3Fe(CN)_6$ cathode solution was also evaluated, but this lowered power density. By these experiments the cathode was identified as the performance limiting electrode.

Consequently, the focus of this work is on the development of improved cathode catalysts for

technical scale MFCs. Potassium ferricyanide cannot be used in a technical wastewater treatment plant, so other solid catalysts for the cathode were investigated. Two carbon clothes, GFD (SGL corporation) and ACN-211 (Kynol corporation) were activated chemically and by thermal treatment. The effect of chemical surface oxidation with Fenton's reagent was investigated. Reflection electron microscopy (REM) indicates that the surface of the treated GFD became rough with increasing the volume of H_2O_2. GFD achieved a maximum performance of 190 mW/m^2, while ACN-211 reached a maximum performance of 450 mW/m^2. Both the untreated ACN-211 and the treated ACN-211 revealed higher and longer lasting power densities than corresponding untreated and treated GFD cloth. REM images of GFD and ACN-211 after chemical activation indicate that many small particles aggregated into large mass and adsorbed on the surface of the samples, which caused a serious fouling. However, the degree of fouling on the surface of ACN-211 is much less as compared to that on the surface of GFD. In addition thermal partial oxidation of ACN-211 at different temperatures was done. Results indicated that the MFC with ACN-211 treated at 400° C for 2 h exhibited the best performance of power density, reaching 470 mW/m^2, which is higher than that of MFCs with ACN-211 treated by Fenton's reagent.

As fibers led to some plugging of the MFC channels, other active cathode materials were investigated. Graphite plus MnO_2 and MoS_2 composites were used as cathode catalysts in the next working phase. An electron conductive paint with suspended solid catalysts was developed and applied on the cathodes. First electrodes were prepared by hand painting, later an automated spraying machine was used. The results demonstrated that MFCs without catalyst reached a power density of only 40 mW/m^2, while the best performance of MFC with graphite plus MnO_2 coating (10:1) was higher than 100 mW/m^2. Comparing with graphite plus MnO_2 coating, the graphite plus MoS_2 paint shows a lower power density but much higher long-term stability than graphite plus MnO_2 coating.

For a stepwise scaling up of MFCs with catalyst on the cathode four MFCs with dimension of 980 cm^2 were constructed and connected in series. Furthermore, mixtures of graphite, γ-MnO_2 and MoS_2 with different weight proportions (20:1:1, 30:1:2 and 30:2:1) were used. During

catalyst preparation the samples were also subjected to ultrasonication to study its influence on particle size and dispersion. The data suggest that the MFC fabricated with the catalyst prepared using graphite, γ-MnO_2 and MoS_2 in a weight proportion of 20:1:1 exhibited the highest optimal power density of 120 mW/m^2. However, after ultrasonic treatment, the power density significantly improved to 183 mW/m^2. It was observed that after using ß-MnO_2, the optimal power density of the MFC fabricated with the catalyst prepared with graphite, ß-$MnO_2$and MoS_2 in a proportion of 20:1:1 was higher than 158 mW/m^2. This was better than that of the MFC fabricated with γ-MnO_2 in the same proportion. The long term performances of the MFCs fabricated using catalysts prepared with different graphite, γ-MnO_2 (ß-MnO_2) and MoS_2 proportions decreased in the order of 20:1:1 (ß-MnO_2) > 20:1:1 (ultrasonic) > 10:1 (ß-MnO_2) >20:1:1 (γ-MnO_2) > 30:2:1 (γ-MnO_2) >30:1:2 (γ-MnO_2).

In the last part, two different structures of TiO_2 (whiskers (W) and nano anatase (A)) supported Co_3O_4 catalysts were synthesized, and the effects of TiO_2 structure and ultrasonic (U) treatment were studied. Motivation for these investigations was to find out if other solid catalysts could reach higher power densities. The MFC with Co_3O_4/TiO_2-W (101 mW/m^2) showed a much higher power density than MFCs with Co_3O_4/TiO_2-A (62 mW/m^2), because of the better dispersion of active Co_3O_4 on TiO_2-W. After U treatment, the power density of MFCs with both catalysts increased remarkably. However, a tiny difference of power density between Co_3O_4/TiO_2-A-U (131 mW/m^2) and Co_3O_4/TiO_2-W-U (135 mW/m^2) was observed, because a better dispersion of Co_3O_4 is reached for both catalysts but the whiskers structure of TiO_2-W is damaged after U treatment. The large pore size of the support and U treatmeant are both beneficial to achieve a better dispersion of active Co_3O_4, which improved MFC performance. But these catalysts did not demonstrate better performance than the manganese dioxide MoS_2 catalyst composition, so for practical application the latter materials were used for coating purposes for scaled-up electrodes with dimensions of 700 mm × 150 mm.

Keywords: microbial fuel cell, electrochemical measurements, Fenton's reagent, MnO_2 catalyst, carbon cloth activation.

Acknowledgements

Firstly, I would like to express my sincere gratitude to my advisor Prof. Dr.-Ing Ulrich Kunz from Institute of Chemical and Electrochemical Process Engineering (ICVT) for this interesting topic and for continuous support throughout my Ph.D. study being always engaged and open-doored for deep discussions. Secondly, my sincere thanks go to Prof. Dr.-Ing. Michael Sievers who was my advisor at Clausthaler Umwelttechnik Forschungszentrum (CUTEC Institute) during this work. He introduced me into the research topic of wastewater cleaning and was always interested in my research.

Furthermore, I would like to thank my colleagues,

Dennis Haupt (CUTEC Institut)

Hinnerk Bormann (CUTEC Institut)

Michael Niedermeiser (CUTEC Institut)

Ottmar Schläfer (CUTEC Institut)

Thorben Muddemann (ICVT and CUTEC Institut)

Student coworker Leandro Gomes Silva e Silva

Furthermore, I would like to thank our partners, Dr. Thorsten Hickmann and Dr. Rouven Henkel from Eisenhuth corporation for constructing and providing composite electrode plates for us. Also I appreciated the following partners, who were always providing new ideas for my work during discussion meetings,

Prof.Dr. Rober Kreutzig (TU Braunschweig)

Prof.Dr Uwe Schröder (TU Braunschweig)

Sebastian Riedl (TU Braunschweig)

Juliane Naujoks (TU Branschweig)

Thomas Deppe (KIT)

Michael Wagner (KIT)

Prof. Harald Horn (KIT)

And all other members of the research teams at ICVT and CUTEC Institute.

During the experiments, I obtained much help from my colleagues Michael Niedermeiser and Hinnerk Bormann, who were responsible for programming of the Labview system. Moreover, my colleague Thorben Muddemann has constructed and programmed the software of the spray machine, which is used for coating process in our research. With the assistance of my colleague Dennis Haupt, we prepared coated cathodes with spray machine successfully.

I also appreciate my wife, Mrs. Nan Jiang. She kept supporting me even during the hardest time of my life in Germany. Maybe I forgot some people, but I collectively thank everyone who helped me during my research.

Finally, we would like to thank Federal Ministry of Education and Research (Bundesministerium für Bildung und Forschung), BMBF, Germany, for funding parts of this study under the contract WTER0219813 and 02WER1317D.

Index

1 Introduction

1.1 Background

Recently, increasing energy shortage and growing awareness of necessary environmental protection, harvesting low-grade waste heat as electrical power has drawn a great deal of attention.[1–4] In addition hydraulic, wind and solar radiation are typical examples of clean energy resources used as alternatives to fossil fuel resources to produce electricity. However, these energy sources are limited by climate and geographical factors. Biomass is one of the important renewable carbon sources and has been recognized as a promising energy supplier for the future.[5] Increasing demand for biofuel has encouraged researchers and politicians worldwide to find sustainable biofuel production systems in accordance with the regional conditions and needs.[6]

Microbial fuel cells (MFCs) are bioelectrochemical devices used to generate electricity from organic matter using exoelectrogenic bacteria.[7] This technology shows promise in both wastewater treatment and sustainable bioenergy conversion applications.[8]In the MFC, electrons liberated from the degradation of the electrolyte organics move through the external circuit to the cathode where oxygen is reduced and a net current/power is generated.[9]

Electricity generation during organic degradation represents a process of directly converting chemical energy within organic matters to electrical energy, which gives rise to a potential for MFC to produce electricity from organic wastewater along with wastewater treatment. The construction of an MFC and its chemical reaction on the electrodes is shown in Fig. 1.1. It can be seen in this figure that the organic reactant is oxidized to CO_2 at the anode, while the oxygen reacts in the cathode. A proton exchange membrane (PEM) is located between anode and cathode for proton exchange.

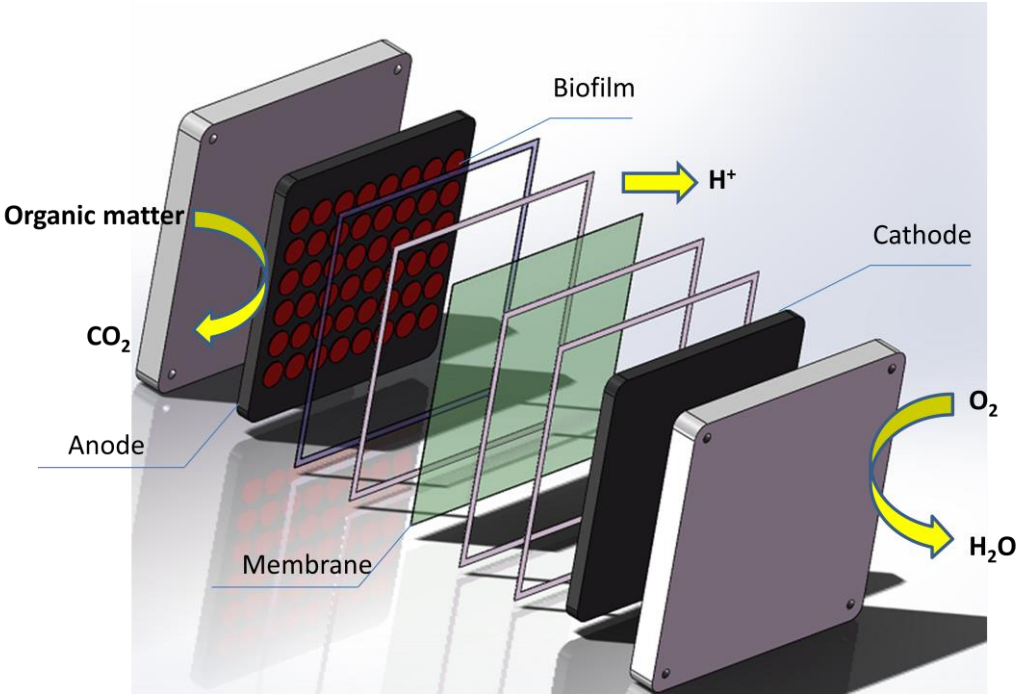

Fig. 1.1: Schematic of a typical two-chamber microbial fuel cell and its reactions

1.2 Construction of MFC

The main MFC-components are the electrodes, separated into the anodic- and cathodic-chamber. Electrons and protons are produced on the anode from the oxidation of soluble organic matters using bacteria as biocatalyst. In the cathode chamber, an electron acceptor is reduced with the electrons transferred via an external circuit and the protons diffused through the solution[10]. Chouler et al. [11] have constructed single chamber MFC, whose anode and cathode were made of carbon cloth. Three different MFCs were developed with polydimethylsiloxane (PDMS) membrane, egg shell membrane and without membrane respectively. It is observed that egg shell possesses a great potential functioning as membrane. The power density of MFC with egg shell has increased from 1 mW/m^2 to 12 mW/m^2 when the distance between the electrodes increased from 4 to 8 mm.

Liu et al.[12] have developed MFC with two chambers separated by a titanium mesh that was used as the anode current collector. Furthermore, granular activated carbon particles enriched with

exoelectrogenic biofilm are fluidized (by stirring) in the anode chamber of the MFC. The maximum power density of 951 ± 10 mW/m^2 was achieved with this construction. For further development of fluidized MFC, Ren et al.[13] have constructed a two-stage laboratory-scale MFC stack, which consisted of MFCs and an anaerobic fluidized bed membrane bioreactor (MFC-AFMBR). They found that AFMBR plays an important role in removing COD, which possessed 43.4% of total COD. This reveals that a combined MFC-AFMBR system could be used to effectively treat domestic wastewater. Thung et al.[14] have even developed a MFC without PEM, which is also defined as membrane-less microbial fuel cell (ML-MFC). In their study, they have evaluated different operational conditions of MFC, which may affect the COD removal rate of MFC. Results showed that despite the constrained power production, the highest COD removal rate has reached 96%. This suggested that ML-MFC can also be used to treat wastewater.

1.3 Microorganisms on the surface of the anode

The bacterium, which is used for the anode, is usually exoelectrogen. An exoelectrogen normally refers to a microorganism that has the ability to transfer electrons extracellularly. Electrons exocytosed in this fashion are produced following ATP production using an electron transport chain (ETC) during oxidative phosphorylation. Convention at cellular respiration requires a final electron acceptor to receive these electrons. A typical example of exoelectrogen is shown in Fig. 1.2, whose priority is that it can directly transfer electrons to a chemical or material that is not the immediate electron acceptor.[15] In this mechanism, electrons from microbial carriers are transported onto the electrode surface either by a microorganism's (Schewanella oneidensis, Geothrix ferementans) own mediator which in turn facilitate extracellular electron transfer or by added mediators. The mediators provide a platform for the microorganisms to generate electrochemically active reduced products.

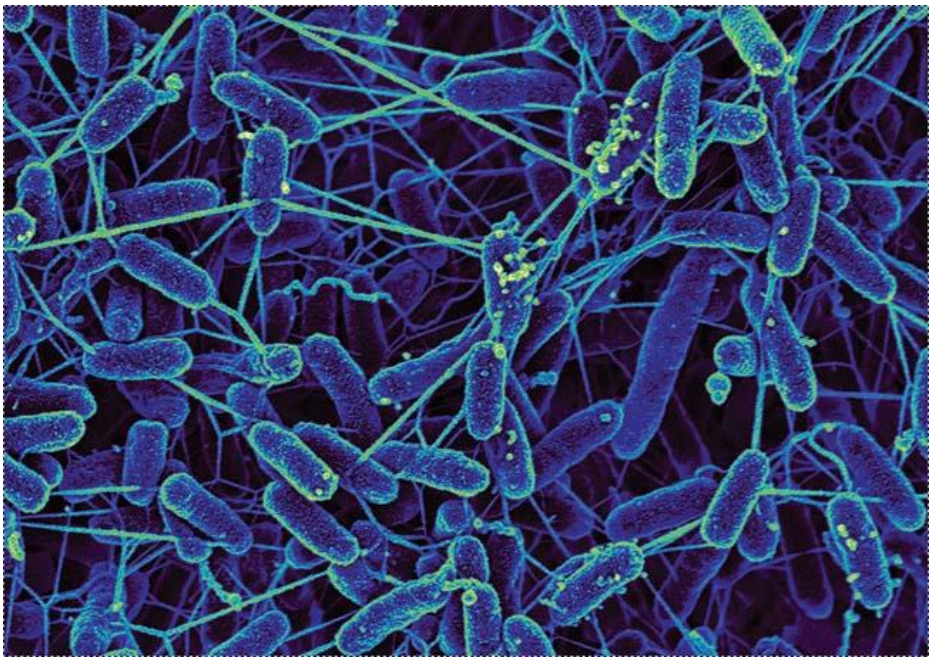

Fig. 1.2 Exoelectrogen with nanowires for transferring electrons

Many researches were conducted, which were focused on the study of bacteria on the anode. Li et al.[16] have used a polymerase chain reaction (PCR) and denaturing gradient gel electrophoresis (DGGE) technology to analyze the bacteria on the surface of the anode. In their study, three different bacteria strains were prepared for experiments, which were clostridium acetobutylicum, anerobic sludge from Luofang wastewater factory, Shenzhen and broth from turmeric wastewater. It is found by PCR-DGGE that 9 different predominant floras on anode were found after operation of MFC. Comparing with other 6 floras, three of the predominant floras produced significantly higher voltage. It has been demonstrated that these three floras possessed a high homology with impure β- proteobacterium. Sun et al. have[17] used two types of wastewater to investigate its influence on the microbial community of the anode. In their study, synthesized wastewater with glucose as main component was used as wastewater A, while wastewater from an anaerobic reactor was used as wastewater B. Results indicated that the predominant flora of wastewater A composed of mainly high G + C Gram-positive bacteria and γ-proteobacteria. Nevertheless, the predominant flora of wastewater B was composed mainly of low G + C Gram-positive bacteria and ε-proteobacteria.

Lin et al.[18] have found by DGGE analysis that the mode of operation (batch and continuous mode), COD concentration and the setup of microorganisms could even influence the structure of the microbial community in the MFC.

1.4 Power generation using MFC

Power output by MFCs has increased considerably over the last decade due to several scientific and technical advances.[19] Unlike enzyme fuel cells in which enzymes are used as biocatalysts,[20] Booki Min et al.[21] have designed a flat plate MFC (FPMFC) to operate as a plug flow reactor combining with a PEM system. They found that the average power density of a MFC operated with domestic wastewater was 72.1 mW/m^2 at a liquid flow rate of 0.39 mL/min. Power generation was sustained at high rates with several organic substrates (all at up to 1000 mg COD/L), including glucose (212 mW/m^2), acetate (286 mW/m^2), butyrate (220 mW/m^2), dextran (150 mW/m^2), and starch (242 mW/m^2). Sona Kazemi et al. have studied the continuous operation of flat plate MFC (FPMFC). A great stability was observed and it resulted in a power density of 44 W/m^3.[22] Yang et al.[23] has established an algae biofilm microbial fuel cell (ABMFC). Results showed that the ABMFC has produced the highest power density of 62.93 mW/m^2, which is 18% higher than ordinary MFC.

There are three main factors that can affect the power generation of MFCs for a given water composition, which are namely anode, membrane and cathode. To improve the performance of the anode, it is necessary to investigate its surface and structure. Logan et al.[24] have developed graphite brush anodes, which were highly conductive, noncorrosive and possessed a high surface area. They constructed a cube (C-MFC) and a bottle (B-MFC) air-cathode MFCs. Results showed that power production in C-MFCs containing brush electrodes at 9600 m^2/m^3 reactor volume reached a maximum power density of 2400 mW/m^2, while the maximum coulombic efficiency (CE) reached the value of 60%. Zhang et al.[25] have used a novel anode, fabricated by electrodepositing manganese dioxide (MnO_2) on carbon felt to improve MFC's power production.

Comparing to a graphite felt anode, the anode capacitance has been improved by 46 times by using this type of anode. Furthermore, The maximum power density of the MFC with the MnO_2-coated anode reached 3580 ± 130 mW/m^2, 24.7% higher than that with the bare carbon felt anode (2870 mW/m^2). It is also found that the electrodeposition time also plays an important role in performance of the anode. Three different electrodeposition times (60 min, 20 min and 5 min) were compared, which were donated as ED60, ED20 and ED5 respectively. Results showed that the power density decreased in the order: ED60-MFC (3580 mW/m^2) > ED20-MFC (3000 mW/m^2) > ED5-MFC (2750 mW/m^2).

It has been shown that the oxygen reduction reaction (ORR) at the cathode is one of the main limiting factors for further improving the output of MFCs.[26,27] An improvement in the cathodic process can lead to a considerable power density increase in MFCs.[28] One of the solutions is to add catalyst on the surface of the cathode. Pt is a typical example. Pt-based catalysts are the best ORR catalysts, however, because of its high cost, it is necessary to study environmental friendly catalysts with lower price. Rossi et al. [29] have investigated the effect of metal-organic framework (MOF) on activated carbon (AC) to improve the performance of the cathode. In their study, Cathodes with the Fe–N–C/AC catalyst were synthetized. During the longterm performance, a power density of 2.78 ± 0.08 W/m^2, was achieved by using MOF catalysts on AC initially. Although the power density decreased by 26% after 8 weeks, it is still 41% higher than that of an AC cathode without MOF. Waston et al.[30] have studied different precursor materials (coal, peat, coconut shell, hardwood and phenolic resin) for AC as catalyst for the cathode. Results showed that cathodes using the coal-derived AC had the highest power densities in MFCs (1620 ± 10 mW/m^2). Furthermore, the peat-based AC performed similarly in MFC tests (1610 ± 100 mW/m^2) and had the best catalyst performance, with an onset potential of E_{onset} = 0.17 V, and n = 3.6 electrons used for oxygen reduction. Gajda et al.[31] have developed Fe-N-C catalyst to improve the performance of air cathode. Results showed that the maximum power density has reached 1300 mW/m^2 when using iron aminoantipyrine (Fe-AAPyr) as cathode catalyst.

Recently, many studies [32] have focused on the effect of manganese dioxide (MnO_2) catalysts on improving the performance of the cathode in MFCs. Because of the low conductivity of MnO_2,

major benefits can be achieved by anchoring MnO_2 nanostructures over carbon supports such as graphite, activated carbon (AC), carbon nanotube (CNT) and graphite oxide (GO). The carbon support (graphite) is expected to increase the electrochemically active surface area and number of active sites to improve the performance of MnO_2 catalysts.[33] Li et al.[34] have developed manganese oxides with a cryptomelane-type octahedral molecular sieve (OMS-2) structure to replace platinum as a cathode catalyst in MFCs. They investigated undoped (ud-OSM-2) and three catalysts doped with cobalt (Co-OMS-2), copper (Cu-OMS-2), and cerium (Ce-OMS-2) to enhance their catalytic performances in granular activated carbon MFC (GACMFC). Results showed that the voltage of the Cu-OMS-2 GACMFC was 214 mV. The cell possessed a relatively high power density of 165 mW/m^2. In addition, the degradation rates of organic substrates in the OMS-2 GACMFCs were twice compared to those in the platinum GACMFCs, which enhanced their wastewater treatment efficiencies. Zhang et al. [35] have investigated the influence of different MnO_2 morphologies on the performance of the cathode. Three manganese dioxide materials, α-MnO_2, β-MnO_2, γ-MnO_2 were compared to platinum (Pt) in air-cathodes of MFCs. Results showed that the power density decreased in the order: Pt (2200 ± 8 mW/m^3) > β-MnO_2 (1300 ± 10 mW/m^3) > α-MnO_2 (920 ± 10 mW/m^3) > γ-MnO_2 (600 ± 11 mW/m^3) > without catalyst (230 ± 5 mW/m^3), showing that β-MnO_2 is an relatively ideal catalyst for MFC. It can also be used as alternative to Pt witch has a much higher price.

Another alternative catalytic material is molybdenum sulfide (MoS_2), which is a silvery black solid that occurs in nature as the mineral molybdenite. Because of its high stability, MoS_2 is usually unaffected by dilute acids and oxygen. In appearance, it is relatively similar to graphite. MoS_2 nanoparticles supported on graphite are also considered as an exciting new catalyst for hydrogen evolution on the nitrogenase enzyme[36]. However, an inherent disadvantage of this material is its low conductivity and insufficient number of active sites. Yuan et al. [37] have used MoS_2 plus CNT composite as catalyst to produce hydrogen in microbial electrolysis cell (MEC) and found that its activity is high. Hou et al. [38] have also developed a MoS_2/nitrogen-doped graphene nanosheet aerogel catalyst for hydrogen evolution in an MEC. They achieved a high output current density of 0.36 mA/cm^2. Furthermore, a hydrogen production rate of 19 m^3/day

was also obtained for the hybrid at a bias of 0.8 V. Our group [5] has also shown that the graphite/MoS_2 composite shows a much higher stability than the graphite/MnO_2 composite. Because of its simple synthetic procedure, and the low cost [39], MoS_2 is promising for future MFC studies.

1.5 Energy harvesting from MFC

Current/power generated from MFC systems is over 3 to 5 orders of magnitude lower compared to traditional hydrogen- or methanol-fueled FC [40] and therefore a smart design is necessary in order to harvest the low energy produced. Alaraj et al. [41] have used a synchronous flyback converter to harvest energy from MFCs, which has a relatively simpler configuration and improves harvesting efficiency by 37.6% compared to a diode based boost converter. Moreover, the proposed harvester was able to store 2.27 J in the output capacitor out of 4.91 J generated energy from the MFC, while the boost converter can capture only 1.67 J from 4.95 J. Boghani et al. [42] have developed a novel strategy of a MFC subsystem. Series connectivity along with maximum power point tracking (MPPT) generates increased power from individual MFCs whilst eliminating cell reversal. In the study, each MFC was connected to a MPPT device which controlled the current sourced from each MFC. They found that the application of MPPT and the connection strategy presented here can increase stack voltages and avoids the reversal of cell voltage, whilst also applying a control mechanism that facilitates peak power extraction from MFCs in real-time. Donovan et al.[43] have constructed a sediment microbial fuel cell (SMFC) using a power management system (PMS) with two DC/DC converters, and digital logic to control energy storage and use. They calculated the process efficiency of PMS. It has been measured that DC/DC1 was operated with an output current of about 1 mA at an efficiency of 70.0%, while the power efficiency of DC/DC2 was 80.6% with an input potential of 4.07 V and an output current of 500 mA. According to the values, the overall system efficiency under these operating conditions was 70.0% × 80.6% = 56.4%. Wang et al. [44] have developed a new approach and system that can actively extract energy from MFC

reactors at any operating point without using any resistors. Results showed that within 18-h test, the energy gained from the MPPC was 76.8 J, 76 times higher than the charge pump (1.0 J) that was commonly used in MFC studies, while the coulombic efficiency obtained from the MPPC was also 21 times higher than that of the charge pump. Furthermore, different numbers (3, 6, 9, and 12) of capacitors during 18-h harvesting were characterized. For 12-capacitor condition, the voltage has not reached the saturated level even after 16 h. The energy storage in the 6, 9, and 12-capacitor conditions was 47.0, 65.6, and 76.8 J, respectively, and the corresponded voltage after 18 h was 2.8, 2.7, and 2.5 V, respectively. Zhang et al. [45] have compared the capacitor-transformer-converter type PMS with pump-capacitor-converter type PMS. They found that the capacitor-transformer-converter type PMS can accommodate lower input voltages, but the charge pump-capacitor-converter type PMS has a slightly higher power efficiency. Furthermore, the charging speed of the capacitor-transformer-converter type PMS is not limited by the charge pump as in the charge pump-capacitor-converter type PMS, resulting in a shorter charging/discharging cycle.

1.6 MFC for real wastewater, manure and urine treatment

Recently, MFCs have been used treating real wastewater, manure and urine. Heidrich et al.[46] have developed MFCs reactors, which can be operated at low temperature without specialized inocula. By treating real wastewater, they have obtained the maximum COD removal rate and Coulombic efficiency of 90% and 25% respectively. Liu et al.[47] have used MFC to treat pharmaceutical wastewater with the initial COD value of 200 mg/L. They obtained the COD removal rate between 92% and 94%. Nikhil et al.[48] have treated pharmaceutical wastewater with much higher COD value comparing to Liu et al. By using the MFC system with total volume of 1 L and surface area of 70 cm^2, they obtained the maximum removal rate of 85%. Qin et al.[49] have used MFC to treat human urine with the COD value of 1448 mg/L. The maximum COD removal rate of 89.1% was achieved by using MFC system with total volume of 75 mL and

surface area of 75 cm^2. Shen et al.[50] have used MFC system with total volume of 600 mL to treat daily manure. The maximum COD removal rate of 75% was achieved in their study. Cerrilo et al.[51] have treated cattle manure with initial COD value of 1500 mg/L and achieved COD removal rate of 84.72%.

1.7 MFC scale up

Scaling up MFCs is challenging based on the need to use inexpensive and non-precious metal materials and to achieve good performance. The use of carbon fiber brushes provides a route to make low-cost anodes, [52–54] and several different cathodes have been constructed without precious metals using AC as a catalyst [55,56]. Liang et al.[57] have developed a 1000 L modularized MFC system, which was operated for more than one year to test its treating ablility for wastewater. Results showed that the concentration of effluent from MFC system remains less than 50 mg/L, while the COD removal rate possessed the value between 70% and 90%. Babauta et al.[58] have scaled up benthic microbial fuel cells (BMFC). They found that by using an in-line flyback converter, the input voltage of BMFC can be held within a relatively optimal range between 0.35 and 0.5 V. When two converters were used, 16 mW of MFC power can be delivered to battery with the efficiency of 77%. In order to improve the performance of MFCs, many works have focused on electrode modification, such as electrochemical treatment [55], metal oxide doping [56] and polymer modification [59].

Alexis et al.[60] have reported a novel membraneless stack design using ceramic plates, with fully submerged anodes and partially submerged cathodes in the same urine solution. In their research, they constructed self-stratifying urine column MFCs (SSC-MFC) with different scales. Comparing to the smaller cells, the larger cells possessed the dimension increase factor of 6. Results showed that the larger MFCs possessed the power density of 12.596 mW/m^2, which is only slightly lower than that of smaller cells (13.836 mW/m^2). This reveals that this SSC-MFC scaling up approach was successful in converting chemical energy in urine into electricity.

1.8 Motivation for this work

As is described in chapter 1.4, the cathode is the main limiting factor for the performance of a MFC. This was demonstrated by application of liquid catholyte (potassium ferrocyanide) in a laboratory MFC. As ferrocyanid solution is not suitable in a real wastewater plant, this work is mainly focused on developing solid ORR catalysts to improve the performance of MFCs.

For this purposes it was necessary to operate a laboratory test system which runs automatically over long time spans. This was accomplished by a Labview (National Instruments) based process control system for data collection and for operation of the electrochemical reactors with adjustable load currents. In the first phase of this study, different types of ORR catalysts such as carbon fiber (ACN and GFD), MnO_2, MoS_2, Co_3O_4 (with brookite, anatase and active carbon as carriers) were prepared and applied in laboratory MFCs. In the further phase, scaling up of MFCs in two size steps was investigated. The scaled up MFCs finally possessed three anode plates with dimension of 700 mm × 150 mm × 7 mm (single anode plate), which are parallel arranged and whose material was polymer carbon composite. The composite electrodes were prepared by Eisenhuth corporation, Osterode, Germany, while ion-exchange membranes and stainless steel cathodes with catalyst (MnO_2 or MoS_2) on the surface are purchased and self-constructed respectively. The membranes and cathodes are arranged on both side of the anode chamber.

2 Start-up behavior of MFCs with the first design

2.1 Experimental

To investigate the properties of the composite plates from Eisenhuth corporation for MFC application, different designs were tested. In a first step a design with flow channels was used comparable to a traditional hydrogen fuel cell. As microorganism growth on the electrodes is essential, it is necessary to improve the surface properties for this purpose. Plates with a surface "as prepared" and with a rouged surface by sand collision were compared.

As a load for the MFCs, constant current sources were applied to evaluate performance of the cells. This has the advantage that load currents can be adjusted in a wide range, which offers convenient variation of the load, not attainable with fixed resistors. The load current was adjusted to the maximum power point of each MFC. Measurements were recorded by a Labview (National Instruments) computer based system.

2.1.1 Measurement of Roughness

The roughness of electrode plates is measured in Institute of Mechanical Engineering (Clausthal University of Technology, Germany)，who uses the MarSurf GD 120 (Mahr Corporation, Germany) to measure the roughness. During the measurement, a test probe is contacted on the surface of the electrode plate. The device scans a certain distance (for electrode plate without sanding 12.5 mm and for electrode plate with sand collision 40.2 mm) with different scanning scales (for electrode plate without sand collision 2.5 mm and for electrode plate with sand collision 8 mm) to measure the arithmetic mean roughness and the average rough deepness of the two different electrode plates.

2.1.2 Wastewater and COD substrate

To make experimental investigations comparable artificial wastewater was prepared. The composition of our model wastewater was: $NaAc \cdot 3H_2O$ = 0.21 g/L, glucose = 0.05 g/L, ribose = 0.05 g/L, glycine = 0.16 g/L, (L-)Cystein = 0.15 g/L, potassium hydrogen phalate = 0.09 g/L, NH_4Cl = 0.31 g/L, KCl = 0.13 g/L, $NaHCO_3$ = 0.10 – 0.15 g/L, vitamine with heavy metal = 12.5 g/L. All the components except Na_2CO_3 are mixed with deionized water. The mixture is than stirred by magnetic mixer. Na_2CO_3 is added to the mixture continuously in order to set the pH value to the range of 8.6 – 8.8. The main components of COD substrate were: $NaAc \cdot 3H_2O$ = 44.32 g/L, glucose = 10.32 g/L, ribose = 9.38 g/L, glycine = 31.2 g/L, (L-)Cystein = 30.3 g/L.

2.1.3 Design of the laboratory MFC

The end plates of our first MFC reactor were made of stainless steel, with anodic and cathodic plates separated by a Nafion 117 membrane. Both anode and cathode were prepared by polymer carbon composite (approximately 85% graphite in an olefinic polymer binder from Eisenhuth Corporation, Germany,) with channels on the surface of the electrode (Fig. 2.1). The surfaces were made rough by sand collision to increase their surface roughness (which denoted as roughened electrode). Each electrode has a dimension of 25cm × 14cm × 1cm. Four individual MFCs with roughened electrodes were connected in series (Fig. 2.2) and denoted as MFC#1, MFC#2, MFC#3 and MFC#4, respectively. As can be seen from Fig. 2.2, the whole stack is connected with two glass containers of 2 L for anodic and cathodic reactants. The nutrition and wastewater are only put into the container at the anode of MFC#1, while the bubbling air flows into the container at cathode of MFC#4. The cathode tap water was enriched with air by bubbling air through the catholyte reservoir. Oxygen in the anode chamber would inhibit electricity generation. Therefore, the system must be designed to keep the bacteria separated from oxygen, which can be realized by using a membrane or separator. Moreover, the separator

should also be used for proton exchange. Nafion 117, which is mainly made of sulfonated tetrafluorethylen-polymer (PTFE), is used as proton exchange membrane between the anode and cathode. Nafion has several advantages in traditional H_2/O_2 fuel cells, such as its high stability against degradation and good proton conductivity. The waste water (using NaAc as additional nutrition for the microorganism) was feed through the cathode and the anode compartment by two pumps.

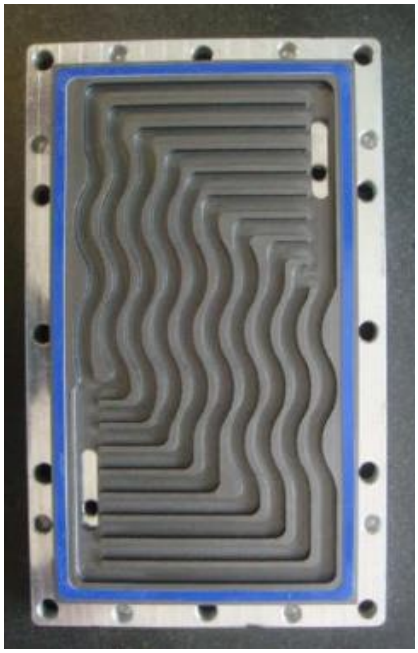

Fig. 2.1: Picture of electrode (250 mm × 140 mm)

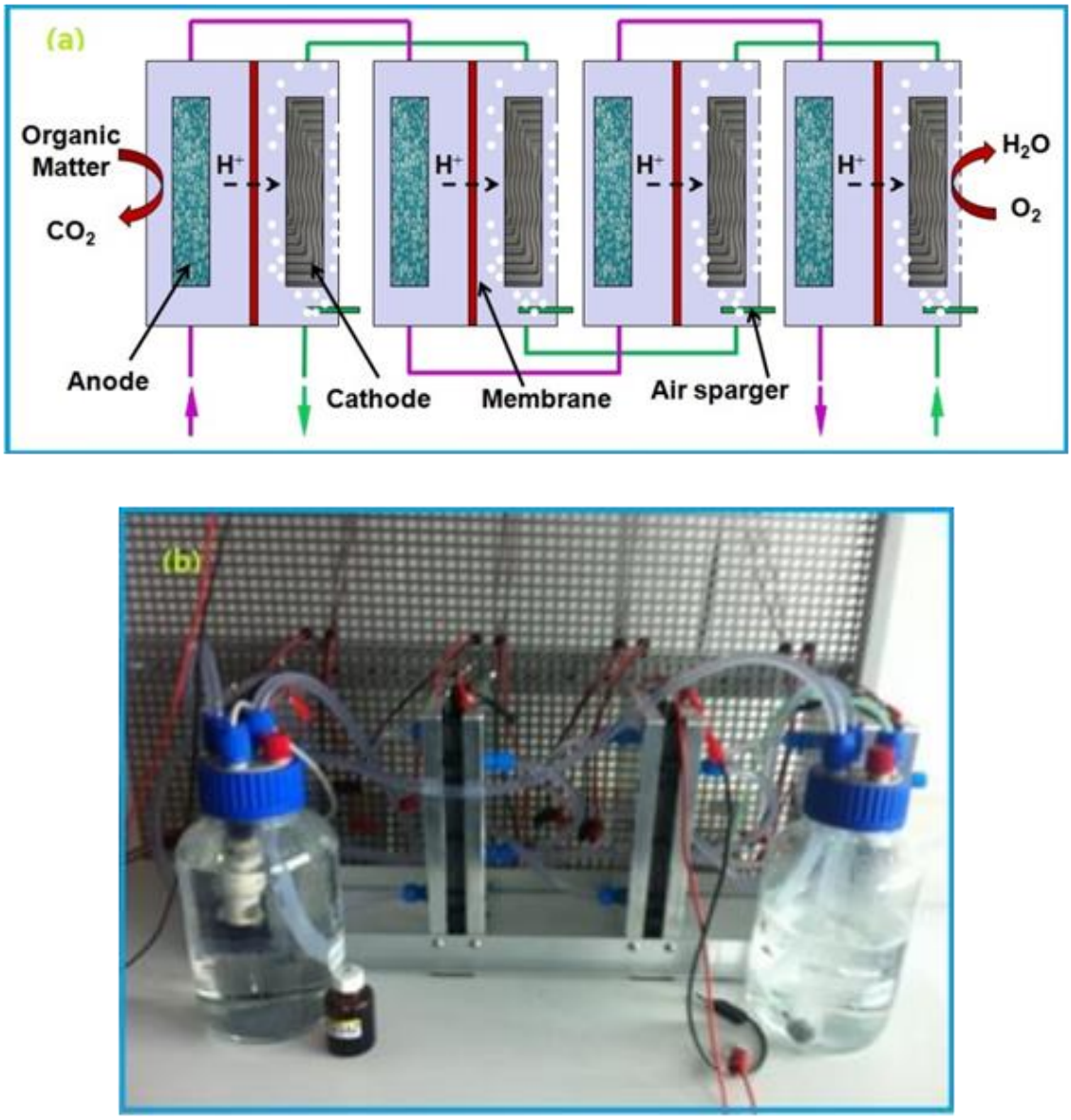

Fig. 2.2: Four individual MFCs connected in series (a) scheme of the MFC stack (b) photograph of the MFC stack

2.1.4 Measurement of COD values

A standard method is used to determine the chemical oxygen demand (COD). During the measurement, 2 mL of sample from the anode water were taken to determine the COD by using a commercial COD analyzer, which is produced by Macherey-Nagel Corporation (Germany), type:

Nanocolor UV/VIS. The COD values are measured under standard condition (298 K and 1 atm). Generating power is one of the main goals of MFC operation, therefore it is necessary to convert as much as possible of the biomass into current and to recover as much energy as possible from the system.

2.1.5 Coulombic and energy efficiency

2.1.5.1 Coulombic efficiency

One of the most important parameters to evaluate the efficiency of MFC is coulombic efficiency η_C, which is given as:

$$\eta_C = \frac{\text{Coulombs recovered}}{\text{Total coulombs in substrate}} \quad (1)$$

According to Eq.(1), the coulombic efficiency η_C can be calculated by the following equation:

$$\eta_C = \frac{M \int_0^t I \, dt}{FbV_{An}\Delta COD} \quad (2)$$

2.1.5.2 Energy efficiency

The energy efficiency is based on energy recovered in the system compared to the energy content of the starting material. Therefore, it is defined as the following equation:

$$\eta_E = \frac{E}{E_{max}}\eta_C \quad (3)$$

With η_E as the energy efficiency; E is cell-voltage; E_{max} is the maximum voltage of the MFC. In our experiments we set a current of 2.5 mA for the determination of this parameter, while the voltage of the MFC is 180 mV.

The maximum potential of MFC can be calculated by the following equation,

$$E_{\max} = \frac{-\Delta G}{bF} \quad (4)$$

With ΔG (Gibbs' enthalpy).

2.2 Results and Discussion

2.2.1 Roughness for different electrode plates

Table 2.1 shows the arithmetic mean roughness (R_a) and the average rough deepness (R_z) of the two different electrode plates (roughened and without roughened). It can be seen that the R_a of an electrode plate with sand collision is 11.8 μm, which is more than two times of that of electrode plate without sand collision (4.9 μm). The similar phenomenon is also observed for the R_z.

Table 2.1: Comparison of roughness between different electrode plate

Electrode plates	R_a/μm	R_z/μm
Electrode plate without roughened	4.9	39.34
Electrode plate roughened	11.8	74.2

2.2.2 Performance of single MFCs

The polarization curves of the single MFCs with electrodes of different roughness are shown in Fig. 2.3. In this first design we did not use a catalyst on the cathode. The data suggested that the optimal power density of the single MFC with roughened electrodes has reached 50 mW/m^2, while the optimal power density of MFC with smooth plates was only 20 mW/m^2, showing that

roughness plays an important role in improving the power density of MFC. The main reason is that higher roughness is beneficial to settlement of microorganisms. According to Fig. 2.3 (b), the optimal power densities of MFCs with and without roughened electrodes reached 2 mA and 6 mA, respectively.

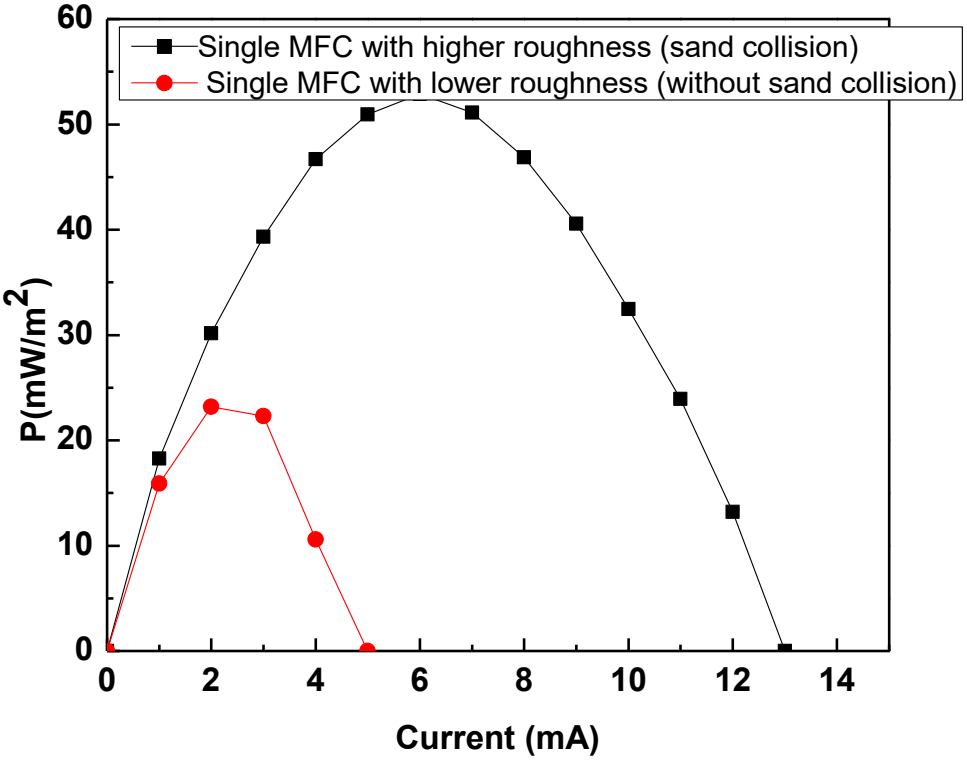

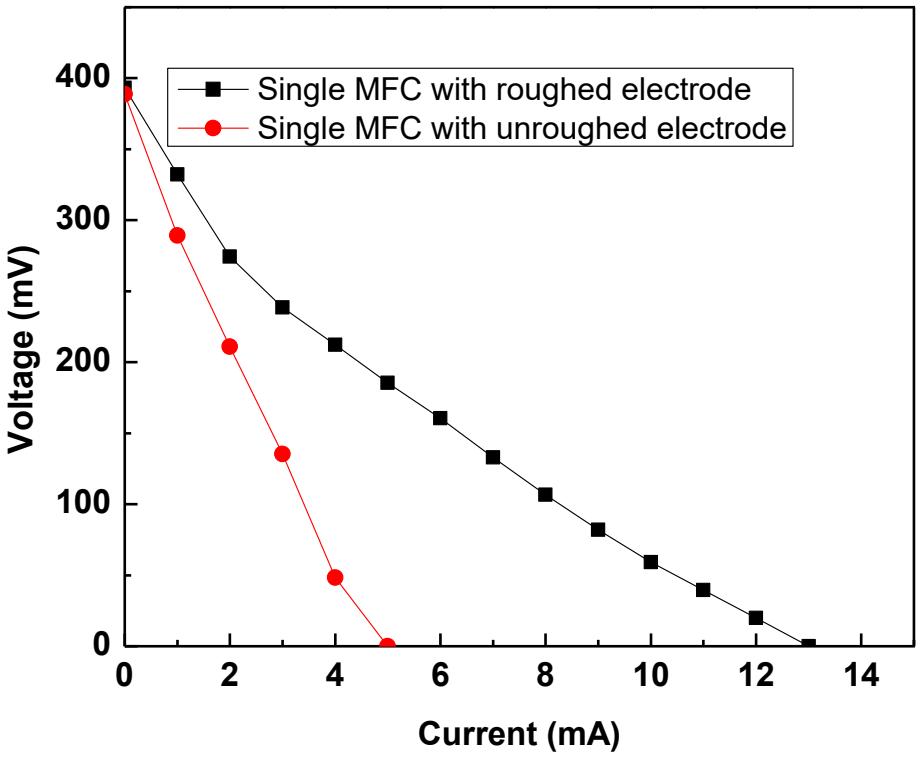

Fig. 2.3 Polarization curves of the single MFCs with electrodes of different roughness (roughened and without roughened)

2.2.3 Performance of roughed MFCs in series and its long term performance

As the power density was higher for the MFCs with the rough plates, these cells were investigated in more detail. The four single MFCs with roughened electrodes were connected in series to further improve power output. The polarization curves of the four series stack MFCs are shown in Fig. 2.4. The data suggested that MFC#1 and MFC#4 produce relatively higher power densities than MFC#2 and MFC#3.Theoretically, the optimal powers of these fuel cells should be equally high. The main reason for the different values of optimal power is probably

because of the different development of microorganisms in the four cells. Each cell developed individually. Fig. 2.4 presents a series of voltage current characteristics and power currents characteristics. The data suggested that the voltage descends with increase of current and it becomes zero at the end of the measurement. A nearly linear decrease of voltage with rising current is observed, the typical sharp decline at the end of such a characteristic is not observed in most MFC investigations as the electrolyte gap is broad and most wastewater has low conductivity. It was observed that the MFCs with higher power densities (MFC#1 and MFC#4) possessed also a relatively higher voltage.

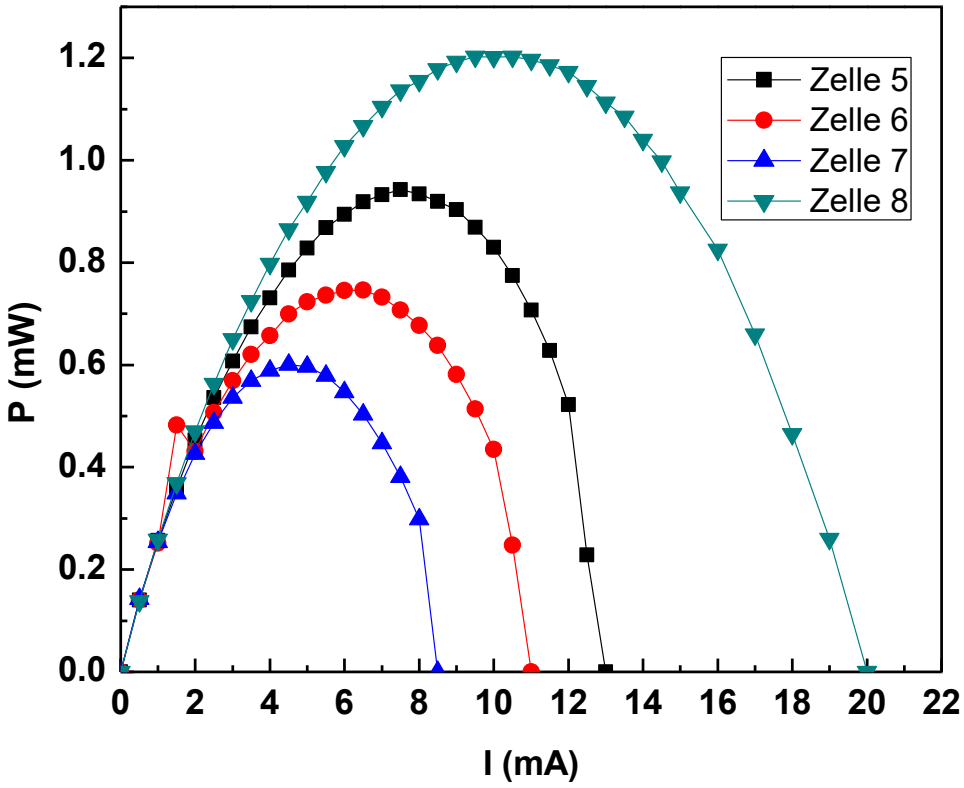

Fig. 2.4: Polarization curves of the four series stack MFC with roughened electrodes

Fig. 2.5 illustrates the long-term performance of the four series stack MFCs, which were

continuously operated for 160 days. Within 12 days, the optimal power of each MFC increased with time. Then, the power densities fluctuated around a value. The optimal power density of each MFC became different from each other gradually after 3 days. Despite of the different optimal power density, the similar tendency was observed for each MFC in the four cell stack. Significant decrease in optimal power of MFCs is observed at the 42th and 102th days which is due to that there was not enough wastewater and nutrient to support the operation of the microorganisms in the MFCs.

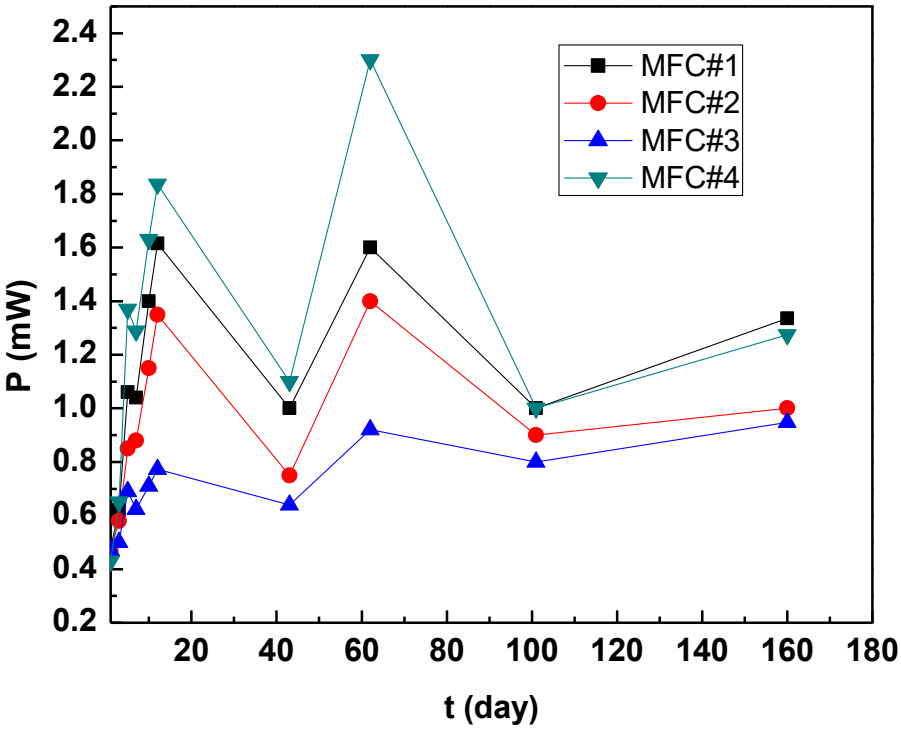

Fig. 2.5: The long-term performance of the four series stack MFCs with roughened electrodes. Depicted is the maximum power determined by measuring current power characteristics by constant current sources.

The optimal power decreased in the sequence: MFC#4> MFC#1>MFC#2>MFC#3. The best performance was achieved at 62 days. The optimal powers of each MFC at 62th and 160th day are

shown in Table 2.2, which suggests that the optimal power of MFC#4 reached 126.5 $mW \cdot m^{-2}$ at 62^{th} day. Zhuang et al.[61] reported a maximum power density of 65.4 mW/m^2 and 97.2 mW/m^2 produced for a stack of forty cells fed with brewery wastewater (between days 25 and 35), respectively. Our results showed that the electrical performance of the four series stack is comparable to the best stack documented thus far. At the end of the experiment (160^{th} day), the MFC#4 in the four series stack produced a maximum power density of 70.05 mW/m^2, a decrease of 44.6% from the highest density obtained at 62^{th} day (126.5 mW/m^2). However, for MFC#1 and MFC#2, the decrease from the highest power density obtained at day 62^{th} to the end of the experiment (160^{th} day) were 16.6% and 21.7%, respectively. For MFC#3 produced the lowest power density among these four MFCs, the power density keeps more stable during the whole experiment. Zhuang et al.[61] evaluated the long-term performance of their forty series stack MFCs. At the end of the experiment, their stack produced a maximum power density of 25.5 mW/m^2, a decrease of 60% from the highest density obtained at day 30 (65.4 mW/m^2). In summary, the optimal powers of the four MFCs tend to become closer to each other after 160 days, which ranged from 52.0 mW/m^2 to 73.4 mW/m^2, showing a considerably stable power output during the period of 160 days. These results and the results reported in the literature indicate that a power density in the range of 25 mW/m^2 to 80 mW/m^2 is the best that can be expected after long time of operation with artificial wastewater if a noncatalytic cathode is used.

Table 2.2: Optimal powers of the four MFCs with roughened electrodes at 160th day

MFC	Maximum Power (mW)		Maximum Power Density (mW/m^2)	
	62th day	160th day	62th day	160th day
MFC#1	1.60	1.34	88.0	73.4
MFC#2	1.40	1.10	77.0	60.4
MFC#3	0.92	0.95	50.6	52.0

MFC#4	2.30	1.28	126.5	70.1

2.2.4 Discussion of coulombic and energy efficiency

NaAc is used as substrate for the MFCs in the experiment. Therefore, the chemical reaction is shown as follows:

$$CH_3COO^- + O_2 \longrightarrow HCO_3^- + H^+$$

The maximum potential of the whole system is 1.09 V.[62]

The average potentials of each MFC in the four cell stack, which were obtained directly from LabVIEW system, are shown in Table 2.3, from which the average potential of the four MFCs is determined as 223.2 mV.

Table 2.3: Potentials of four series stack MFCs

MFCs	Potential (mV)	Average potential (mV)	Energy efficiency(%)
MFC#1	238.2	223.2	5.47
MFC#2	217.3		
MFC#3	201.5		
MFC#4	235.8		

The COD removal is needed for coulombic energy calculations. In order to calculate the COD difference (ΔCOD), both the start and end samples were detected. The results of change in COD (ΔCOD) values for the four series stack MFCs are shown in Table 2.4.

Table 2.4: COD values of the start and end samples for the four series stack MFCs with roughened electrodes

Day	COD ($mg \cdot L^{-1}$)		Duration (h)	Current (mA)
	Start sample	End sample		
159th	2888	2836	19.2	4.5
160th	3665	3565	18.8	5.5

The COD value measurement at 159th day (Table 2.4) is taken as an example for energy efficiency calculation. The measurement interval and ΔCOD are 19.2 h and 52 $mg \cdot L^{-1}$, respectively. According to Eq.(2), the coulombic efficiency of the four MFCs is calculated as 26.8%, which corresponds to the theoretical value in the range of 12- 95%.[15] Aelterman et al. [63] have obtained coulombic efficiency of 12.4% by connecting six MFC stacks in series, which is lower than 26.8%. Appling Eq.(3)–(4), the energy efficiency is calculated to be 5.47%. Logan et al. [15] have obtained a value range for coulombic efficiencies, which lies in the range of 2 – 50%, which means that the result corresponds to the expectation.

2.2.5 Performance of MFCs with $K_3Fe(CN)_6$ as catholyte

Since power production from MFCs can be limited by the overpotential of the oxygen reduction reaction (ORR) at the cathode[64], measures are taken to improve the performance of the cathode. One of the methods is to add cathodic fuel to the catholyte. In these experiments, $K_3Fe(CN)_6$ solutions with different concentrations (50 mM, 100 mM and 200 mM) were prepared. The pH values were set to 7 by sodium carbonate. During the experiments, the $K_3Fe(CN)_6$ solution was injected into the cathode container. The obtained results are shown in Fig. 2.6. It can be seen from Fig. 2.6 that the output power density of the MFCs without adding $K_3Fe(CN)_6$ solution were around $52 - 73\ mW/m^2$. With increasing $K_3Fe(CN)_6$ concentration to 100 mM, first the output power densities increased slowly, then increased rapidly. However, with further

increasing $K_3Fe(CN)_6$ concentration from 100 mM to 200 mM the increase became slow. Choi et al.[65] have measured cyclic voltammograms of thionin and $Fe(CN)_6^{3-}$ in pH = 7 phosphate buffer at a carbon electrode. Results show that reduction of $Fe(CN)_6^{3-}$ is diffusion controlled. $Fe(CN)_6^{3-}$ can easily be reduced to $Fe(CN)_6^{4-}$, which indicates that this compound is an ideal cathodic fuel. Bruce et al. [66] also reported that the internal resistance with the 22.5 cm^2 Pt cathode and dissolved oxygen was 960 Ω, while the internal resistance of the system with ferricyanide was only 800 Ω. Thus, the improved power densities can be explained by the great mass transfer efficiency with concentrated ferricyanide solution. At low $Fe(CN)_6^{3-}$ concentration, the reduction is mass transfer controlled. As a result, the output power density increased slowly with increasing $K_3Fe(CN)_6$ concentration. At higher concentration of $K_3Fe(CN)_6$, the effect of $Fe(CN)_6^{3-}$ on the output power densities is significant since large amount of $Fe(CN)_6^{3-}$ can be reduced to $Fe(CN)_6^{4-}$ rapidly. Among the four series stacked MFCs, the output power density of MFC #3 is the highest, which reaches 560 mW/m^2 at $K_3Fe(CN)_6$ concentration of 200 mM. This value is 10.8 times higher than that of MFC#3 without adding $K_3Fe(CN)_6$ solution at the same conditions. Aelterman et al.[63] have prepared $K_3Fe(CN)_6$ catholyte with KH_2PO_4 as buffer solution and obtained similar results. The output power densities have almost tripled with the value of 308 W/m^3 (series) and 263 W/m^3 (parallel).

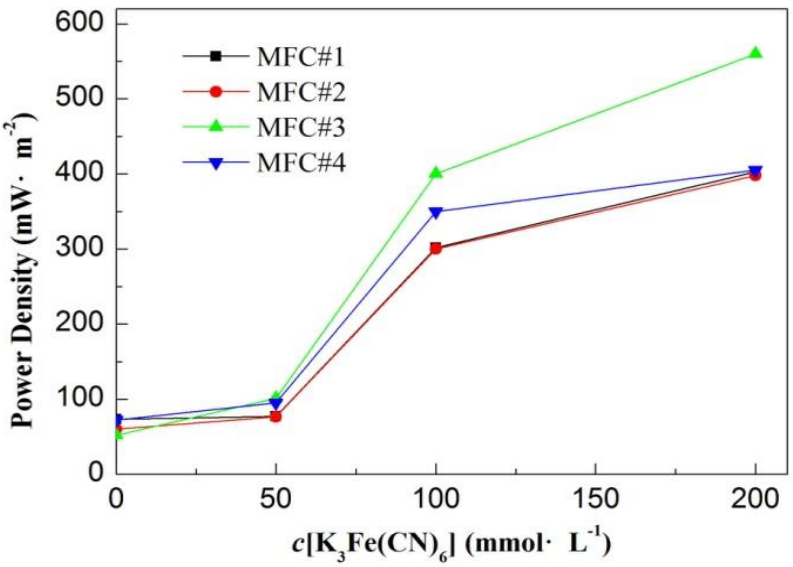

Fig. 2.6: Improvement of MFCs powers by adding $K_3Fe(CN)_6$ to catholyte

2.3 Conclusions

In a first approach surface properties of composite electrodes were investigated. Composite electrodes with rough surface, prepared by sand collision, exhibited higher power density compared to smooth plates. The power density of single MFCs with roughened electrodes is 50 $mW \cdot m^{-2}$, which is two times as high as that of MFC with electrodes without treatment by sand collision, showing that roughness plays an important role in improving power density. A stack of four cells was constructed with the roughened electrodes to further improve the power density. Long-term performances of the MFCs were studied over 160 days. Results showed that the optimal power of the stack decreased in the sequence: MFC#4> MFC#1>MFC#2>MFC#3. A maximum power density output of 126.5 mW/m^2 was achieved at 62^{th} day, which shows that series connection of MFCs can improve the power output. The optimal powers of the four MFCs almost were kept stable after 62^{th} day and tend to become closer (which ranged between 52.03 and 73.41 mW/m^2) to each other at 160^{th} day. The coulombic efficiency of the four cell stack is 26.8%, while the energy efficiency is 5.47%. The output power densities of each MFC in the four cell stack ascend rapidly with increasing $K_3Fe(CN)_6$ concentration, a maximum power density of 560 mW/m^2 was observed at $K_3Fe(CN)_6$ concentration of 200 mM. This value is 10.8 times higher than without adding $K_3Fe(CN)_6$ solution, keeping all other parameters at same conditions. Our results showed that the electrical performance of the four cell stack in the current study is comparable to the best stacks documented thus far for noncatalytic cathodes using artificial wastewater.

3 Continuous electricity generation of MFCs with potassium ferricyanide

From the experiments with the first MFC construction it is obvious, that further improvement can be achieved by catalytic cathodes. In addition, the experience of the first laboratory experiments have to be transferred to the real world. Therefore, artificial wastewater was no longer used, but wastewater from a municipal plant was used in the laboratory reactors. The first step was to investigate if in real wastewater the cathode is the performance limiting electrode, then solid catalysts and a method for electrode coating had to be developed.

3.1 Experimental

3.1.1 Wastewater and COD Substrate

The purpose of our study is to examine the new combined catalyst coatings in real wastewater and study the first stage of scale up towards commercial scale MFCs. The wastewater with the initial COD value of 250 to 300 mg/L was provided by a municipal wastewater treatment plant in Goslar, Germany. After sometime when the MFC have consumed nutrition contained in the wastewater, a solution of 200 g/L glucose and 200 g/L NaAc dissolved in distilled water was used to supply the microorganism with nutrition. This approach was used as it was much more convenient than to use daily fresh batches of wastewater from Goslar.

3.1.2 Design of MFC

According to the experience with the first cell design, it is necessary to have composite plates with wider channels with less plugging. The MFC system was designed to keep the bacteria on the anode separated from the cathode solution and to separate the aneorobic and aerobic

compartments also. This is realized by using a membrane or separator. Moreover, the separator should also be used for proton exchange. During the experiments proton exchange membranes were used as separator between anode and cathode compartment of the MFCs (manufacturer: Fumatech Corporation; type: FKE 50). As electrodes a polymer/graphite composite (approximately 85 % graphite in an olefinic polymer binder) was used, as it is known that microorganism can settle easily on graphite which is a major compound in these plates. These materials were prepared by Eisenhuth Corporation (Germany) and are also used in other electrochemical reactors like batteries or electrolyzers. The conductive plates can be easily manufactured by polymer processing methods, resulting in low cost. Flat plates of the new design with channels for the wastewater flow are depicted in Fig. 3.1.

Fig. 3.1: Constructions of our improved electrode (150 mm × 150 mm)

3.1.3 Measurement of COD Values

A standard method is used to determine the chemical oxygen demand (COD). During the measurement, 2 mL of sample from the anode water were taken to determine the COD by using a commercial COD analyzer, which is produced by Macherey-Nagel Corporation (Germany), type: Nanocolor UV/VIS. The COD values are measured under standard condition (298 K and 1 atm).

3.1.4 Measurement of power density and MFC-bottleneck identification

State of the art in MFC research is the use of resistors with fixed values as an electric load. The resistor is needed to allow the microorganism to release their generated electrons. This method works, but is not the best approach to load the MFCs electrically. MFCs are electrochemical reactors with living organism on the electrodes. This results in fluctuations of power density which cannot be forecast. Therefore a fixed resistor does not fit optimal to the variable power output of the MFC. The better the microorganism can give of produced electrons the better they can live and the better the bio-film on the electrodes will develop. Our approach is different from the well-known resistor load. The MFCs are loaded with constant current sources. The current is adapted to the prevailing power capability of the MFC. So the MFCs were loaded individually with different constant currents, each MFC is connected with an own constant current source. Simultaneously the potential was measured. From these data the current density/voltage characteristic and the current density/power density characteristic were calculated on-line by LabView software (National Instruments). These data are not constant over time but change during the operation of a MFC. This is caused by changing supply with nutrition, varying supply with oxygen and individual development of the microbial film on the electrodes. So it is necessary to measure these data several times a day and adjust the applied load current to the maximum power point in the current density/power density characteristic of each MFC. In Fig. 3.2 four possible situations are depicted. By comparison of voltage and current of the freshest

measurement with the stored data from the previous measurement the status of operation is identified. In the next step the load current is adjusted stepwise towards the direction of the power maximum. The time interval for the measurements can be chosen freely as well as the current increments, so this method can be adapted to different sizes of MFCs. By this approach each MFC was operated at the individual maximum power point in the current density/power density characteristic and a rapid development of the microorganism could be reached leading to a fast power production. Materials with beneficial properties can be easily detected and be used for the development of industrial MFCs. All materials can be compared at the maximum power point this material in combination with the other materials of construction can deliver. The LabView program structure for controlling the constant current values is shown in Fig. 3.3. Here I want to thank my colleagues Michael Niedermeiser and Hinnerk Bormann for the programming of the Labview system.

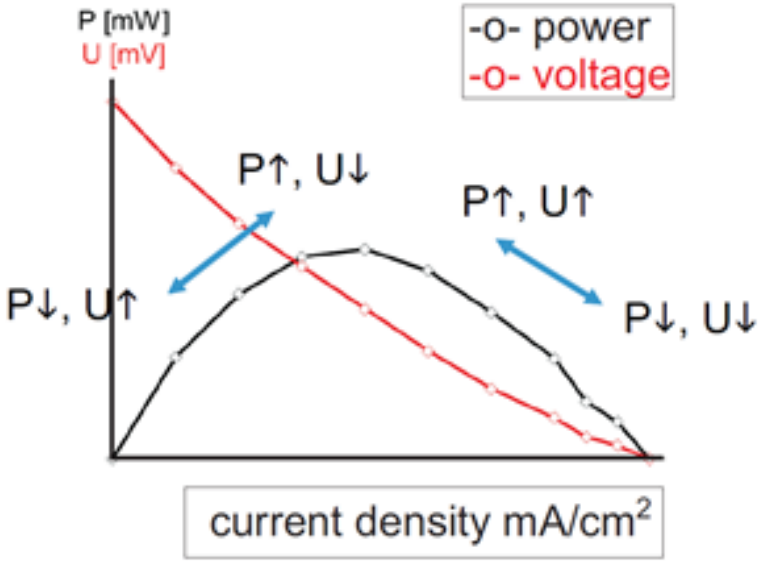

Fig. 3.2: Strategy for optimization of MFC power output by software controlled load currents

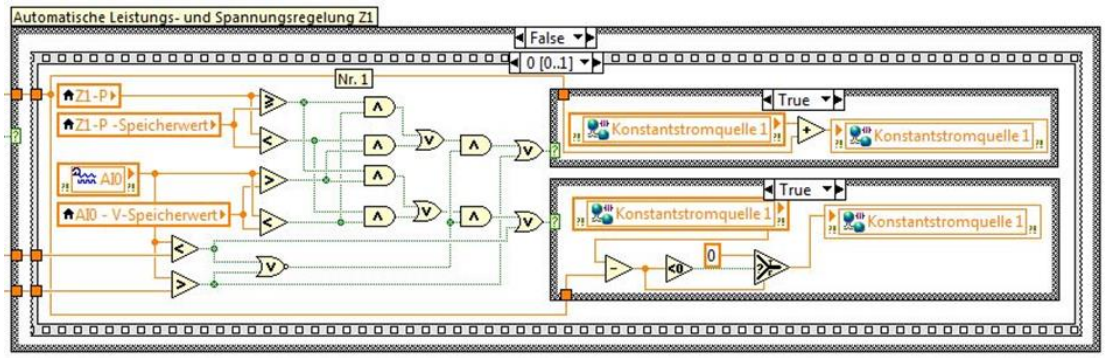

Fig. 3.3: Logic flow sheet for the program routine in LabView software to adjust the MFCs to individual maximum power production

Before the cathode with a catalytic coating is used for a MFC, a MFC with an uncoated stainless steel cathode was set up and the polarization curve was measured by using a reversible hydrogen reference electrode (RHE) as it is shown in Fig. 3.4. The implementation of a reference electrode directly into the MFC allows to confirm clearly which electrode is the rate determining one. We adapted a method described in literature, described by He and Nguyen[67]. During assembly of the MFC the membrane was left larger than the surface area of the MFC. The membrane outside the cell was immersed into a beaker filled with diluted sulfuric acid. In the beaker a commercial hydrogen reference electrode (Gaskatel company, Kassel, Germany) was inserted. So by the membrane a conductive ionic connection between the MFC and the reference electrode was created. With this arrangement is it possible to measure anode and cathode potentials individually not disturbing the inner construction of the MFC with additional measuring electrodes and capillaries. Simultaneously the cell voltage was measured. By rising the load current with the constant current source it could be observed that the cell voltage begins to drop when the cathode voltage begins to change. This indicates that the cathode is the power limiting electrode in a MFC.[5]

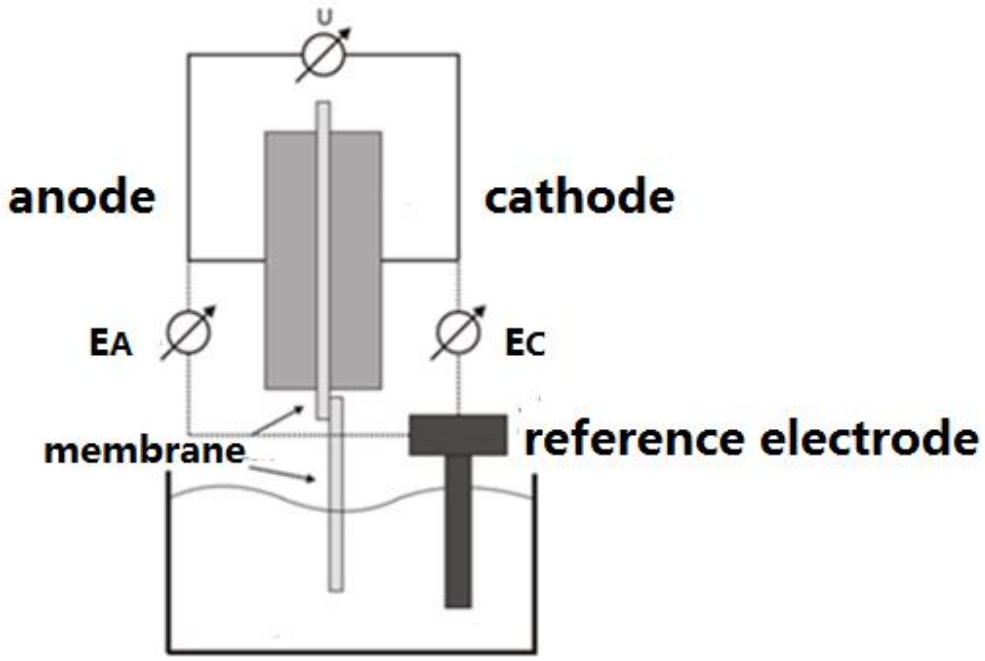

Fig. 3.4: Application of a reference electrode (RHE) to measure anode and cathode potentials individually

The implementations of the reference electrodes are shown in Fig. 3.5. The polarization (U–i) curves were recorded by increasing the current density, in order to portray the tendency curves of electrode potentials with the increase of current.

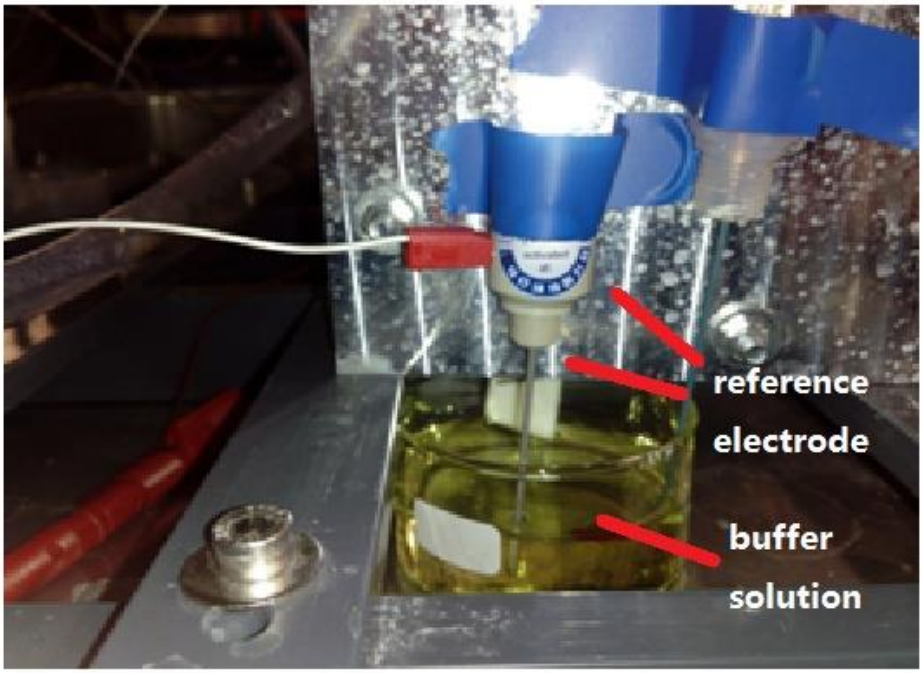

Fig. 3.5: Reference electrodes with buffer solution (pH=7)

3.1.5 Preparation of $K_3Fe(CN)_6$ Solution

During experiments, $K_3Fe(CN)_6$ solutions with concentrations of 5 mM, 10 mM and 30 mM are prepared, respectively. Sodium carbonate is added into solutions until pH value reaches 7. The produced solutions are than added as cathode solution in order to measure the characteristic curves.

3.2 Results and discussion

3.2.1 Long term performance of MFC with Pt

Platinum is well known as a good oxidation catalyst for the ORR. To compare own catalyst developments during a first phase, a MFC was built with an air cathode, which possessed a Pt load

of 0.5 g/m^2. Fig.3.6 shows the long term performance of a MFC with air cathode. The data suggested that the power density increased with time firstly and then reached its highest value of 191 mW/m^2 at 28th day. However, the power density decreased after reaching the highest value. After 51 days test, the power density possessed the value of only 31 mW/m^2, probably because the Pt was poisoned during the long term run by catalyst poisons contained in the wastewater. As catalyst poisons cannot be avoided in real waste water the conclusion is, that platinum is not suited for this application. Furthermore, because of Pt's high price, it is necessary to use novel catalyst or catholyte to improve the performance of MFC.

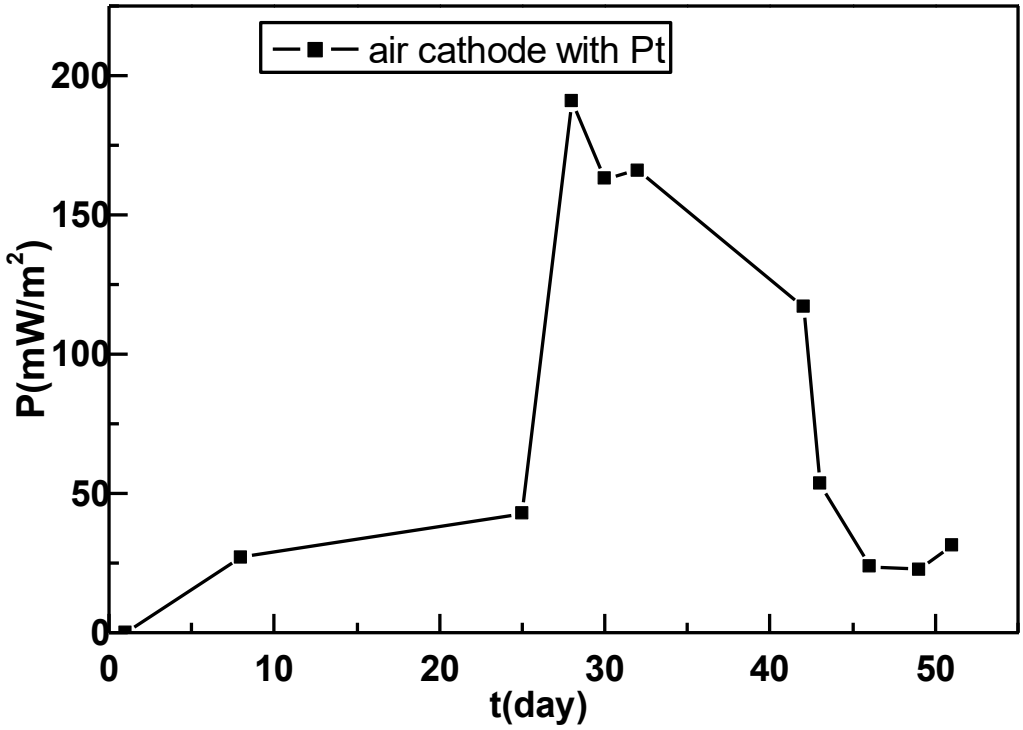

Fig. 3.6: The long-term performance of a MFC with Pt as ORR catalyst (air cathode)

3.2.2 Potentials of Electrodes with $K_3Fe(CN)_6$

The effect of injection of $K_3Fe(CN)_6$ solution (Soda as buffer solution to keep the pH value the same as other experiments) to the cathode solution with sparging air on the performance of the

MFC was evaluated and results are shown in Fig. 3.6. It can be seen in Fig. 3.7(a) that the potential of the cathode tends to become much more stable with increase of current for $K_3Fe(CN)_6$ solution concentration of 30 mM than those of for 5 mM and 10 mM. When the current reached 25 mA, the potential of the anode ascended rapidly and reaches the same value as the cathode, which made the voltage of the MFC became zero. Compared with the results obtained with lower $K_3Fe(CN)_6$ solution concentration of 5 mM and 10 mM, the cathode with higher $K_3Fe(CN)_6$ solution concentration of 30 mM possessed a relatively higher potential and the power density is also much higher, showing that the performance of the cathode can be improved by increasing the $K_3Fe(CN)_6$ concentration. The polarization curves of the MFC with different $K_3Fe(CN)_6$ concentrations are shown in Fig.3.6(b). The data in Fig. 3.7(b) suggested that power densities are lower than 280 mW/m^2 when the $K_3Fe(CN)_6$ concentration is lower than 10 mM. However, with increasing the $K_3Fe(CN)_6$ concentration to 30 mM a high power density of 560 mW/m^2 is achieved, which is 2 times higher when compared with that found for the $K_3Fe(CN)_6$ concentration of 10 mM.

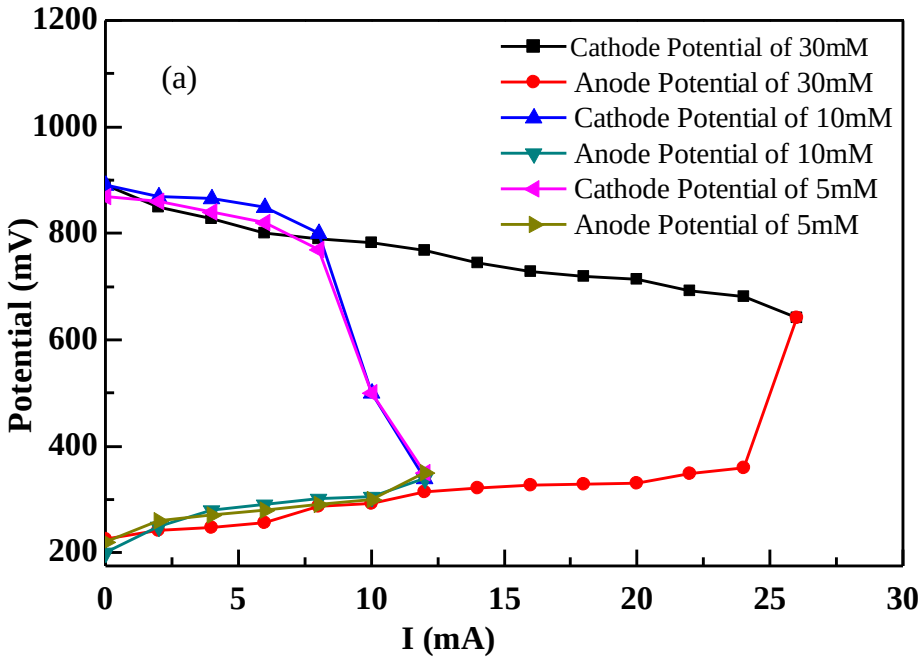

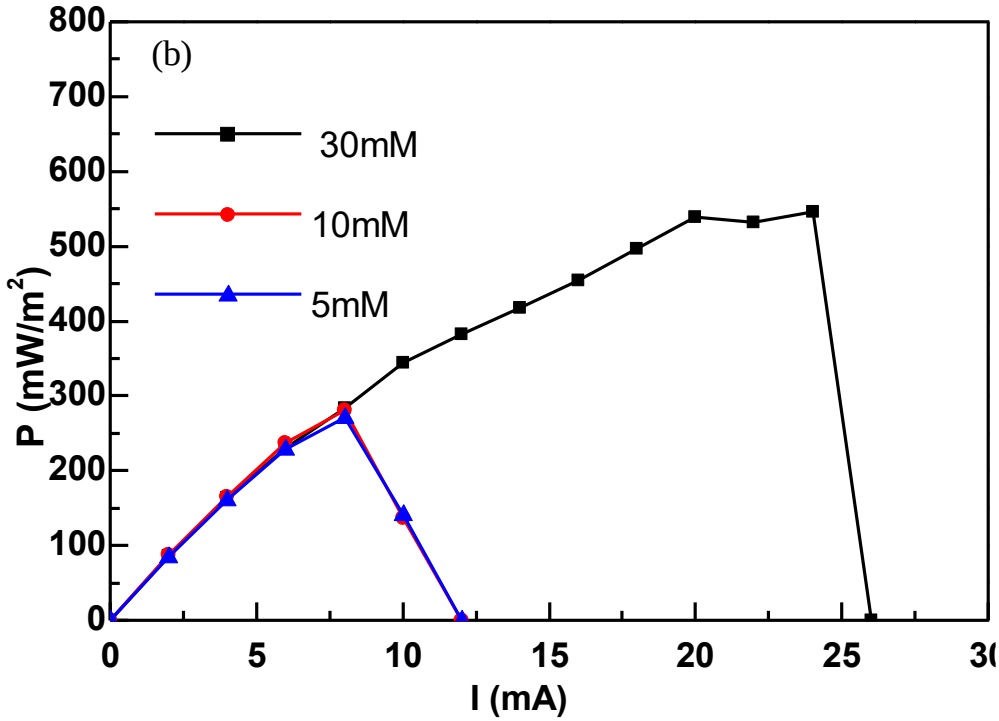

Fig. 3.7: Effect of the $K_3Fe(CN)_6$ concentration on potential curve (a) and polarization curve (b) of MFC

3.2.3 Evaluation of long-term performance

Fig. 3.8 illustrates the long-term performance of MFC, which were continuously operated with 30 mM $K_3Fe(CN)_6$ solution with sparging air for 25 days. The power density increased with time firstly and then increased slightly after 10^{th} day. A high power density of 1020 mW/m^2 is achieved at 10^{th} day. The same tendency is observed for the anode, which also increased with time firstly and then increased slightly after 10^{th} day. The breaking current reached a high value of 40 mA at 10^{th}day. The best performance of breaking current is also achieved at 25^{th} day, whose value reached 45 mA, showing that the performance of anode can be improved by adding $K_3Fe(CN)_6$ to cathode solution continuously. This indicates that the microorganism on the anode notice that the cathode is getting better and they are able to adapt to this cathode development.

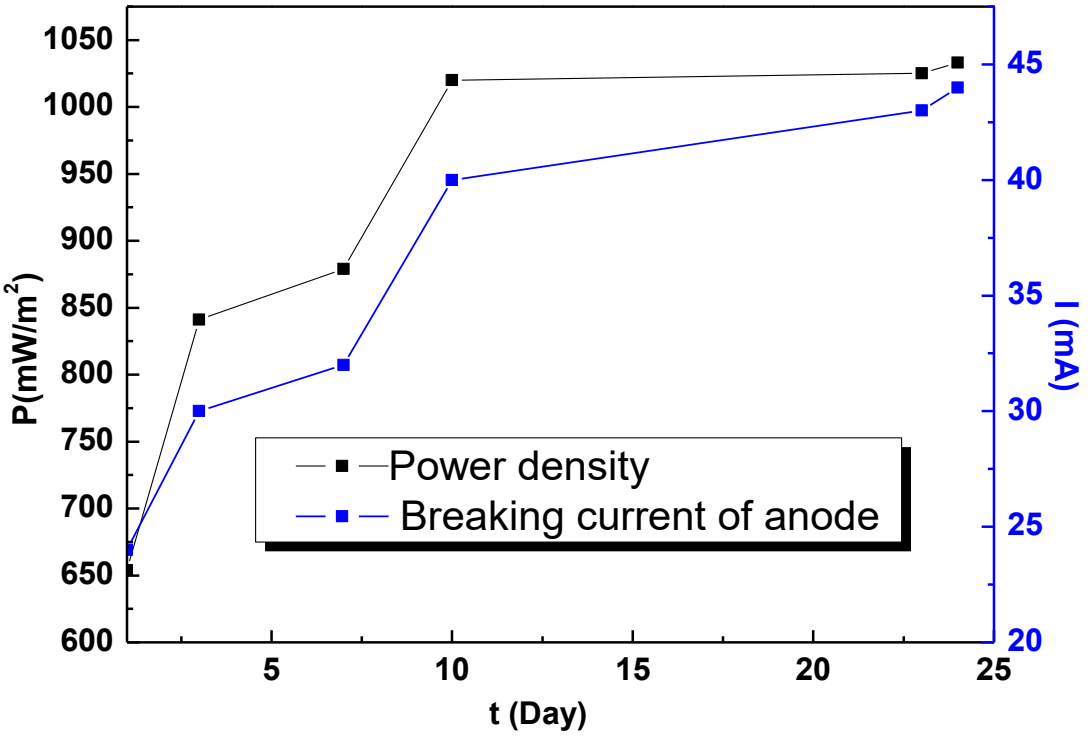

Fig. 3.8: The long-term performance of MFC with $K_3Fe(CN)_6$ solution concentration of 30 mM

3.2.4 Influence of oxygen on power density

Rabaey et al.[68] achieved a high power density in a MFC using a ferricyanide cathode solution (4310 mW/m^2), but they have not studied the power production in that system with dissolved oxygen. In this work, the effect of oxygen on power density of MFC with $K_3Fe(CN)_6$ cathode solution is evaluated and the results are shown in Fig. 3.9. It can be seen from Fig. 3.8, for a MFC with sparged air only, the optimal power density is only 59 mW/m^2, which is very low. The optimal power density for a MFC with sparged air is improved from 59 mW/m^2 to 1005 mW/m^2 by using $K_3Fe(CN)_6$ cathode solutions. The MFC with $K_3Fe(CN)_6$ cathode solutions without sparged air showed optimal power density of 1260 mW/m^2, which is much higher than that of

MFC sparged with air. This shows that sparging air into $K_3Fe(CN)_6$ cathode solution causes decrease in the optimal power density of MFC significantly. Our result was similar to that obtained by Wei et al. [65], who found the MFC with $K_3Fe(CN)_6$ only showed an output power density of 181 mW/m^3, while the MFC with $K_3Fe(CN)_6$ cathode solutions sparged with air showed an output power density of 149 mW/m^3. The main reason is that compared to the potential of an oxygen electrode (0.401 V), the $Fe(CN)^{3-}$ reactant showed a higher potential of 0.46 V[66] when the pH value of the solution is higher than 7. The sparged air may probably have reduced the potential of the cathode and resulted in the descent of power density. There are several advantages for $K_3Fe(CN)_6$. Firstly, for the system with $K_3Fe(CN)_6$, there is no need to use air pumps for continuously sparging of air, which could reduce energy consumption. Secondly, the maximum output power density of the system using $K_3Fe(CN)_6$ cathode solution was more than 20 times higher than that with aerated cathode solution because there is little polarization of the cathode in the former. Thirdly, $K_3Fe(CN)_6$ and its reduction product, which are environmentally friendly, have no effect on continuous cathode reaction. Therefore, $K_3Fe(CN)_6$ is a promising cathodic electron acceptor for wastewater treatment in MFC.[69] The only disadvantage is that large quantities would be necessary in a real wastewater plant.

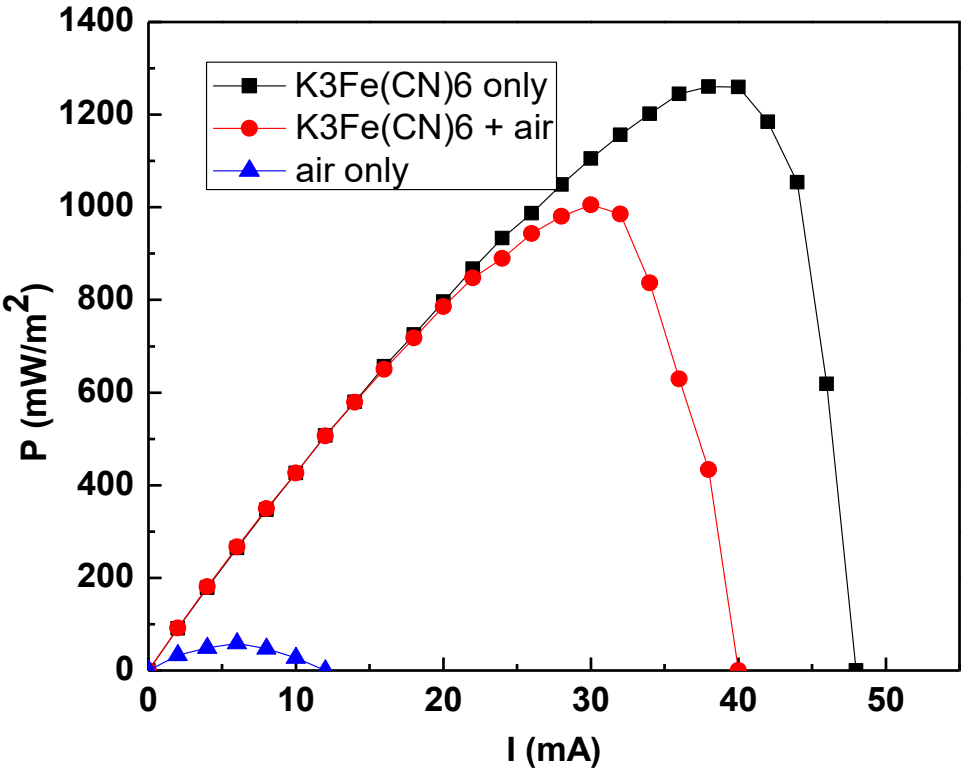

Fig. 3.9: Polarization curves of MFC with $K_3Fe(CN)_6$ cathode solution only and sparged with oxygen

3.2.5 Coulombic and energy Efficiency

The coulombic and energy efficiencies are evaluated within one month and the results were shown in Fig. 3.10. According to Fig. 3.10, the $K_3Fe(CN)_6$ solution was added as the cathode solution at the 7th day. It can be seen from Fig. 3.9 that the coulombic efficiency was about 12.6% before using $K_3Fe(CN)_6$. However, after adding $K_3Fe(CN)_6$ as cathode solution the coulombic efficiency was significantly increased from 12.6% to 32.2% (at 10th day), which was 2.55 times when compared to that of using dissolved oxygen. The energy efficiency was about 2.6% before using $K_3Fe(CN)_6$. However, after adding $K_3Fe(CN)_6$ into cathode solution the energy efficiency was significantly increased from 2.6% to 10.6% (at 10th day), which was 4.08 times when compared to that of using dissolved oxygen. The best performance is achieved at the 36th day

with MFC using $K_3Fe(CN)_6$ without sparging air. The MFC showed a highest coulombic efficiency of 34.2%, while the energy efficiency reached 13.3%, showing that the efficiencies can be improved by using $K_3Fe(CN)_6$ solution only.

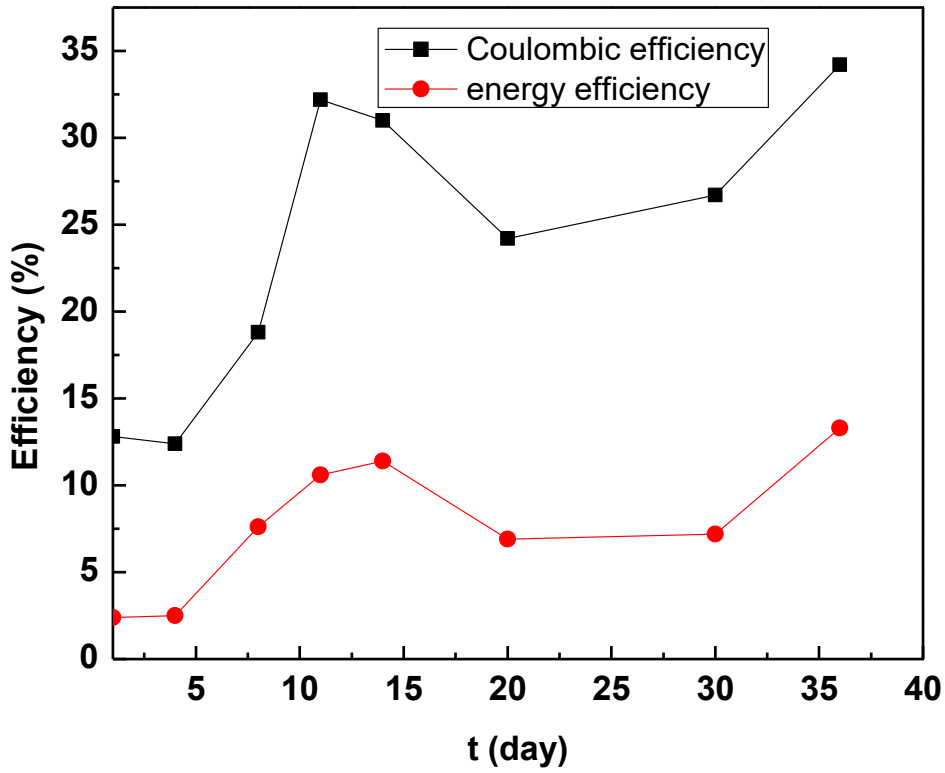

Fig. 3.10: Long term performance of coulombic and energy efficiency (From 1st to 6th day with sparging air only, from 7th day to 32nd day with $K_3Fe(CN)_6$ and sparging air and from 32nd day and 37th day with $K_3Fe(CN)_6$ only)

3.2.6 Long term performance of COD degradation rate

Fig. 3.11 illustrates the long term performance of COD degradation rate. $K_3Fe(CN)_6$ solution was added into cathode solution at the 1st day. A significantly increased COD degradation rate was observed between 1st day and 4th day. The best performance is achieved at 10th day (between 1st and 25th day), whose COD degradation rate has reached maximum of 72.3%, showing that

$K_3Fe(CN)_6$ plays an important role in improving COD degradation rate of wastewater. The best performance was achieved at 30th day with MFC using $K_3Fe(CN)_6$ solution only, the maximum COD degradation rate has reached 73.5%.

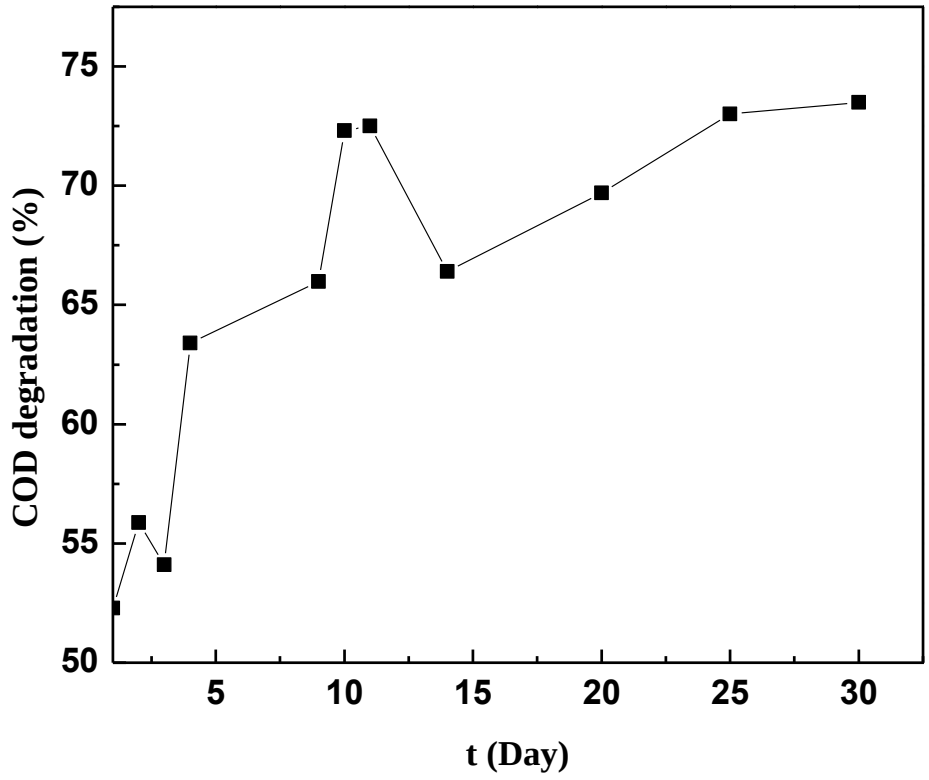

Fig. 3.11: Long term performance of COD degradation rate (From 1st to 25th day with sparing air and from 25th day to 30th day without sparging air)

3.3 Conclusions

Pt is relatively unstable for our system, between 28th day and 51st day, the power density of MFC with Pt as ORR catalyst has descended from 191 mW/m^2 to 31 mW/m^2. Therefore, it is necessary to use novel catalyst or catholyte to improve the performance of MFC. $K_3Fe(CN)_6$ is an ideal electron cathodic acceptor for MFCs with liquid cathode. The performance of the cathode can be

improved significantly by adding $K_3Fe(CN)_6$ solution into cathode solution. A high power density of 560mW/m^2 is achieved with $K_3Fe(CN)_6$ solution concentration of 30 mM. A high power density of 1020 mW/m^2 is achieved at 10^{th} day. The best performance of breaking current is achieved at 25^{th} day, whose value reached 45 mA, showing that the performance of the anode can be improved continuously by adding $K_3Fe(CN)_6$ to the cathode solution.

The effect of oxygen on power density is evaluated, and the data suggested that the power density of MFC with only $K_3Fe(CN)_6$ (1260 mW/m^2) is higher than that of MFC with $K_3Fe(CN)_6$ sparged with air (1005 mW/m^2). A significant increase of coulombic and energy efficiencies is observed by using $K_3Fe(CN)_6$ instead of using dissolved oxygen. The coulombic efficiency of a MFC after adding $K_3Fe(CN)_6$ into the cathode solution was 32.2 %, which was 2.55 times higher when compared to that of using dissolved oxygen (12.6%). The energy efficiency of a MFC after adding $K_3Fe(CN)_6$ into the cathode solution was 10.6%, which was 2.55 times when compared to that of using dissolved oxygen (2.6%). The best performance is achieved at the 36^{th} day. The coulombic efficiency possessed the value of 34.2%, while the energy efficiency has reached 13.3%, showing that $K_3Fe(CN)_6$ has a positive influence on improving efficiencies of MFCs.

A significantly increased COD degradation rate was observed between 1^{st} day and 4^{th} day. The best performance is achieved at 10^{th} day (between 1^{st} and 25^{th} day), whose COD degradation rate has reached maximum of 72.3%, showing that $K_3Fe(CN)_6$ plays an important role in improving COD degradation rate of wastewater. The best performance was achieved at 30^{th} day with MFC using $K_3Fe(CN)_6$ solution only, the maximum COD degradation rate has reached 73.5%. However, $K_3Fe(CN)_6$ is not suitable for industrial utilization, it is necessary to develop new forms of catalysts in the next working phase.

4 Activated carbon cloth as cathode catalysts

4.1 Measurement of power density and MFC-bottleneck identification

As ferricyanid is not suited for application in a real wastewater plant other materials were considered. Two kind of carbon cloth were activated by oxidation and tested as cathode, (GFD from SGL corporation, Germany and ACN-211 from Kynol corporation, Germany).

4.2 Treatment of graphite felts

4.2.1 Treatment with Fenton's Reagent

Each piece of graphite felt (12.8 cm×11.7 cm), was dipped in four beakers containing 200 mL 0.02 M ferrous solutions ($FeSO_4$, pH = 3) for 1 h under ambient conditions, respectively. Then, 50, 100 and 150 mL H_2O_2 (30%) were added into the beakers and each solution was diluted to 400 mL with deionized water, respectively. After separately treated with the above H_2O_2 solutions until no gas evolution can be observed (0.5–2 h), graphite felts were immersed in 0.1 M H_2SO_4 under ultrasonication for 30 min to remove the attached $Fe(OH)_3$. The obtained samples washed with deionized water until the pH of wash water became neutral, then were dried in an oven at 50 ^oC for 10 h. The as-prepared graphite felts were denoted as GFD-*x*, where *x* is the H_2O_2 (30%) volume used to prepare the Fenton's reagent in mL, respectively. And the GFD-0 stands for the parent graphite felt without treatment with Fenton reagent. Another type of graphite felt, which is used in our experiments, was ACN-211, which is produced by Kynol Corporation, Germany. Table 4.1 shows the technical data of ACN-211 and GFD samples. Compared to GFD, ACN-211 possesses a relatively higher specific surface area (1500 m^2/g). The relatively large specific surface area of ACN-211 is beneficial to the cathodic reaction of MFC. The same methods are also used for ACN-211, which are denoted as ACN-211-*x*, *x* = 0, 50, 100

and 150 according to the volume of H_2O_2 used.

Table 4.1: Technical data of carbon fiber felts

Article No.	Carbon fiber content (%)	Weight (g/m^2)	Apparent thickness(mm)	Specific surface area(m^2/g)
ACN-211	100	180	2.5	1,500
GDF	100	70	2.5	200

4.2.2 Treatment by thermal modification

The ACN-211 graphite felt, which showed better performance, is treated under different temperatures (300° C, 400° C and 450° C) and times of duration (2 h, 5 h, and 10 h) to study the effect of thermal treatment. The samples are denoted as ACN-211-T-y, T is the treatment temperatures and y is times of duration.

4.2 Results and discussion

4.2.1 Characterization of graphite felts treated with Fenton reagent

Fig. 4.1 illustrates the surface morphology of these GFD-*x* samples. It can be seen from Fig. 4.1 that there are some particles on the surface of untreated sample GFD-0 (Fig. 4.1(a)), which can hinder the approach and adsorption of oxygen and the electron transfer. [70, 71] The particles on the surface of GFD-x reduced with increasing the concentration of H_2O_2. Furthermore, the surface of the sample became relatively rough with increasing the concentration of H_2O_2. For GFD-150, the particles vanished and the surface became more etched and rougher (Fig. 4.1(d)).

Fig. 4.2 illustrates the REM images of ACN-211-*x*, which are treated by Fenton reaction with different volumes of H_2O_2. The similar phenomenon of GFD-*x* is also observed for ACN-211-*x*.

The particles on the surface of ACN-211-x reduced with increasing the concentration of H_2O_2. Furthermore, the surface of the sample became relatively rough with increasing the concentration of H_2O_2. For ACN-211-150, the particles vanished and the surface became more etched and rougher (Fig. 4.2(d)). In addition, it can be seen from Fig.4 that compared to GFD-*x*, smaller holes on the surface of ACN-211-*x* can be seen. This roughened surface of the ACN-211-*x* is beneficial to promote the adsorption ability of oxygen, which would improve the performance of MFC.

Gao Chao et al. [72] have treated graphite felts with different concentration of H_2O_2 for the vanadium redox flow battery and obtained similar results. They found that when H_2O_2 reaches a relatively high level, the fibers become slender and are corroded like tree root, showing that some carbon fibers have been shed from the felt body. Meanwhile, the mechanic strength was deteriorated, showing that the oxidation process could remove the surface contamination or the inhibitory layer, but could also slightly destroy the surface of the graphite felt simultaneously.

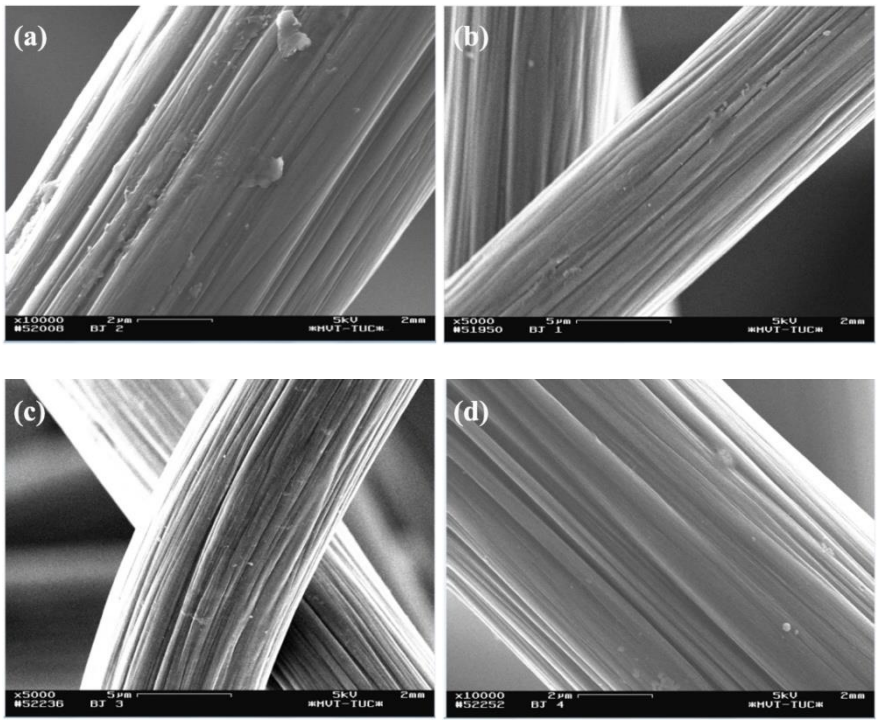

Fig. 4.1: REM images of GFD-*x*; (a) GFD-0, (b) GFD-50, (c) GFD-100 and (d) GFD-150.

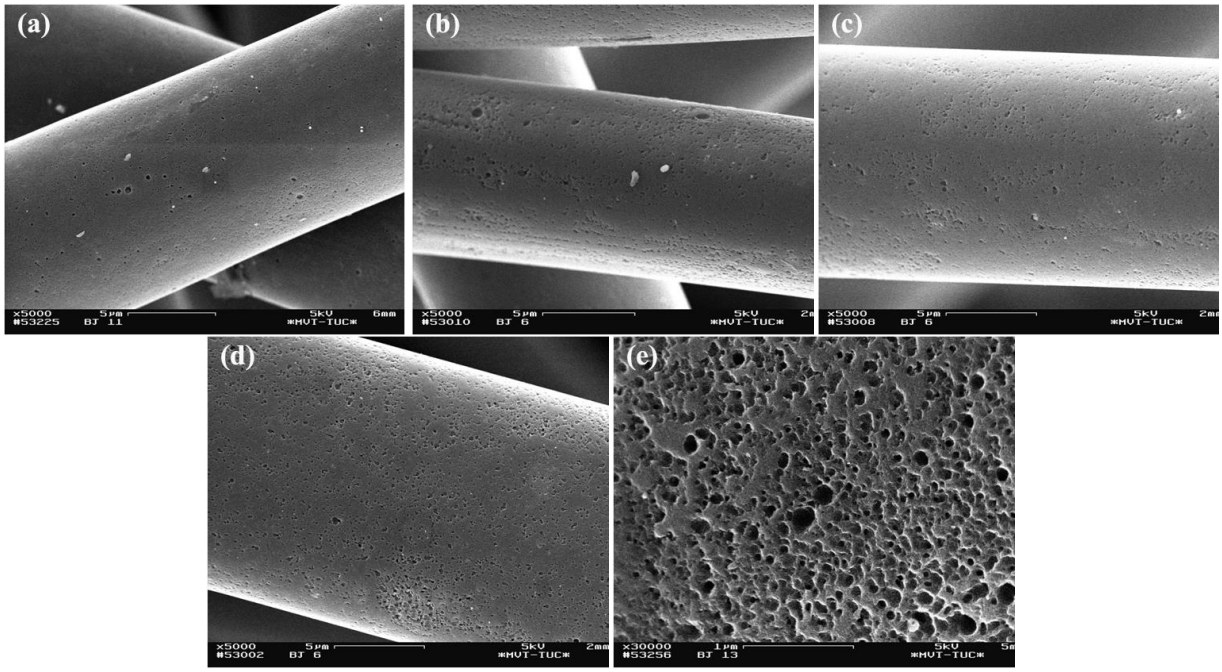

Fig. 4.2: REM images of ACN-211-*x*; (a) ACN-211-0, (b) ACN-211-50, (c) ACN-211-100, (d) ACN-211-150 and (e) ACN-211-150 (Large scale).

4.2.2 Evaluation of start-up behavior and long term performance

Untreated samples GFD-0 and ACN-211-0 are put into use in order to analyze its start-up behavior. Fig. 4.3 illustrates the output power density of MFC with untreated GFD-0 and ACN-211-0 within 33 days. It can be seen in Fig. 4.3 that for GFD-0 the power density was relatively low at the first 6 days and then it increased rapidly with time and reached a maximum of 154 mW/m^2 at 13^{th} day. The similar phenomenon is also observed for ACN-211-0. However, comparing with GFD-0, the maximum power density of ACN-211-0 is much higher, which is achieved at 13^{th} day with the value of 270 mW/m^2. The main reason is that ACN-211-0 possesses a relatively high specific surface area, which is beneficial for the cathodic reaction.

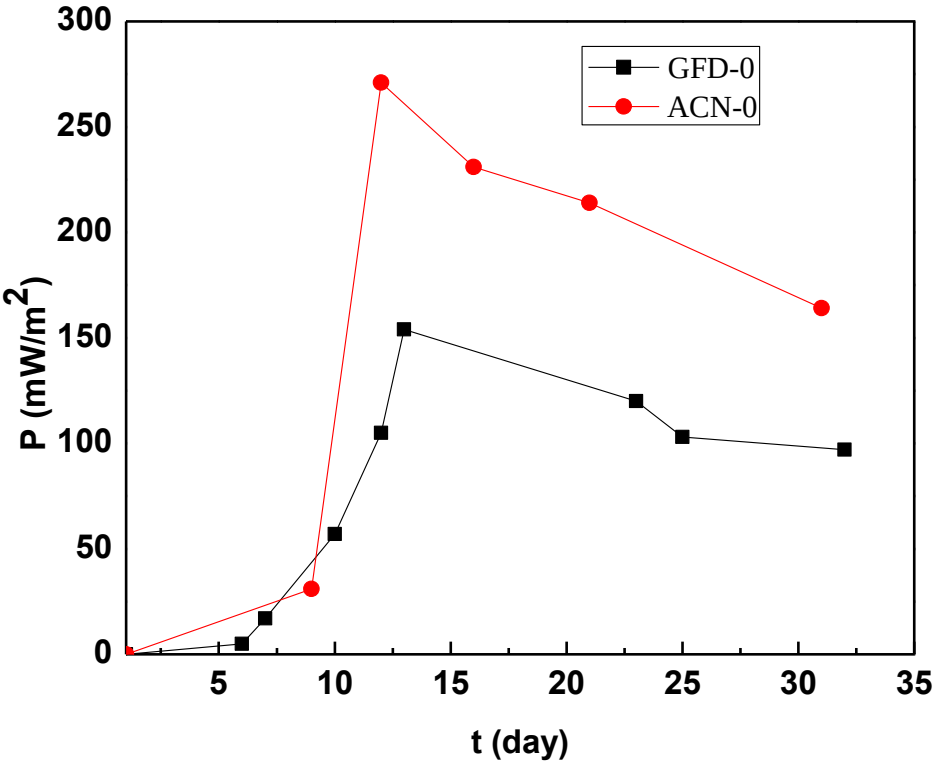

Fig. 4.3: Power density of MFC with untreated GFD and ACN-211

In order to observe the influence of Fenton reagent on the catalytic activity, the long term performance of MFCs with GFD-*x*, treated by different H_2O_2 concentrations, were measured and results were illustrated in Fig. 4.4. The MFCs with GFD-*x* were constructed at different days, whose start-up behaviors were also analyzed at the beginning of long term performance. It can be observed in Fig. 4.4 that the power density of MFCs with treated GFD increased with time much faster than that of the MFC with untreated sample. The optimal power densities are observed at the 20^{th} day and the MFC with GFD-100 reached optimal value of 190 mW/m^2, while the MFCs with GFD-150 and GFD-50 reached optimal value of 180 mW/m^2 and 140 mW/m^2, respectively. The optimal value decreased in the order: GFD-100 > GFD-150 > GFD-50 > GFD-0. This can be explained by the fact that the GFD became more etched and rougher with increasing the H_2O_2 concentration, which is beneficial for adsorption of Fe^{2+}. After reaching the optimal values, all

the power densities of MFCs with GFD-*x* decreased rapidly with time and decreased to lower than 35 mW/m^2 at 25th day. This is possibly due to deactivation of the catalytic groups during the chemical reaction. To show this the REM images of GFD after chemical reaction were analyzed (Fig. 4.5). It can be observed in Fig. 4.5 that many small particles aggregated into large mass and adsorbed on the surface of GFD, which caused a serious fouling.

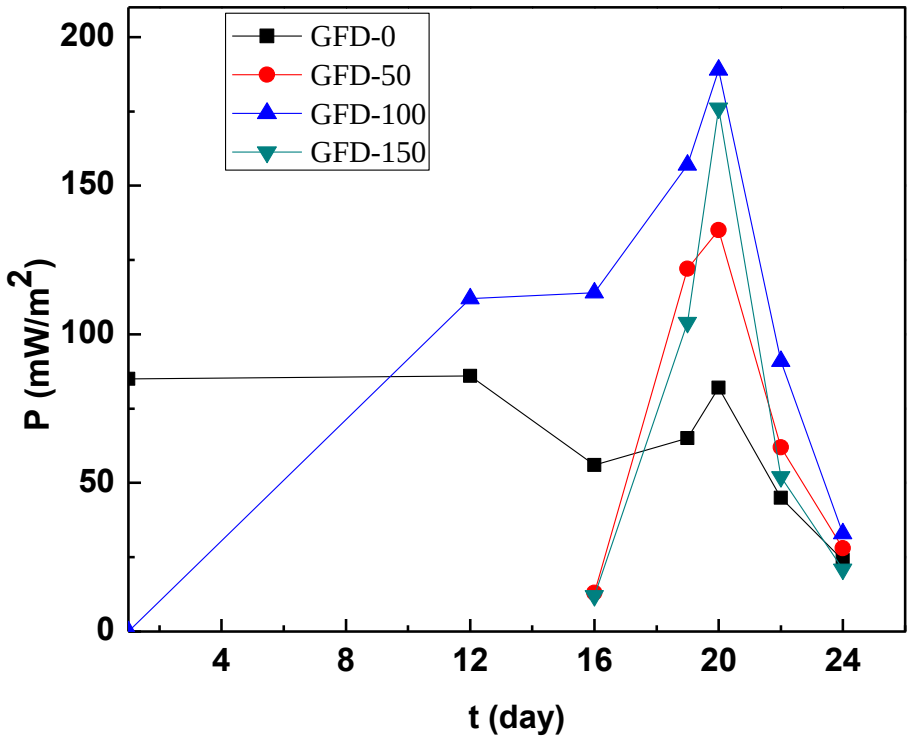

Fig. 4.4: Effect of H_2O_2 volume on the long term performance of MFCs with GFD-*x*

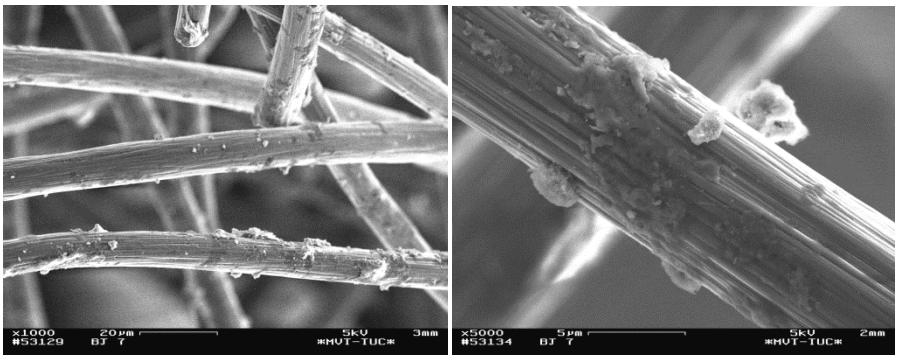

Fig. 4.5: REM images of GFD-100 after chemical reaction

Fig. 4.6 illustrates the long term performance of MFCs with ACN-211-*x*, which was treated by different H_2O_2 concentrations. Results are illustrated in Fig.4.6. It can be observed in Fig. 4.6 that the MFCs with ACN-211-*x* reached the optimal value of power density immediately after construction (for ACN-211-0 is 230 mW/m^2, ACN-211-50 is 380 mW/m^2, ACN-211-100 is 260 mW/m^2 and for ACN-211-150 is 450 mW/m^2). The optimal power density decreased in the sequence: ACN-211-150 > ACN-211-50 > ACN-211-100> ACN-211-0. The power densities descended after reaching the optimal value rapidly. For all the MFCs with ACN-211- *x*, the power densities maintained higher than 100 mW/m^2 at 35th day. Compared to the MFCs with GFD-*x*, the MFCs with ACN-211- *x* exhibited much higher power densities and are more durable. To explain what could be the reason, the REM images of ACN-211-100 after chemical reaction were analyzed, which is shown in Fig. 4.7. Again many small particles aggregated into large mass and adsorbed on the surface of ACN-211, however, the degree of fouling is much less compared to the GFD (Fig. 4.5). Therefore, the higher surface area and better anti fouling performance of ACN-211 are responsible to its relatively high power density during long term running.

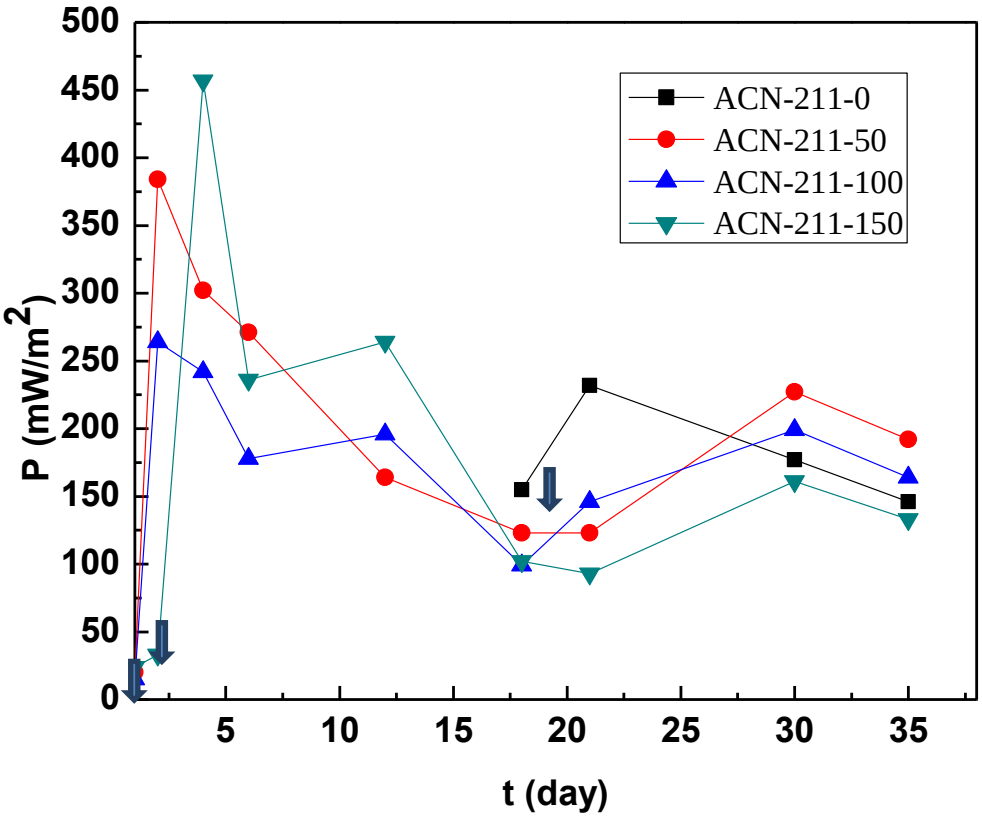

Fig. 4.6: Effect of H_2O_2 volume on the long term performance of MFCs with ACN-211- *x*

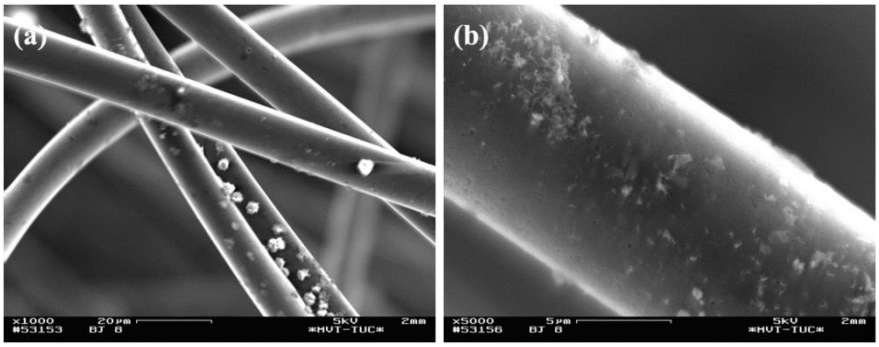

Fig. 4.7: REM images of ACN-211-100 after chemical reaction

4.2.3 Characterization of ACN treated with thermal modification

Fig. 4.8 illustrates the surface morphology of ACN-211 samples, which are treated for 2 h under different temperatures. It can be seen in Fig. 4.8(a) that there are some particles adsorbed on the surface of ACN-211-300-2. With increasing thermal treatment temperature to 400 ° C, the amount of particles became less and their size was getting smaller (Fig. 4.8(b)). However, the amount of particle became larger with increasing the treatment temperature to 450 ° C. In addition, some big pits were formed on the surface of the carbon fiber (Fig. 4.8(c)). This showed that the chemical structure was broken at higher temperature. The similar phenomenon was also observed in Fig. 4.8(d) and Fig. 4.8(e). From Fig. 4.8(e), it can clearly be seen that these particles have blocked the holes on the surface of the carbon fiber. Therefore, excessive high temperature is not beneficial to the cathodic reaction of MFC.

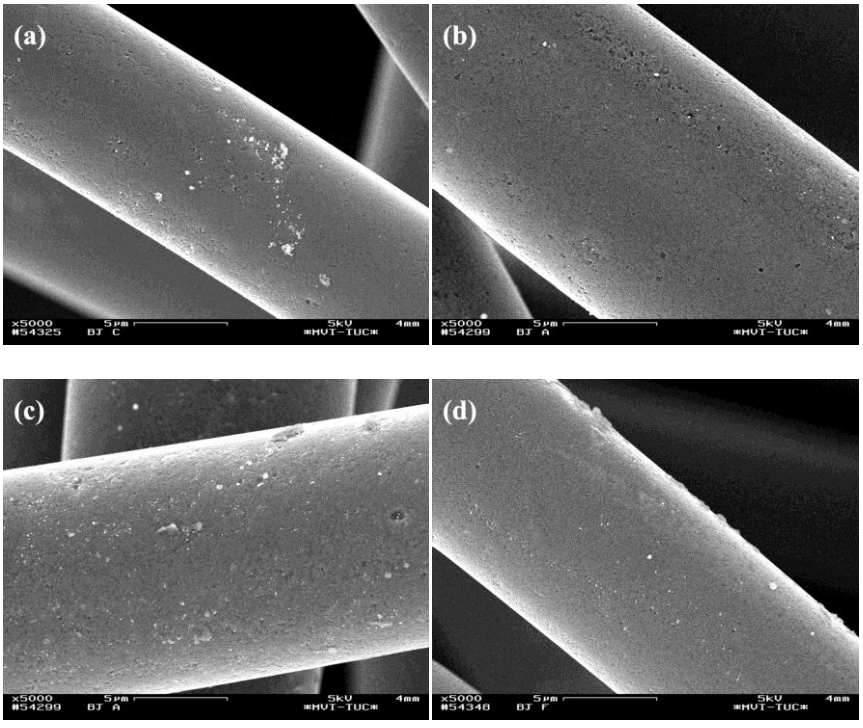

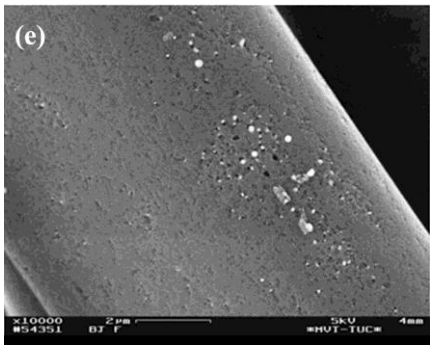

Fig. 4.8: REM images of ACN-211-T-2 with thermal modification; (a) 300 ° C, (b) 400 ° C, (c) 450 °C, (d) 500 °C and (e) 500 °C (Large scale)

Fig. 4.9 illustrates the surface morphology of these ACN-211 samples, which are treated under 400 °C for different times. It can be seen in Fig.11 that the amount of particles on the surface of ACN-211-400-y became larger with increasing time of thermal treatment, which would block the holes on the surface of the carbon fiber.

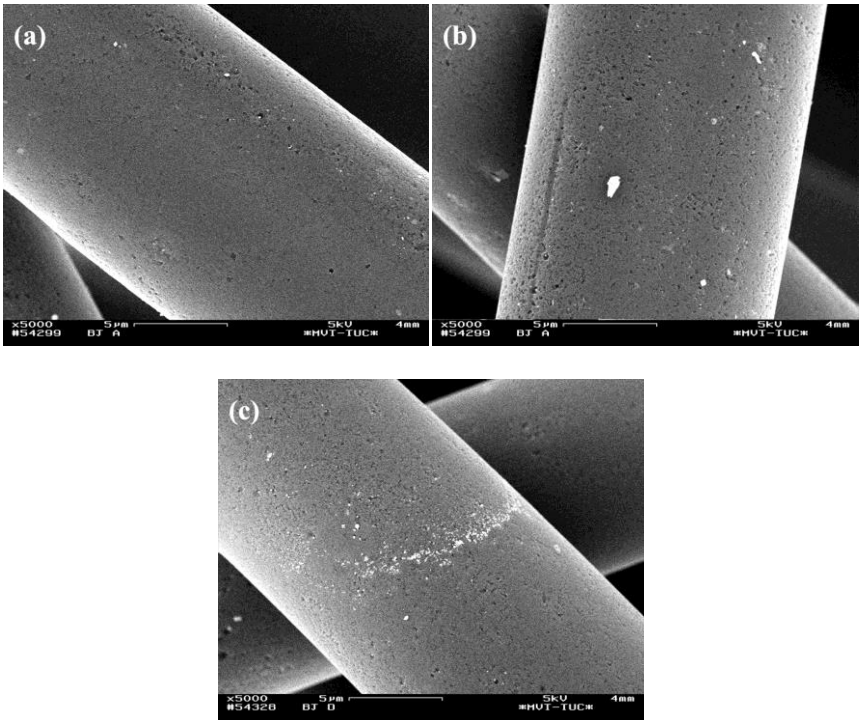

Fig. 4.9: REM images of ACN-211-400-y with thermal modification; (a) 2 h, (b) 5 h, (c) 10 h.

4.2.4 Start-up behavior and long term performance of MFCs with thermally treated ACN-211

Fig. 4.10 shows the start-up behavior and long term performance of MFC with untreated ACN-211-0 and treated ACN-211-T-2. The data suggested that the optimum power density of MFC with ACN-211-300-2 was slightly lower than ACN-211-0. Then the optimum power density of MFC increased with increasing the treatment temperature, reached a maximum at 400 °C (the value is 470 mW/m^2 at 18th day), and then decreased. The optimum power density decreased in the sequence: ACN-211-400-2 > ACN-211-450-2 > ACN-211-0 > ACN-211-300-2, showing that 400 °C is optimal temperature for thermal modification. This is possibly because some of the chemical structure of ACN-211 was broken at higher thermal treatment temperature (Fig. 4.8, REM analysis).

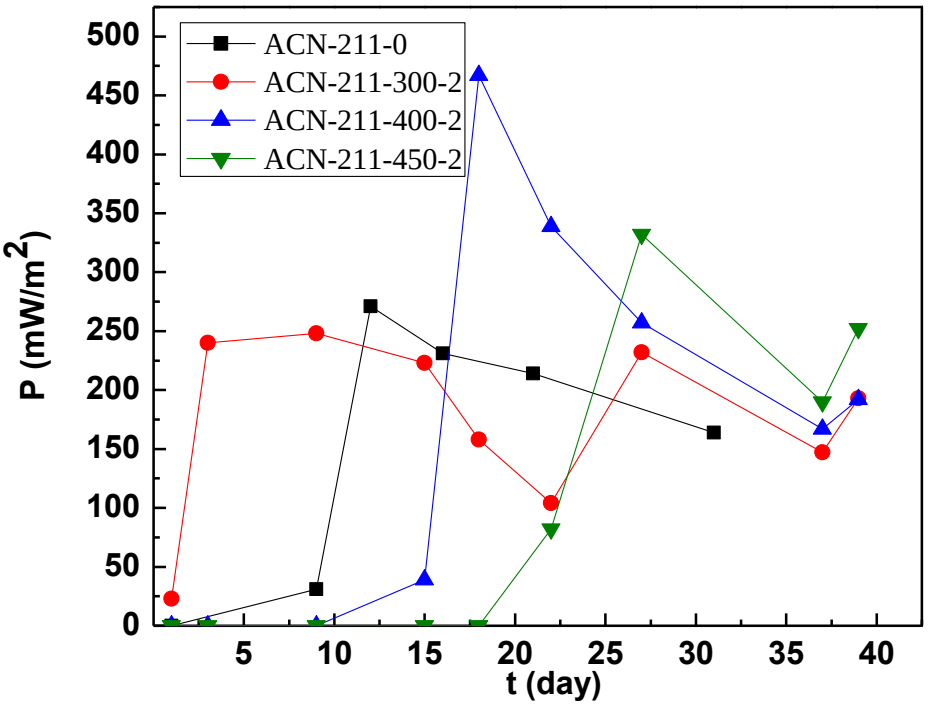

Fig. 4.10: Effect of thermal modification temperature on the start-up behavior and long term performance of MFC with ACN-211-T-2

Fig. 4.11 shows the start-up behavior and long term performance of MFC with thermal modification treated ACN-211 under 400 °C and different time durations. The data suggested that the MFC with ACN-211-400-2 exhibited the highest optimum power density of 470 mW/m^2, while the ACN-211-400-10 possessed a relatively low value, which is 150 mW/m^2. The optimum performance of MFC decreased in the sequence: ACN-211-400-2 > ACN-211-400-5 > ACN-211-400-10. The main reason is that many particles on the surface of ACN-211 can be destroyed under relatively long time duration of thermal treatment (Fig. 4.9, REM analysis). Therefore, the optimal conditions of thermal modification are 400 °C and 2 h.

The ACN-211-150, which treated with Fenton reagent, exhibited optimum power density of 450 mW/m^2. However, the power density decreased rapidly and tended to 130 mW/m^2 at 35th day. As compared to the ACN-211-150, the ACN-211-400-2 exhibited higher optimum power density of 470 mW/m^2. In addition, the power density tended to a higher value of 190 mW/m^2 40th day. This shows that the thermal treatment is also one of the promising modification methods for improving the GFs performance.

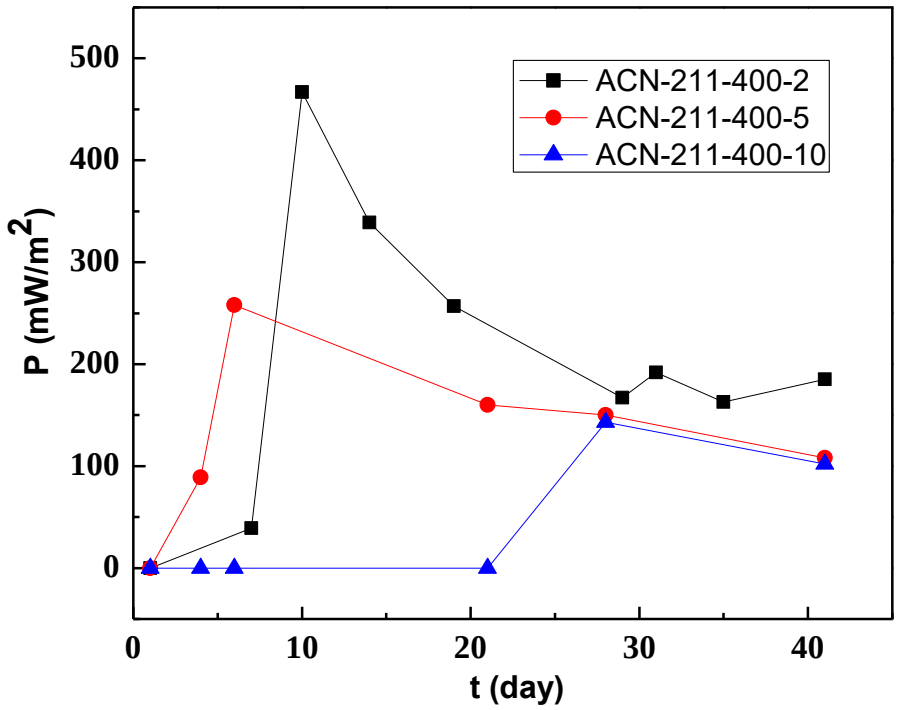

Fig. 4.11: Effect of thermal modification time on the start-up behavior and long term performance of MFC

4.2.5 Long term performance of COD degradation rate

Fig. 4.12 illustrates the long term performance of COD degradation rate of ACN-211-*x* and GFD-*x* samples. The Data in Fig. 4.12 suggested that the best COD degradation rate of GFD-*x* group is achieved with the value of 45% at 12th day and maintained at this level till 45th day. For ACN-211-*x* group, the best COD degradation rate of 57.1% was reached at 4th and maintained at this level till 21th day. However, the degradation rate descended slightly to 49.5% after achieving the best performances. After 30 days, the COD degradation rate became stable with the value of about 50%, showing the COD degradation performance of the MFC could maintain at this level for long term operation.

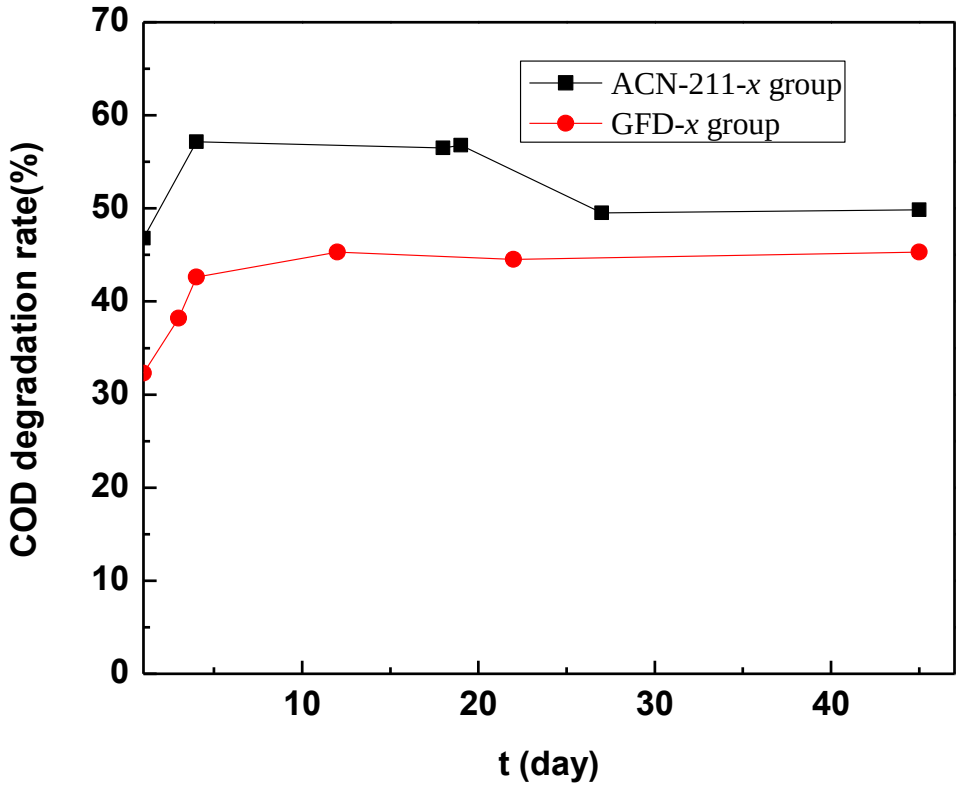

Fig. 4.12: Long term performance of COD Degradation rate of ACN-211-*x* and GFD-*x* groups

4.2.6 Coulombic and Energy Efficiency

Fig. 4.13 illustrates the Coulombic and energy efficiency of ACN-211-*x* and GFD-*x* samples during long term operation. The data suggested that the optimum coulombic efficiency and energy efficiency for GFD-*x* group were 20.1 % and 6.1 %, respectively. In addition, the coulombic efficiency and energy efficiency maintained around these levels during long term operation. The best performance was achieved at 12^{th} day with the values of 35 % for coulombic efficiency and 10% for energy efficiency. Between 12^{th} day and 45^{th} day, the average coulombic efficiency was about 31% and the average energy efficiency was about 8 %. As compared with GFD-*x* group, the ACN-211-*x* group possessed both higher coulombic efficiency and energy efficiency.

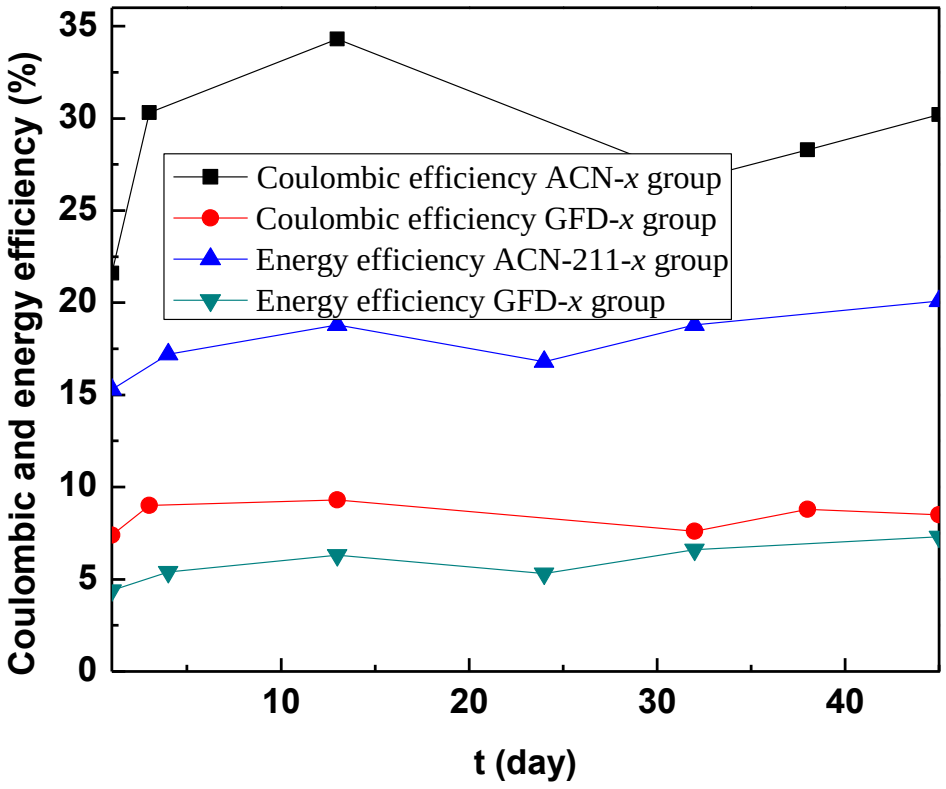

Fig. 4.13: Long term performance of coulombic and energy efficiency

4.3 Conclusions

The MFCs with GFs (GFD and ACN-211) treated by different amounts of H_2O_2 were constructed in this part of the study. Surface morphology of GFs treated with different concentrations of H_2O_2 was observed by REM. Some small particles were observed on the surface of untreated samples, which can hinder the approach and adsorption of oxygen and the electron transfer. By treating the GFs with Fenton reagent, the particles on the surface became less and the surface became relatively rough. With further increasing of H_2O_2 concentration to 150 mL, the particles vanished and the surface became more etched and rougher.

For untreated GFD-0, the maximum power density of 154 mW/m^2 was reached at 13th day, which

is relatively low. Comparing with untreated GFD-0, the maximum power density of untreated ACN-211-0 is much higher, which is achieved at 13th day with the value of 270 mW/m^2. The main reason is that ACN-211 has a relatively high specific surface area, which is beneficial for cathodic reaction.

For the treated GFD-*x*, the MFC with GFD-100 exhibited the best performance with optimal power density of 190 mW/m^2. The optimal value decreased in the order: GFD-100 > GFD-150 > GFD-50 > GFD-0. Among the ACN-211-*x*, the MFC with ACN-211-150 exhibited the best performance with optimal power density of 450 mW/m^2. Unlike the GFD-*x*, the power densities of the treated ACN-211-*x* descended after reaching the optimal value and fluctuated around a certain value instead of dropping sharply to lower than 35 mW/m^2 at 25th day, showing that ACN-211-*x* is more durable. REM images of GFD-100 and ACN-211-100 after chemical reaction indicate that many small particles aggregated into large mass and adsorbed on the surface of samples, which caused a serious fouling. However, the degree of fouling on the surface of ACN-211-100 is much less compared to the GFD-100. Therefore, the higher surface and better anti fouling performance of ACN-211 are responsible for its relatively high power density during long term running.

The thermal modification of ACN-211, which showed better performance, at different temperatures (300 °C, 400 °C and 450 °C) and times (2 h, 5 h and 10 h) were performed and the effects of treatment conditions on the performance of MFC are also studied. The MFC with ACN-211 treated under 400°C and 2 h exhibited the best performance of power density with the maximum value of 470 mW/m^2, which is higher than that of MFC with ACN-211 treated by Fenton's reagent.

The long term performances of coulombic and energy efficiency for both GFD group and ACN-211 group are also studied. The data suggested that the optimal performance of coulombic efficiency for GFD group is 20.1 %, while the optimal performance of energy efficiency is 6.1 %. The coulombic efficiency of 35 % and energy efficiency of 10 % are achieved by using ACN-211 group in MFC. This showed that the COD degradation rate, coulombic and energy efficiency of MFCs with ACN-211 group are better than those of MFCs with GFD group. The best

performance of COD degradation rate of ACN-211 group is 56 % between 19th and 21st day, during which the MFCs are reconstructed by ACN-211 and become stable at around 50 % within 45 days. Comparing with GFD, the ACN-211 possesses both higher coulombic efficiency and energy efficiency.

Another aspect observed was some plugging of the channels by biomass. The carbon fibers act like a filter, causing that some channels were plugged. Compared to $K_3Fe(CN)_6$, the power density of ACN-211 and GFD is much lower, therefore other solid ORR catalyst were studied.

5 Graphite plus MnO_2 and MoS_2 paints as oxygen reduction cathode catalyst of MFC

5.1 Experimental

5.1.1 Wastewater and COD Substrate

In the next step other solid catalysts were investigated. The test conditions were the same as for the previous experiments. The same wastewater and feeding procedure was used.

5.1.2 Measurement of COD Values

The same method as used before was applied.

5.1.3 Preparation of graphite plus MnO_2 and graphite plus MoS_2 paints for evaluation in laboratory scale MFCs

In this part of the work metal compounds were tested as catalyst. As these materials are poor electron conductors a conductive paint was developed in which the catalysts were suspended. For the preparation of the cathode dispersion, MnO_2 received by EMD Millipore Corporation in USA (article number 805958), MoS_2 by Metallpulver24 Corporation in Germany (article number 22020) and graphite RA by Eisenhuth Corporation Germany were mixed and suspended with a binder solution.

Graphite and MnO_2 (or MoS_2) were mixed with the weight proportion of 10:1, 5:1 and 3:1 respectively. As a polymer binder a solution made of 150 mL butanone and 7.5 g celluloid (taken from table tennis balls) was prepared. It may be that the use of celluloid from table tennis balls seems unusual, but the benefit is that this material is highly flexible and contains no additives which could be harmful for our water environment. In addition the properties (like flexibility) are

well regulated by international sports regulations. So reproducibility is guaranteed. The mixture of MnO_2 (MoS_2) and graphite is added into the celluloid butanone solution. 80 ml binder solution was mixed with 17.6 g of graphite catalyst mixture. The components were chosen considering the aspect that no poisonous materials should be used in a water treatment plant. Coating can be done by hand with a paintbrush or an automated spraying machine. In our research, the catalysts are coated by use of a manual paintbrush on the surface of the cathode with an average loading ratio of 0.16 g (catalyst) / g (cathode). 1.4301 AISI 304 stainless steel meshes (w_{mesh} = 1.8 mm, d_{wire} = 0.32 mm) by Spörl KG Präzisionsdrahtweberei Corporation (Germany) with dimension of 150 mm × 150 mm were used as cathodes. A sample of a stainless steel cathode with graphite plus MnO_2 composite coating and four in series connected MFCs with stainless steel as cathode carrier material is given in Fig. 5.1.

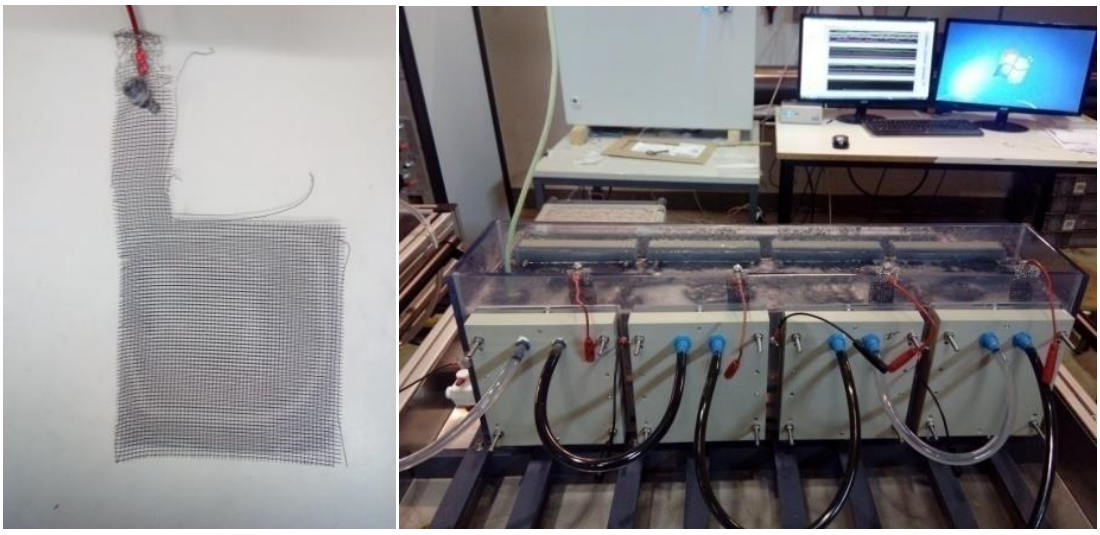

Fig. 5.1: Stainless steel mesh with graphite plus MnO_2 composite (left) and in series connected smaller laboratory scale MFCs (right) (150 mm×150 mm)

5.1.4 Scaling up of MFCs

To reach the next step in scale up, four MFCs with active anodic area of 700 mm × 140 mm

were used for catalyst evaluation. The scaled up MFCs in series are shown in Fig. 5.2, an insight to the design also.

To enlarge the reaction area of the new design, the anode plates have two sides with channels. These were produced by our project partner Eisenhuth Corporation (Germany). In our research, the catalysts are coated by use of a manual paintbrush on the surface of the cathode with an average loading ratio of 0.16 g (catalyst) / g (cathode). Stainless steel meshes (1.4301 AISI 304; w_{mesh} = 1.8 mm, d_{wire} = 0.32 mm for fine mesh and w_{mesh} = 3.15 mm, d_{wire} = 0.56 mm for rough mesh) from Spörl KG Präzisionsdrahtweberei Corporation (Germany) with dimension of 700 mm × 140 mm are used as cathode coated with catalytic composite, which are graphite plus MnO_2 composites with mixing proportion of 10:1. This composition was used since it had the best performance during the catalyst evaluation with the smaller test cells. One of the MFCs was constructed with additional graphite felts (ACN-211 by Kynol Corporation, Germany) for further increasing surface area on the cathode to improve power density. Table 5.1 shows the technical data of ACN-211. This one was used in our experiments because it had the highest specific surface area. For comparison other available types of carbon felts from the same corporation were also listed in Table 5.1. The surface area of ACN-211 is 1500 m^2/g with carbon fiber content of 100 %.

Different cells with different electrode materials and separators were used for comparison, Table 5.2 shows the used materials. Furthermore, different membranes were also used for the MFCs, which are FKE-50 with thickness of 0.05 - 0.07 mm and conductivity of 3 mS/cm and FKS-130 with thickness of 0.11-0.13 mm and conductivity of 5 mS/cm (Fumatech Corporation, Germany) [73].

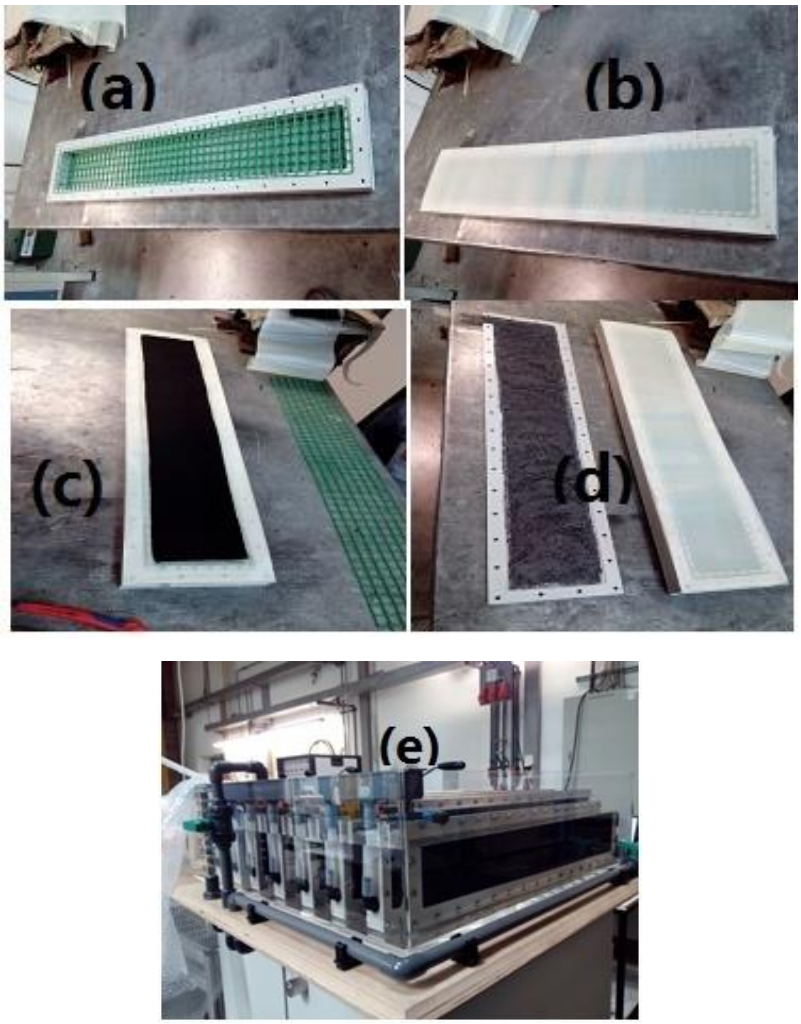

Fig. 5.2: Materials of scaled up MFCs (a) PVC frame for anode plates, (b) Proton exchange membrane, (c) ACN-211for improving power density, (d) Coated stainless steel mesh with graphite plus MnO_2 composite as cathode, (e) assemble scaled up MFCs

Table 5.1: Technical data of carbon fiber felts from Kynol Corporation

Article No.	Carbon fiber content (%)	Weight (g/m^2)	Apparent thickness(mm)	Specific surface area(m^2/g)
ACP-304	50	50	0.2	630
STV-505	50	50	0.2	700
ACN-157	100	90	1.5	1,500
ACN-211	**100**	**180**	**2.5**	**1,500**

Table 5.2: Materials used for the different MFCs

Cell No.	Membrane (byFumatech Corp.)	Stainless Steel mesh Cathode carrier (by Spörl KG Präzisionsdrahtweberei Corp.)	ACN-211 (byKynol Corp.)
1	FKE-50	rough/fine	-
2	FKE-50	fine/fine	-
3	FKE-50	fine/fine	on bothsides
4	FKS-130	fine/fine	-

5.2 Results and Discussion

5.2.1 Start-up behavior of MFCs with graphite plus MnO_2 paint

Four small MFCs (cell No.1a, 2a, 3a, 4a; each with 225 cm^2 active area) with graphite plus MnO_2 paint with the graphite plus MnO_2 weight proportion of 10:1 were connected in series with the wastewater supply. Their start-up behaviors and long term performance were evaluated (Fig.5.3, up). The depicted data are the maximum power point data determined by the LabView control system. The data in Fig.9 suggested that the power densities increased slightly with time within nine days. However, the power densities increased rapidly and reached relatively high values (for cell No.4a 110 mW/m^2, for cell No.1a, 2a and 3a 150 mW/m^2) at the 10^{th} day and then tended to fluctuate around a value of 70 mW/m^2. This behavior that the power densities develop over longer times with fluctuations is quite common in MFCs. Zhang et al. [74] have used carbon nanotubes (CNT) with coated MnO_2 as cathodic catalyst and achieved an optimal power density of 200 mW/m^2 by using anaerobic sludge collected from the Liede municipal wastewater

treatment plant (from Guangzhou, China), which is slightly higher than that obtained in our experiments. But they used CNT as carrier, which is much more expensive than graphite. A cathode without a catalyst for the oxygen reduction reaction in our experiments reached only a power density of about 40 mW/m^2. The power density could be improved by more than 50 mW/m^2 (Fig.5.3, down) by the application of MnO_2 as a catalyst, this is an increase of a factor of more than two. Suresh Babu Pasupuleti et al. have developed membrane-free single-chamber cell by using RuO_2 as coating on the surface of the Ti cathode [75]. A maximal power density of only 70 mW/m^2 was achieved at 27^{th} day during the long term performance, which is lower than that of MFCs in our research. In addition the application of noble metals as catalysts in MFCs is not efficient regarding costs. This demonstrates that a low cost MnO_2 catalyst can play an important role in improving the power density generation of MFCs by increased electrochemical cathode activity.

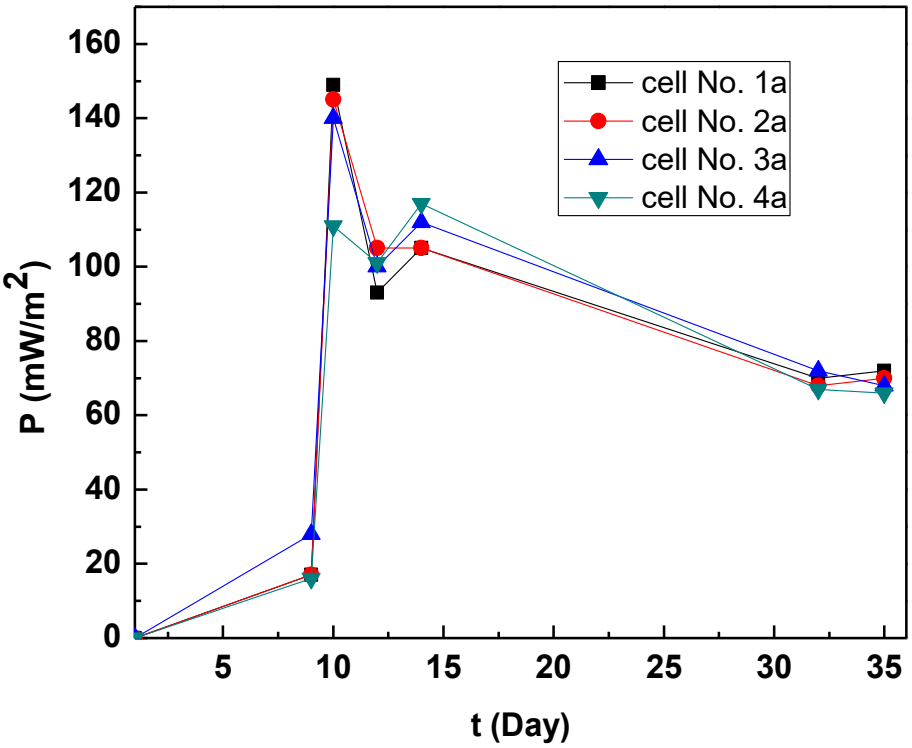

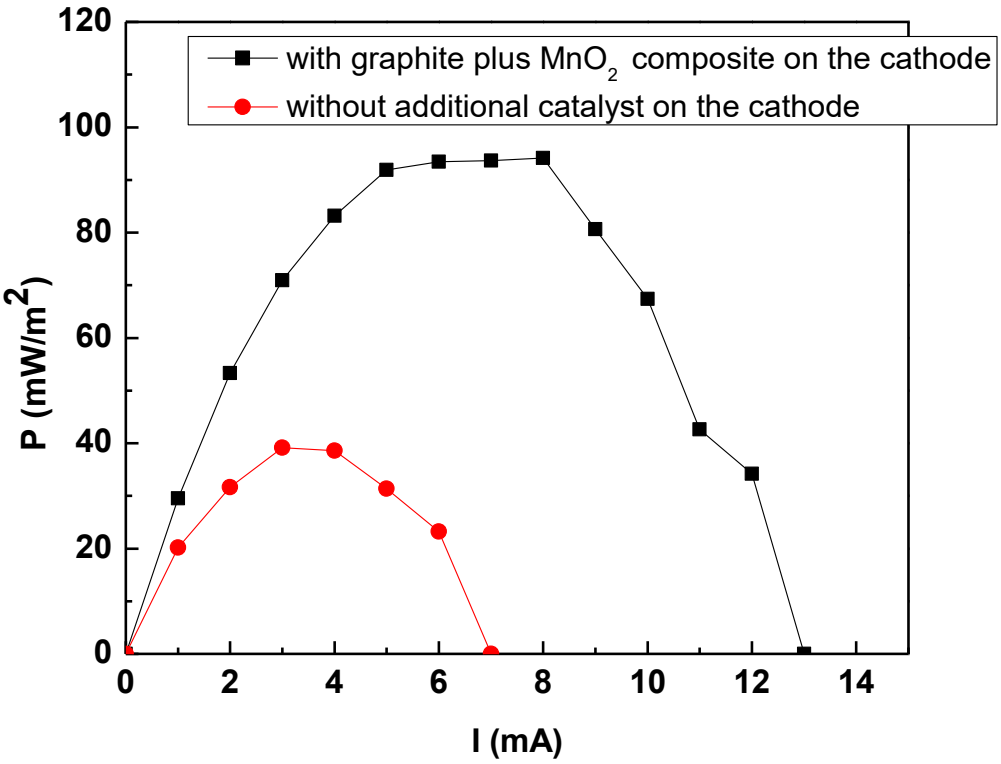

Fig. 5.3: Power density development over time (up) and output power densities of an improved and unimproved MFCs after 2 weeks (down)(red curves, not improved MFC; black curves, improved MFC)

5.2.2 Long term performance of graphite plus MnO_2 paints with higher proportion of MnO_2

To study the influence of catalytic paint composition we varied the graphite:MnO_2 ratio. The loading with catalytic paint on the electrodes was kept constant. Higher MnO_2 loadings were reached. Fig.5.4 shows the long term performance of MFCs with graphite plus MnO_2 paints of 5:1 and 3:1. The arrows in Fig. 5.4 show the time, in which graphite plus MnO_2 composites with graphite plus MnO_2 proportions (5:1 and 3:1) are used. The data suggested that after reaching the best performance, the power densities of MFCs descended rapidly. The best performances were achieved in MFCs with graphite plus MnO_2 proportion of 5:1 and 3:1 at 30^{th} and 20^{th} day

respectively, whose values are 109 mW/m^2 and 114 mW/m^2 respectively. In comparison to the performance of graphite plus MnO_2 composite with graphite plus MnO_2 proportion of 10:1, the power densities of graphite plus MnO_2 composites with graphite plus MnO_2 proportion of 5:1 and 3:1 are relatively low, showing that higher proportion of MnO_2shows no effect on improving the power density of MFCs.

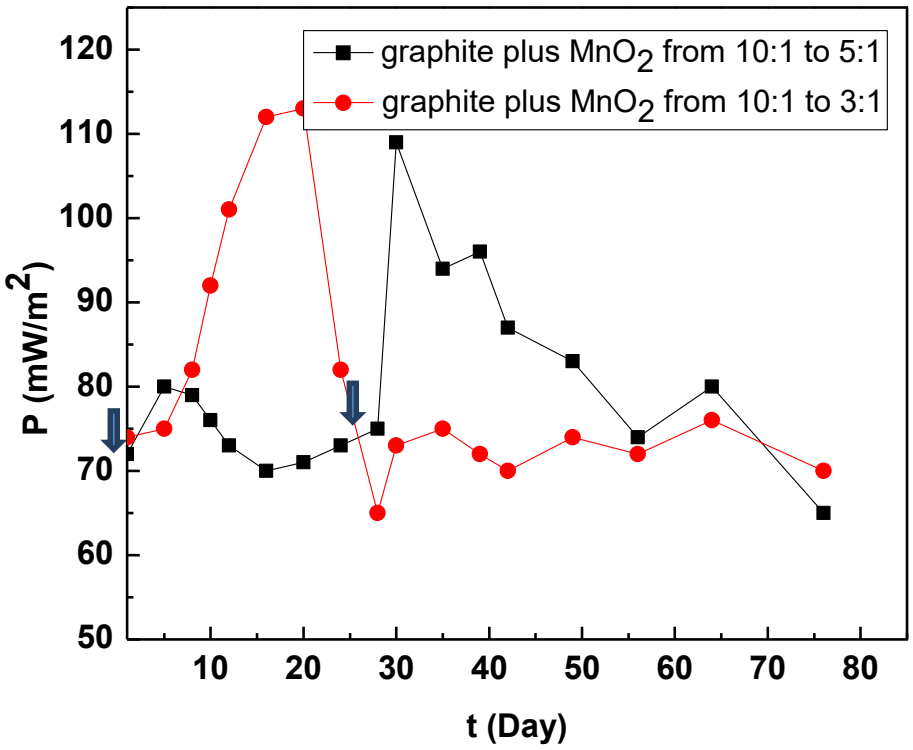

Fig. 5.4: Long term performance of a cathode with graphite plus MoS_2paints. Arrows show cathode installation from 10:1 to 5:1 and 10:1 to 3:1

5.2.3 Long term performance of graphite plus MoS_2 paint

The long term performance of MFCs with graphite plus MoS_2 paint of 10:1 ratio is given in Fig. 5.5. The arrow in Fig. 5.5 shows the time, in which graphite plus MoS_2 paint was installed and

used. The data suggested that the power density of a MFC increased after using graphite plus MoS_2 paint. Despite of the relatively low power density at 30th day, the best performance is achieved at 65th day with the value of 90 mW/m^2. After reaching the best performance, the power density fluctuated with the value of 85 mW/m^2. Comparing with graphite plus MnO_2 composite, the power density of graphite plus MoS_2 composite increased much more slowly with time and its value is also relatively lower than graphite plus MnO_2 composite. However, the graphite plus MoS_2 composite shows a much higher stability than graphite plus MnO_2 composite. Therefore, in order to achieve a higher power density and stability contemporarily, MnO_2 and MoS_2 should be mixed with a certain proportion.

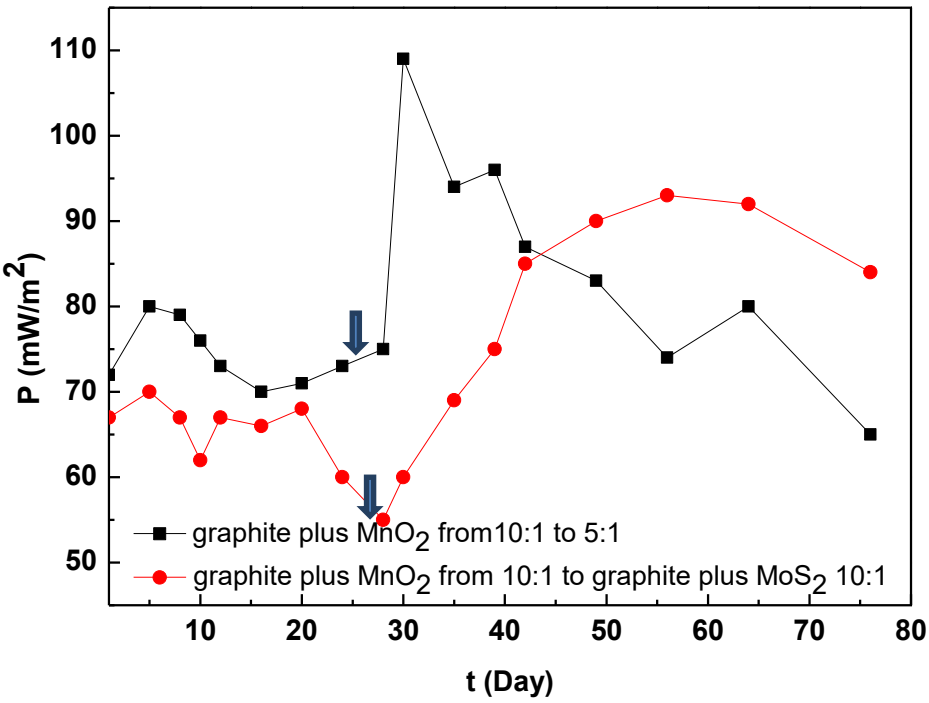

Fig. 5.5: Long term performance of a cathode with graphite plus MnO_2 paints. Arrows show cathode installation from 10:1 to 5:1 and from 10:1 to MoS_2 paint (10:1)

5.2.4 Performance of MFCs with different MnO_2/MoS_2 mixing proportions

The combination of different catalysts (MnO_2 and MoS_2) is necessary for further improvement of power density. The power density performance of MFCs with different MnO_2 plus MoS_2 proportions is shown in Fig. 5.6. The data suggested that the MFC with mixed catalysts with graphite plus MnO_2 plus MoS_2 proportion of 20:1:1 possessed the highest power density during experiments (125mW/m^2 at 5^{th} day). It can be seen in Fig. 5.6 that the power density of MFC with mixed catalysts with graphite plus MnO_2 plus MoS_2 proportion of 30:1:2 possessed the value of 85 mW/m^2 at the beginning and descended rapidly after starting operation. The power density fluctuated around a value of 35 mW/m^2 after the 7^{th} day. However, comparing with the MFC with mixed catalysts with graphite plus MnO_2 plus MoS_2 proportion of 30:2:1, the power density of MFC with graphite plus MnO_2 plus MoS_2 proportion of 20:1:1 shows a better performance, showing that 20:1:1 is the optimal mixing proportion in our experiments.

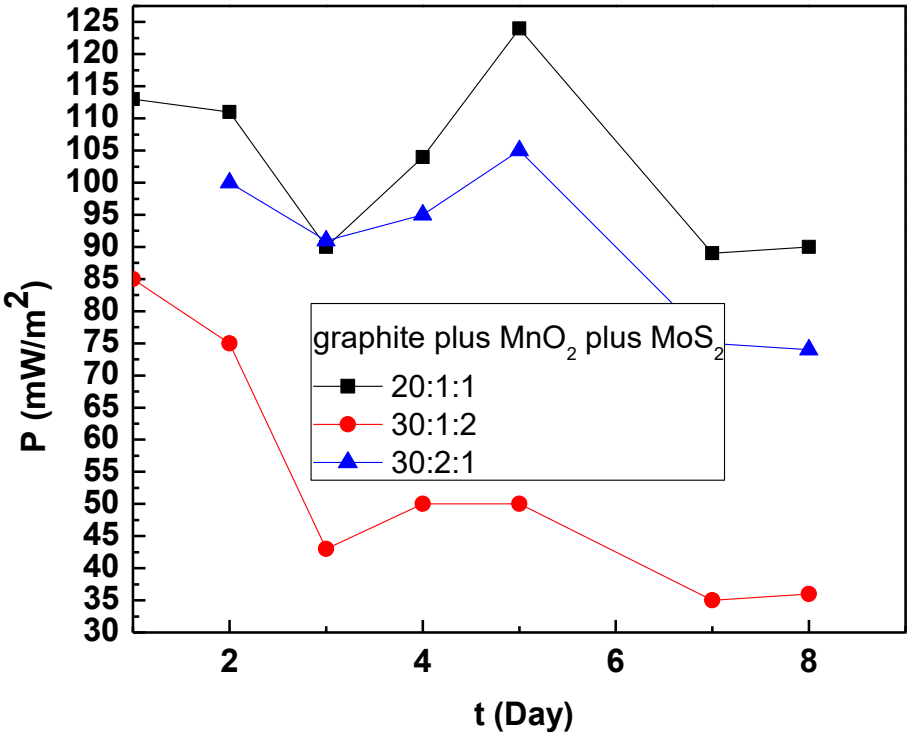

Fig. 5.6: Performance of MFCs with cathodes based on the combination of MnO_2 and MoS_2 proportions as indicated

5.2.5 Coulombic and energy efficiency

The coulombic and energy efficiencies of the whole MFC system (all cells together) were calculated by measured COD values. Fig. 5.7 shows the long term performance of coulombic and energy efficiencies. The data suggested that the coulombic efficiency fluctuated between 20% and 35% from 1st day to 45th day, while the energy efficiency fluctuated between 5% and 10%. The best performances are achieved at 59th (36.8%) and 60th (38%) day, at which the graphite plus MnO_2 composites (5:1 and 3:1) and graphite plus MoS_2 (10:1) composite were used. However, because of decrease of power density after achieving the best performance, both the coulombic and energy efficiencies decreased to 15.8 % and 3.8 % respectively.

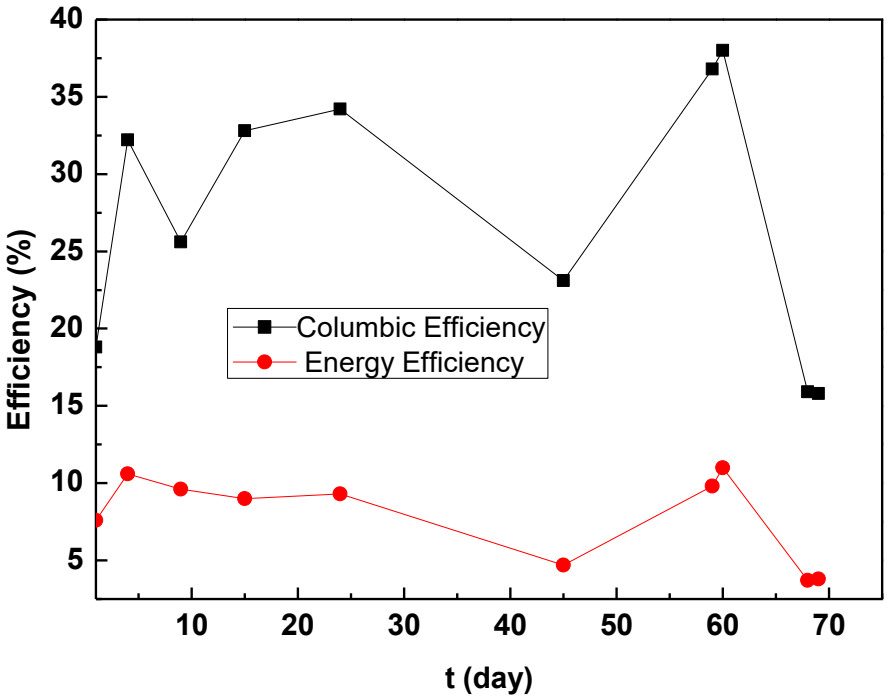

Fig. 5.7: Average coulombic and energy efficiency of the whole MFC stack during long term operation (All the measurements were taken at maximum power point of MFC.)

5.2.6 Start-up behavior of scaled up MFCs

Different cell components and material combinations were tested with the best MnO_2/MoS_2 catalyst determined in the smaller laboratory cells. Fig. 5.8 shows the start-up behavior of MFCs with larger dimensions, from cell No.1b to 4b. According to Table 2, cell No.1b is constructed with a rough and a fine steel mesh, while cell No.2b is constructed with two fine steel meshes on both sides of the anode. It can be seen in Fig. 5.8 that the power density of cell No.1b increased with time at the beginning and fluctuated around a value of 75 mW/m^2 after ten days. The data suggest that the power density of cell No.2b increased continuously until the 39^{th} day and then fluctuated around a value of 125 mW/m^2. The best performance is achieved at 39^{th} day with the value of more than 200 mW/m^2, whose main reason is that a fine stainless steel mesh possesses a

relatively large surface area (Table 5.1), which is beneficial for both coating process and cathodic reaction. The similar phenomenon is also observed by Suman et al., who used carbon felt and stainless steel mesh assembly as cathode [76]. According to Table 5.2, the difference between cell No.2b and 3b is that cell No.3b is constructed with additional graphite felts on the stainless steel cathode. It can be seen in Fig. 5.8 that the power density of cell No.3b increased with time from 1st day to 37th day and possessed a higher power density than cell No.2b. However, the power density of both cells No.2b and 3b decreased after 37 days, whose main reason is that there was not enough substrate (laboratory failure!) to support the power densities of MFCs. It can be seen in Fig. 5.8 that the power density of cell No.3b is still higher than that of cell No.2b after decrease, showing that an additional graphite felt plays an important role in improving the performance of catalytic coated stainless steel mesh cathodes. According to Table 5.2, cell No.2b and 4b were equipped with different proton exchange membranes (FKE 50 and FKS 130 by Fumatech Corp.).As it is mentioned in chapter 2, the FKE-50 membrane possesses thickness of 0.05 - 0.07 mm and conductivity of 3 mS/cm, while FKS-130 possesses a thickness of 0.11 - 0.13 mm and conductivity of 5 mS/cm. The data in Fig. 5.8 suggested that the power density of cell No.4b increased with time during the first 37 days. The best performance is achieved at the 37th day with the value of 195 mW/m^2. It can be seen in Fig. 5.8 that the power density of cell No.4b was higher than that of cell No.2b during the first 37 days, showing that the membrane seems to influence power density of the MFCs. But considering the high conductivity of the membranes in comparison to the low conductivity of the wastewater a real effect of membrane conductivity seems not probable. However, the power density of cell No.4b decreased after achieving the best performance and fluctuated around a value of 100 mW/m^2, which is similar with cell No.3b. The main reason is also lacking of substrate in anode chamber as described above. However, comparing with the power density of cell No.2b, the power density of cell No.4b is still higher at 51st day. By these experiments the best combination of the materials used in our research was found. The combination graphite plus MnO_2 plus MoS_2 in proportions of 20:1:1 as a coating on fine stainless steel mesh combined with carbon felt ACN 211 resulted over longer times in the most satisfying performance. Here I want to thank my colleagues Dennis Haupt and Thorben

Muddemann for their helpful assistance during all these cell tests.

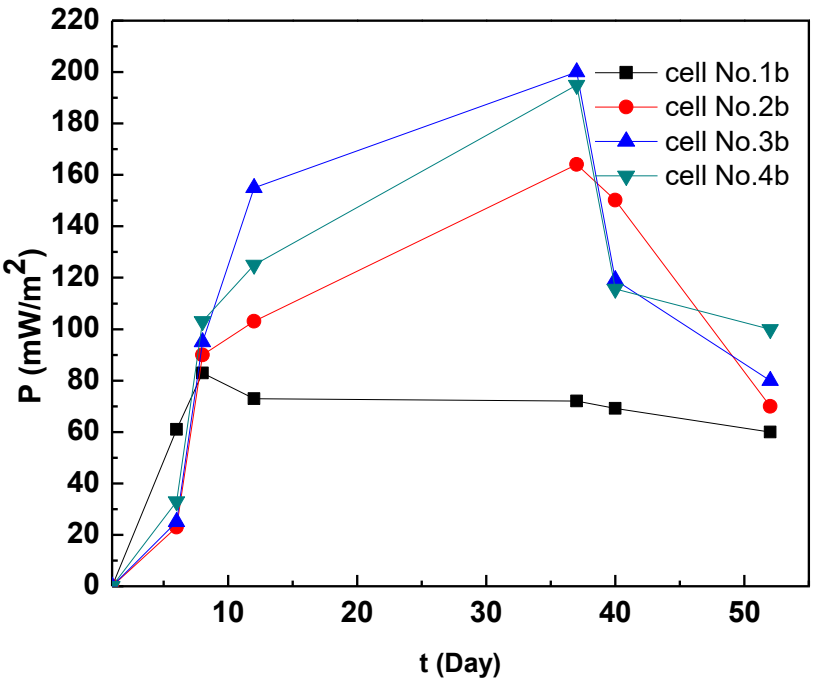

Fig. 5.8: Start-up behavior of scaled up MFCs

5.3 Conclusions

A MFC with uncoated stainless steel cathode is firstly constructed and the polarization curve as well as the individual electrode potentials is measured by using a reversible hydrogen reference electrode (RHE) which does not disturb the inner construction of the MFC. The data reveal that the voltage of MFCs descends with increasing load current. When the load current reaches a value too high for the cell to deliver the cathode potential descends rapidly showing that the cathode is the limiting factor for MFC power. Therefore, it is necessary to enhance the cathode performance by adding an electrocatalyst on the cathodes surface.

A low cost MnO_2 catalyst can play an important role on improving the power density generation of MFCs by increased electrochemical activity on the cathode. A cathode without a catalyst for the

oxygen reduction reaction reached only a power density of about 40 mW/m^2 in our experiments with real wastewater. The best performance of MFC with graphite plus MnO_2 composite (10:1) was more than 100 mW/m^2. The best performances of graphite plus MnO_2 composites with 5:1 and 3:1 are achieved at 30^{th} and 20^{th} day respectively, whose values are 109 mW/m^2 and 114 mW/m^2 respectively. Comparing with the performance of graphite plus MnO_2 composite with 10:1, the power densities of graphite plus MnO_2 composites with 5:1 and 3:1 are relatively low, showing that higher proportion of MnO_2 shows no effect on improving the power density of MFCs. An explanation may be that the higher concentration of the not conducting binder in the catalyst paint lowers the paint conductivity. Comparing with graphite plus MnO_2 paint, the power density of graphite plus MoS_2 paint increased much more slowly with time and its value is also relatively low. However, the graphite plus MoS_2 paint shows a much higher stability than graphite plus MnO_2 paint. Therefore, in order to achieve a higher power density and stability over long operation times, MnO_2 and MoS_2 should be mixed together with a certain proportion.

The power density performance of MFCs with different MnO_2 plus MoS_2 proportions is studied and the data suggested that the MFC with mixed catalysts with MnO_2 plus MoS_2 proportion of 1:1 possessed the highest power density during experiments. The power density of MFC with mixed catalysts with MnO_2 plus MoS_2 proportion of 1:2 possessed the value of 85 mW/m^2 at the beginning and descended rapidly after the construction. Comparing the MFC with mixed catalysts with MnO_2 plus MoS_2 proportion of 2:1, the power density of MFC with MnO_2 plus MoS_2 proportion of 1:1 shows a better performance, showing that 1:1 is the optimal mixing proportion. For the scaled up MFCs, the best performance of cell No.2b is achieved with the value of more than 200 mW/m^2, which is higher than that of cell No.1b with a rough stainless steel mesh. So a fine stainless steel mesh should be used. In addition a fine mesh is easier to handle during assembly. The power density of cell No.3b with graphite felts ACN-211 increased with time from 1^{st} day to 37^{th} day and possessed a higher power density than cell No.2b. However, the power density of both cell No.2b and 3b decreased after 37 days, whose main reason is that there was not enough substrate to support the power densities of all MFCs. In addition we observed a plugging of the graphite felts by microbial films, which may contribute to power decline. The power

density of cell No.3b is still higher than that of cell No.2b after decrease, showing that graphite felt plays a role in improving the performance of catalytic stainless steel coated mesh. Considering this, the additional costs and the observed trend to plugging we cannot recommend the application of felt electrodes in real wastewater. Considering the membrane it is obvious that the membrane has a slight influence on power performance. As membranes are expensive MFC components the cheapest membrane which is available should be used. The MnO_2 catalyst possesses a great potential for improving the performance of MFC, therefore, it is necessary to investigate the performance of MnO_2 catalysts with different crystal forms in the next working phase.

6 Effect of different MnO_2 catalysts on the performance of MFCs

6.1 Experimental

6.1.1 Preparation of graphite/$MnO_2$and graphite/MoS_2 composite

For preparing the cathode dispersion, MnO_2 was received by Guangzhou Chun Zheng Chemical Corporation in China, MoS_2 by Metallpulver24 Corporation in Germany (article number 22020) and graphite RA by Eisenhuth Corporation Germany.

New form of MnO_2 (ß-MnO_2) catalyst is also studied in our research, which was prepared according to the method of Zhang et al.[77] In which, $KMnO_4$, ethanol and water were mixed together and then sealed and maintained at 125 ^oC for 24 h before cooling down to room temperature. After washed and dried, the precipitates were calcined at 300 ^oC for 5 h. The catalyst was cooled to room temperature before putting into use.

Graphite, MnO_2 and MoS_2 are mixed in a weight proportion of 20:1:1, 30:1:2 and 30:2:1 respectively. As a polymer binder a solution made of 150 mL butanol and 7.5 g celluloid (taken from table tennis balls) is produced. The mixture of MnO_2, MoS_2 and graphite is added into the butanol solution. The components were chosen considering the aspect that no poisonous materials should be used in a water treatment plant. In our research, the catalysts were coated by paintbrush on the surface of cathodes with the average loading ratio of 0.16 g (catalyst) /g (cathode). In order to study the influence of ultrasonic treatment on the performance of MFC, graphite, MnO_2 and MoS_2 which are mixed in a weight proportion of 20:1:1 are also treated under ultrasonication for 30 min. Stainless steel meshes (w = 1.8 mm, d = 0.32 mm) from Spörl KG Präzisionsdrahtweberei Corporation (Germany) with dimension of 150 mm × 150 mm were used as cathode. A sample of a stainless steel cathode with graphite/MnO_2 composite coating and four in series hydraulically connected MFCs with stainless steel as cathode carrier material is given in Fig. 6.1.

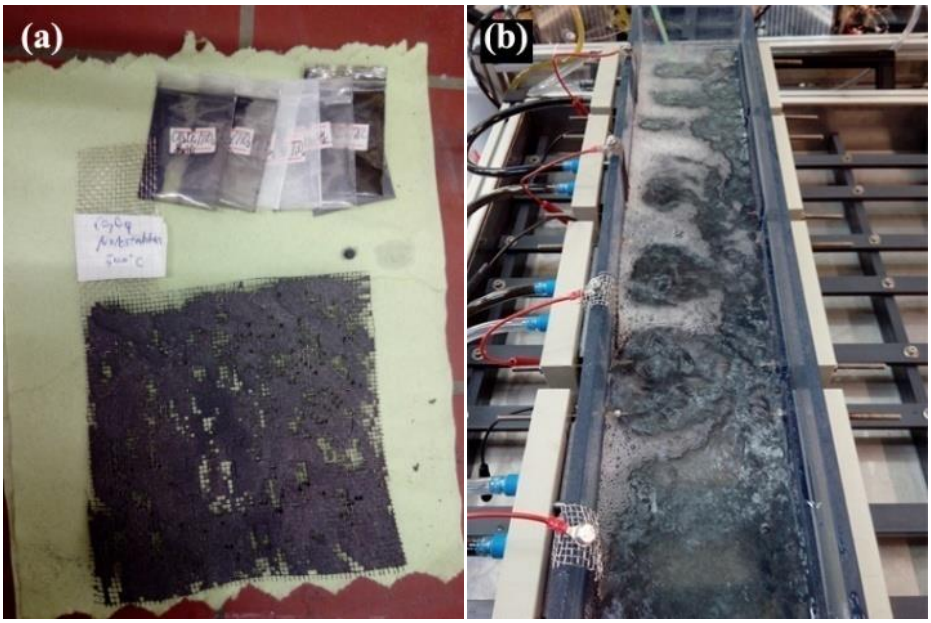

Fig. 6.1: Stainless steel mesh with catalyst (a) and four in series connected MFCs (b).

6.1.2 Characterization

The X–ray powder diffraction (XRD) analysis were recorded on a D/max-2200PC-X-ray diffractometer (40 kV, 20 mA) using CuKα radiation (0.15404 nm), scan range from 10 to 80° at a rate of 10°/min. The typical physico-chemical properties of supports and catalysts were analyzed by BET method using Micromeritics adsorption equipment of NOVA2000e. All the samples were outgassed at 200 °C until the vacuum pressure was 6 mm Hg. The morphological and surface composition characterization of the samples were obtained using scanning electron microscopy (SEM, NOVA600, FEI) and energy dispersive X-ray spectrometry (EDS).

6.2 Results and Discussions

6.2.1 Characterization of MnO_2 and MoS_2

XRD patterns were used to identify and confirm the crystalline phases of samples used as catalysts (Fig. 6.2) . It can be observed from Fig.4 that for purchased γ-MnO_2, the peaks at 2θ = 22.3°, 37.1°, 42.4°, 56.6°, 65.7° and 67.3° (PDF: 03-0953) can be seen, which confirmed that the purchased MnO_2 sample was γ-MnO_2. For as-prepared β-MnO_2, the peaks at 2θ = 28.7°, 37.3°, 41.0°, 42.8°, 46.1°, 56.7°, 59.4°, 64.8°, 67.2°, 68.6°, 72.3° and 72.4° can be seen, which confirmed that the prepared MnO_2 sample was β-MnO_2. For MoS_2, the sharp peaks at 2θ = 14.4°, 29.0°, 32.7°, 33.5°, 35.9°, 39.5°, 44.2°, 49.8°, 56.0°, 58.3°, 60.1°, 62.8°, 70.1°, 72.8° and 76.0° (PDF: 37-1492) can clearly be seen, which confirmed that the sample was MoS_2 of good crystallinity.

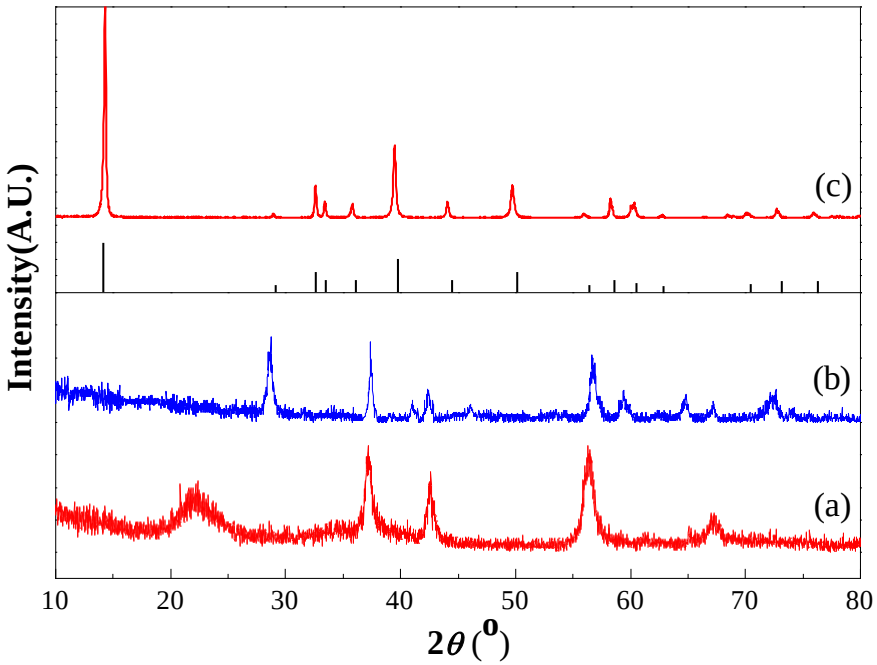

Fig. 6.2: XRD patterns of the purchased γ-MnO_2 (a), as-prepared ß-MnO_2 (b) and MoS_2 (c) catalysts

Table 6.1 shows the textural properties of different catalysts. It can be observed from Table 6.1 that the surface area, pore volume and diameter of γ-MnO_2 were 57.1 $m^2 \cdot g^{-1}$, 0.072 $cm^3 \cdot g^{-1}$ and 4.9 nm, respectively. While for ß-MnO_2, the surface area, pore volume and diameter were 68.3 $m^2 \cdot g^{-1}$, 0.281 $cm^3 \cdot g^{-1}$ and 16.5 nm, respectively. This shows that the ß-MnO_2 possessed a higher surface area than that of γ-MnO_2. In addition, the pore diameter and pore volume of ß-MnO_2 were 2.9 times and 2.4 times larger than those of γ-MnO_2, respectively. The above results showed that the structures of the γ-MnO_2 and ß-MnO_2 catalysts were significantly different even though their compositions are the same. The ß-MnO_2 is more likely to be a better catalyst than γ-MnO_2 owing to its textural properties. This will further discussed later. For MoS_2, the surface area, pore volume and diameter were 7.7 $m^2 \cdot g^{-1}$, 0.038 $cm^3 \cdot g^{-1}$ and 19.2 nm, respectively. Comparing with γ-MnO_2 and ß-MnO_2, the MoS_2 catalyst possessed a lower surface area with a relatively low pore volume.

Table 6.1: Textural properties of γ-MnO_2, MoS_2 and ß-MnO_2catalysts

Sample	$S_{BET}/(m^2 \cdot g^{-1})$	$V_p/(cm^3 \cdot g^{-1})$	D/(nm)
γ-MnO_2	57.1	0.072	4.9
β-MnO_2	68.3	0.281	16.5
MoS_2	7.7	0.038	19.2

Fig. 6.3 illustrates SEM morphologies of the γ-MnO_2, MoS_2 and ß-MnO_2catalysts. It can be observed from Fig. 6.3 that γ-MnO_2 catalyst showed an irregular form and rough edges (Fig. 6.3(a)). The morphologies of the γ-MnO_2 and ß-MnO_2 catalysts are significantly different. The ß-MnO_2 catalyst clearly maintains the whisker structure (Fig. 6.3(c)). Comparing with those

MnO_2 catalysts, the morphology of MoS_2 catalyst (Fig. 6.3(b)) is much more regular with several layers.

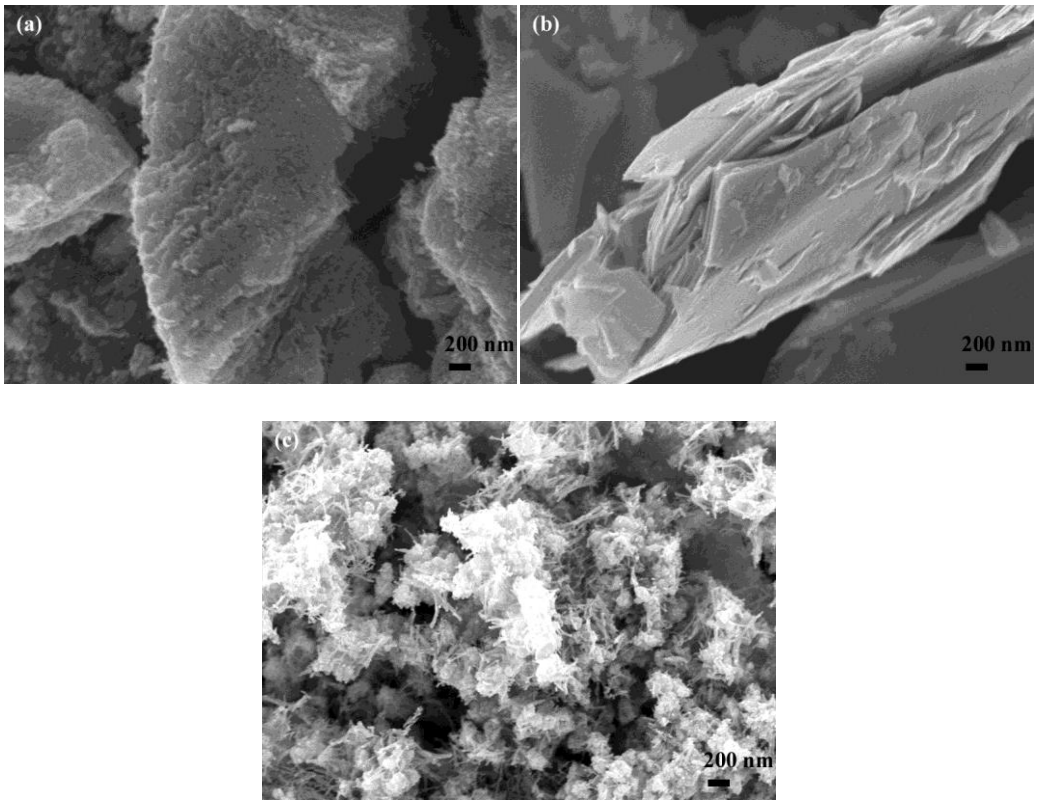

Fig. 6.3: SEM morphologies of γ-MnO_2 (a), MoS_2 (b) and ß-MnO_2 (c) catalysts

6.2.2 Polarization curves of MFC with different catalysts

The power density performance of MFCs with different graphite, γ-$MnO_2$and MoS_2 proportion is shown in Fig. 6.4 (up). The data suggested that the optimal power densities of MFCs with catalysts prepared by graphite, γ-MnO_2 and MoS_2 in a proportion of 30:1:2 and 30:2:1 were lower than 60 mW/m^2. The MFC fabricated with a catalyst prepared by graphite, γ-MnO_2 and MoS_2 in a proportion of 20:1:1 possessed the highest optimal power density of 120 mW/m^2.

This value is two times the optimal power of the MFCs fabricated using the catalysts prepared by graphite, γ-$MnO_2$and MoS_2 in a proportion of 30:1:2 and 30:2:1. This shows that the proportion of graphite has significant effect on the power density. A RHE is also used in our experiments for measuring the potential of single electrode and the data is shown in Fig. 6.4 (down). The similar results were obtained. It can be seen that the cathode potential of MFC fabricated with a catalyst prepared by graphite, γ-$MnO_2$and MoS_2 in a proportion of 20:1:1 descended slower than those of MFCs with other mixing proportions. The main reason is that the MFC fabricated with a catalyst prepared by graphite, γ-$MnO_2$and MoS_2in a proportion of 20:1:1 possesses the highest optimal power density.

The influence of ultrasonic treatment on the performance of power density of MFC is shown in Fig. 6.5. The data suggested that the MFC fabricated with a catalyst prepared by graphite, γ-MnO_2 and MoS_2 in a proportion of 20:1:1 with ultrasonic treatment possessed a significantly higher power density (183 mW/m^2) than the one without ultrasonic treatment, showing that ultrasonic treatment plays an important role in improving the power density of MFC. The possible reason maybe that the ultrasonic treatment can promote a good mix of the graphite, γ-MnO_2 and MoS_2, and therefore can produce more uniform composite. This would play a positive role in energy production. Sang et al.[78] have pretreated different sludge types for MFC and found that the ultrasonic pretreatment has changed the physical structure of sludge and therefore, a higher electricity production was obtained.

The influence of different MnO_2 morphologies on the performance of power density of MFC is shown in Fig. 6.6. The data suggested that the optimal power density of MFC fabricated with a catalyst prepared from graphite and ß-MnO_2 in a proportion of 10:1 was 140 mW/m^2, which is higher than that of MFC fabricated with a catalyst prepared form graphite, γ-MnO_2 and MoS_2 in a proportion of 20:1:1, showing that the performance of ß-MnO_2 with a whisker structure was much better than γ-MnO_2. This can be attributed to the higher surface area, larger pore size and great pore volume of ß-MnO_2 (Table 6.1). It should be noted that the higher surface area is beneficial to expose more active sites, which would enhance the catalytic performance. While the larger pore diameter and pore volume would facilitate the diffusion rates of the reactant, which is

beneficial towards chemical reactions over the catalysts. Furthermore, the average oxidation state (AOS) of manganese oxide would also play a role in the performance. Shen et al. [79] have measured the AOS value of different manganese oxide samples via a magnetic method and found that the ß-MnO_2 possessed the highest AOS value (4.23) comparing with γ-MnO_2 (4.04). Zhang et al.[80] have tested three manganese dioxide materials, α-MnO_2, ß-MnO_2, γ-MnO_2 as cathodic catalysts in air-cathode MFCs and found that ß-MnO_2 appeared to hold the highest catalytic activity. They concluded that the high catalytic activity of ß-MnO_2 is due to its high BET surface and AOS value. Comparing with MFC fabricated with a catalyst prepared from graphite and ß-MnO_2 in a proportion of 10:1, the MFC fabricated with a catalyst prepared from graphite, ß-$MnO_2$and MoS_2 in a proportion of 20:1:1 possessed even a higher power density, which is 158 mW/m^2. This indicated that addition of MoS_2 is beneficial to enhance the MFC performance.

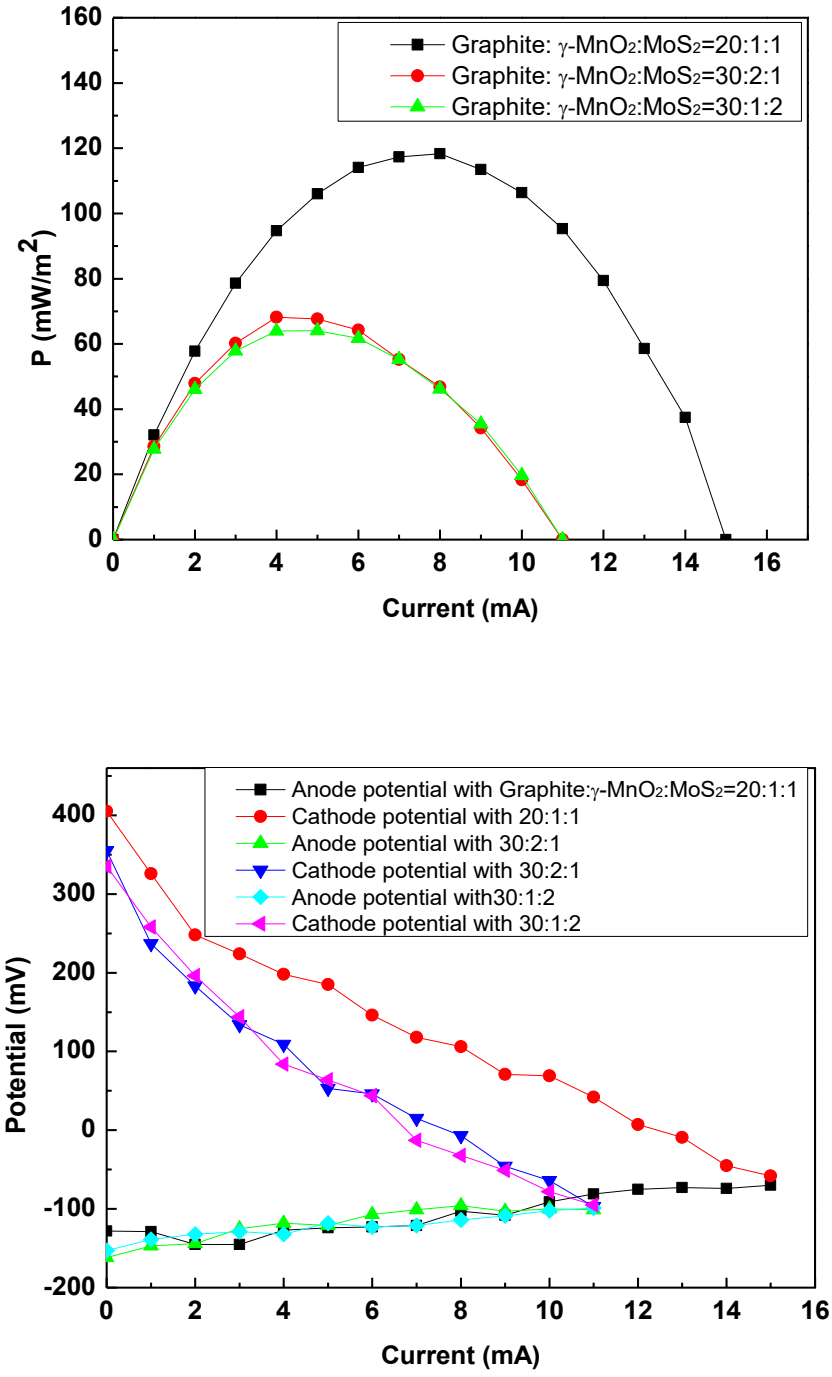

Fig. 6.4: Power densities of MFCs with cathodes based on the catalysts prepared using graphite, γ-MnO_2 and MoS_2 in different proportions as indicated (up) and the corresponding potential measurement (down)

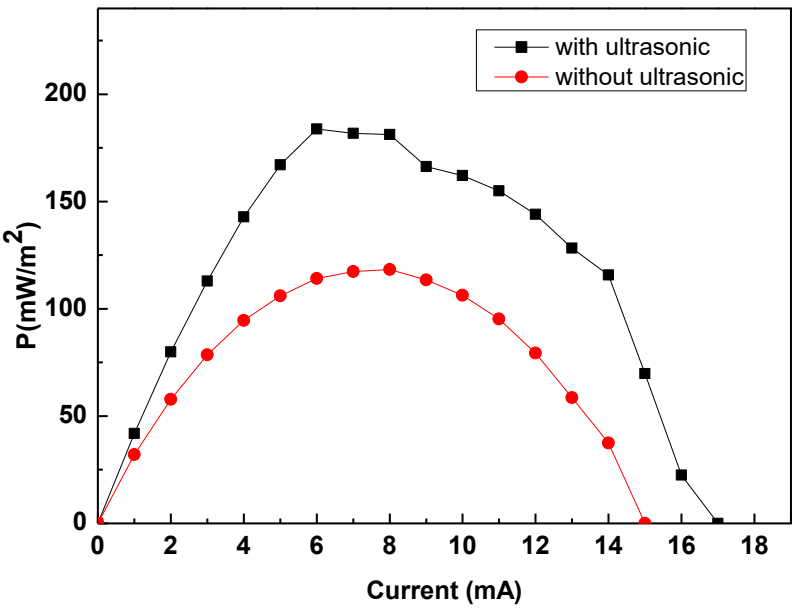

Fig. 6.5: Power densities of MFCs with cathodes based on the catalyst prepared using graphite, γ-MnO_2 and MoS_2 in a proportion of 20:1:1 with and without ultrasonic treatment

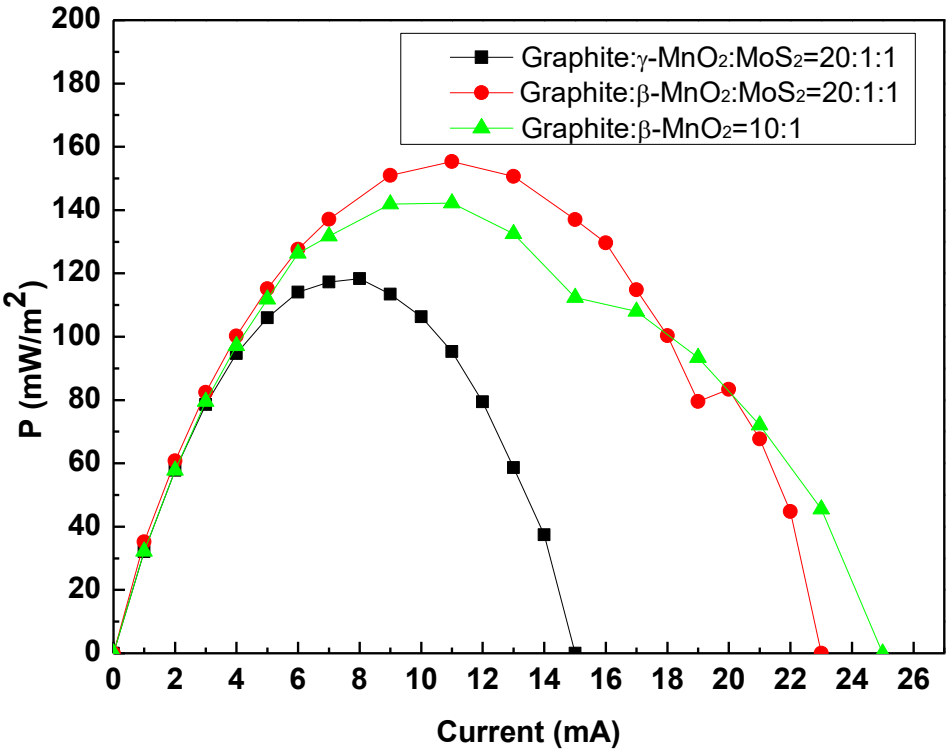

Fig. 6.6: Power densities of MFCs with cathodes based on the catalysts prepared using graphite, ß-MnO_2 (γ-MnO_2) and MoS_2.

6.2.3 Long term performance of MFC fabricated with a catalyst prepared by different proportions

The long term performance of MFCs with catalysts prepared with different graphite, γ-MnO_2 (ß-MnO_2) and MoS_2 proportions is shown in Fig. 6.7. The data suggested that for all the samples, the power densities became stable after 12^{th} day and a slight descend is observed. The MFC fabricated with the catalyst prepared from graphite, γ-$MnO_2$and MoS_2 in a proportion of 20:1:1 achieved the highest power density of 125 mW/m^2 on 5^{th} day. The power density of MFC fabricated with a catalyst prepared from graphite, γ-$MnO_2$and MoS_2 in a proportion of 30:1:2 possessed the value of only 85 mW/m^2 at the beginning and descended rapidly after starting operation. However, after 12^{th} day, the power density of MFC fabricated with a catalyst prepared from graphite, γ-MnO_2 and MoS_2 in a proportion of 20:1:1 fluctuated around the value of 95 mW/m^2, which is still much higher than those of MFCs catalysts prepared from graphite, γ-MnO_2 and MoS_2 in proportions of 30:1:2 (35 mW/m^2) and 30:2:1 (75 mW/m^2). This demonstrated that among the MFC fabricated with a catalysts prepared from different graphite, ß-MnO_2 and MoS_2 proportions, the MFC fabricated with a catalyst prepared from graphite, ß-MnO_2 and MoS_2in a proportion of 20:1:1 showed the highest power density.

The power density of MFC fabricated with a catalyst prepared from graphite, ß-MnO_2 in a proportion of 10:1 is 140 mW/m^2 on the 1^{st} day, which is better than those of MFC fabricated with a catalyst prepared from graphite, γ-MnO_2 and MoS_2 combinations. While the MFC fabricated with a catalyst prepared from graphite, ß-MnO_2 and MoS_2 in a proportion of 20:1:1 showed the power density of 165 mW/m^2 on the 1^{st} day, and fluctuated around the value of 142 mW/m^2, which is the highest among all the tested combinations. This observation agrees well with the results of power densities analysis described above (Fig. 6.7), which indicated that the

performance of crystallized ß-MnO_2 is much better than γ-MnO_2. However, it can also be observed that the power density of the MFC fabricated with a catalyst prepared from graphite, γ-MnO_2 and MoS_2 in a proportion of 20:1:1 with ultrasonic treatment possessed the highest power density only at the first 4 days. After 4 days, the power density became lower and possessed the value of 114 mW/m^2 on the 17^{th} day.

It can be observed in Fig. 6.7 that almost all the power densities with different catalysts have descended with time and fluctuated around a certain value. We used the mixture of graphite and MnO_2 with proportion of 10:1. The data suggested that because of the growth of microorganism, the power density increased rapidly at the beginning. However, the power density decreased and fluctuated around a value, which is lower than the highest value in the long term performance. This phenomenon could be attributed to both the degradation of microorganism on the anode side and deactivation of catalysts because of chemical reaction for a long time. This observation is in accordance with results obtained by Zhou et al.[80] They have developed a MFC stack and investigated the long term behavior of power density for 180 days. They showed that after 30 days, the power density decreased from 4 W/m^3 to 1.5 W/m^3 within 150 days, which was stable. The long term performances of the MFCs fabricated using catalysts prepared with the different graphite, γ-MnO_2 (ß-MnO_2) and MoS_2 proportions were decreased in the order of 20:1:1 (ß-MnO_2) > 20:1:1 (ultrasonic) >10:1 (ß-MnO_2) >20:1:1 (γ-MnO_2) > 30:2:1 (γ-MnO_2) >30:1:2 (γ-MnO_2).

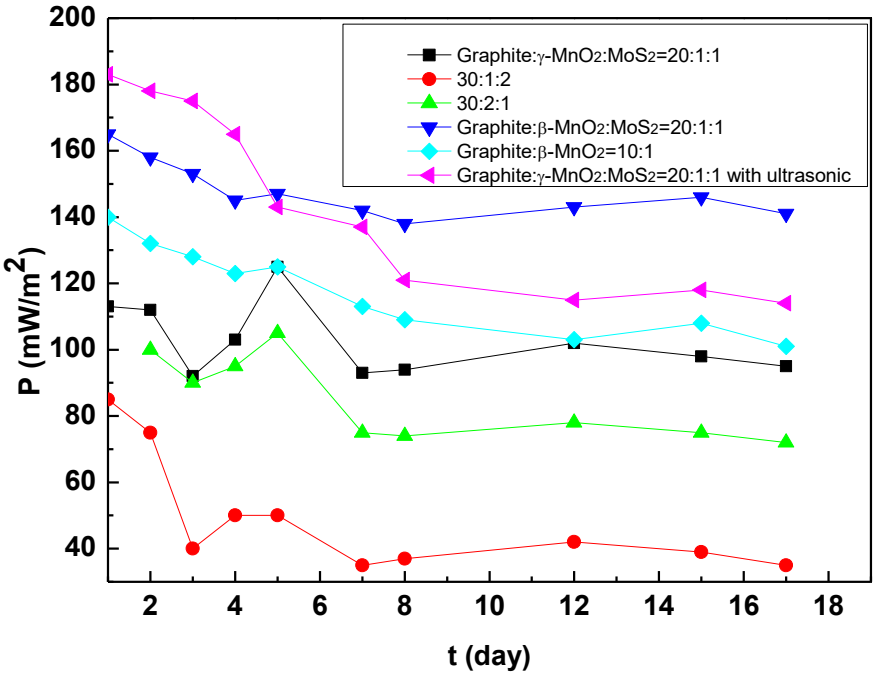

Fig. 6.7: Long term performances of MFCs with cathodes based on the catalysts prepared using graphite, ß-MnO_2 (γ-MnO_2) and MoS_2 in different proportions

6.3 Conclusions

Mixtures of graphite, γ-MnO_2 and MoS_2 at different weight proportions (20:1:1, 30:1:2 and 30:2:1) were prepared and used as oxygen reduction catalysts in MFCs. To further investigate the effect of different MnO_2 morphologies on the MFC performance, ß-MnO_2 with a whisker structure was also prepared. It was observed that among the graphite, γ-MnO_2 and MoS_2 combinations, the MFC fabricated with the catalyst prepared from graphite, γ-MnO_2 and MoS_2 in a proportion of 20:1:1 possessed the highest optimal power density of 120 mW/m^2, which was two times the optimal power of the MFCs fabricated using the catalysts prepared with graphite, γ-MnO_2 and MoS_2 in proportions of 30:1:2 and 30:2:1. When compared with the graphite, γ-MnO_2 and MoS_2 combination, the optimal power density of the MFC fabricated with a catalyst

prepared using graphite, ß-MnO_2 and MoS_2 in a proportion of 20:1:1 was higher (158 mW/m^2), showing that the performance of ß-MnO_2 with a whisker structure was much better than that of γ-MnO_2 owing to its higher surface area, larger pore diameter and great pore volume. Furthermore, the ß-MnO_2 possessed a higher oxidation state than γ-MnO_2, which is also an important reason for better performance of ß-MnO_2.

For long term performance, the MFC fabricated using the catalyst prepared with graphite, ß-MnO_2 and MoS_2 in a proportion of 20:1:1 possessed a power density of 165 mW/m^2 on the 1st day, which fluctuated at ~142 mW/m^2 and was the highest among all the combinations tested. This observation agrees well with the power density analysis described previously (Fig.8), which indicates that the performance of crystallized ß-MnO_2 was much better than γ-MnO_2. The long term performances of the MFCs fabricated using catalysts prepared with the different graphite, γ-MnO_2 (ß-MnO_2) and MoS_2 proportions were decreased in the order of 20:1:1 (ß-MnO_2) > 20:1:1 (ultrasonic) > 10:1 (ß-MnO_2)>20:1:1 (γ-MnO_2) > 30:2:1 (γ-MnO_2) > 30:1:2 (γ-MnO_2). This reveals that the catalyst prepared using graphite, ß-MnO_2 and MoS_2 in a proportion of 20:1:1 was optimal. In order to make a precise comparison of other catalysts with MnO_2 and MoS_2, we developed Co_3O_4 catalysts with different support materials in the next chapter.

7 Graphite plus Co_3O_4 paints as oxygen reduction cathode catalyst of MFC by using different forms of TiO_2

7.1 Experimental

7.1.1 Synthesis of Co_3O_4 catalyst

Cobalt oxide is known to be a good oxidation catalyst. In this research, two TiO_2 materials of different morphologies, anatase TiO_2 whiskers (TiO_2-W) and anatase TiO_2 nano particles (TiO_2-A), were used as supports to synthesize supported Co_3O_4 catalysts for the cathode. The TiO_2-W was synthesized following the procedure as described in the literature[81], while the TiO_2-A was purchased from Cofermin Chemicals GmbH, Germany. Firstly, 4 g of TiO_2 support was added into 100 mL of $Co(NO_3)_2$ solution (8 wt%) and impregnated for 24 h at room temperature. After filtrated and dried at 80 ^oC, the solid was calcined at 350 ^oC for 2 h. The obtained catalysts are denoted as Co_3O_4/TiO_2-W (whiskers TiO_2) and Co_3O_4/TiO_2-A (anatase TiO_2), respectively. The as-prepared Co_3O_4/TiO_2-W and Co_3O_4/TiO_2-A, which were treated under ultrasonic for 30 min, are denoted as Co_3O_4/TiO_2-W-U and Co_3O_4/TiO_2-A-U, respectively. The synthesized four kinds of catalysts are characterized by XRD, BET and SEM.

7.1.2 Preparation of cathode with Co_3O_4 catalyst

Graphite and each of the as prepared four Co_3O_4 catalysts was mixed with the weight proportion of 10:1, respectively. As a polymer binder a solution made of 150 mL butanone and 7.5 g celluloid (taken from table tennis balls) was produced. The polymer binder was produced according to our previous publication[5]. It may be that the use of celluloid from table tennis balls seems unusual, but the advantage is that this material is highly flexible and contains no additives which could be

harmful for the environment. In addition the properties (like flexibility) are well regulated by international sports regulations. Therefore, the reproducibility is guaranteed. The mixture of Co_3O_4 catalyst and graphite is added into the celluloid butanone solution. The 80 mL binder solution was mixed with 17.6 g of graphite catalyst mixture. The components were chosen considering the aspect that no poisonous materials should be used in a water treatment plant. Coating can be done by hand with a paintbrush or an automated spraying machine. In our research, the catalysts are coated by use of a manual paintbrush on the surface of the cathode with an average loading ratio of 0.16 g (catalyst)/g (cathode). 1.4301 AISI 304 stainless steel meshes (w_{mesh} = 1.8 mm, d_{wire} = 0.32 mm) by Spörl KG Präzisionsdrahtweberei Corporation (Germany) with dimension of 150 mm × 150 mm are used as cathodes.

7.2. Results and Discussion

7.2.1 Characterization of supports and catalysts

XRD patterns were used to identify the crystalline phases of the supports and catalysts (Fig. 7.1). As can be seen from Fig. 7.1(a) that the samples showed clear TiO_2 peaks at 2θ = 25.2°, 37.8°, 48.0°, and 55.0°, which confirmed that TiO_2-A and TiO_2-w are both of anatase TiO_2 phase. After loading Co_3O_4, the peaks TiO_2 are broadened for all the sample and the peaks of Co_3O_4 can be seen at 2θ = 36.9° and 65.2°, showing that Co_3O_4 phase are formed on surface of the samples. The crystalline phases are remained unchanged after U treatment.

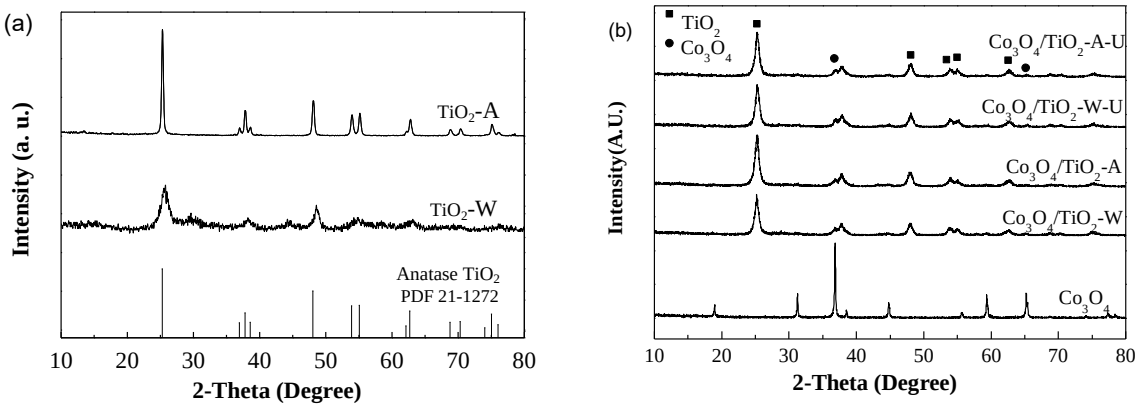

Fig. 7.1: The XRD patterns of supports (a) catalysts (b)

Fig. 7.2 illustrates the morphology of the supports and as-prepared Co_3O_4 catalysts. It can be observed from Fig. 7.2 that the TiO_2-A showed uniform small particles with diameters of 50 nm. The morphology of the Co_3O_4/TiO_2-A catalyst was similar to that of TiO_2-A (Fig. 7.2(a)). The TiO_2-W catalyst (Fig. 7.2(b)) clearly shows the TiO_2 structure appearing as whiskers, with a diameter about 150 nm. However, the whiskers structure of support was broken and aggregated after loading of Co_3O_4 (Fig. 7.2(b)). Comparing with Co_3O_4/TiO_2-A, the Co_3O_4/TiO_2-A-U shows a higher surface, which is shown in Fig. 7.2(c). The similar phenomenon is also observed in Co_3O_4/TiO_2-W-U (Fig. 7.2(d)). However, the whisker structure of support is damaged after U treatment.

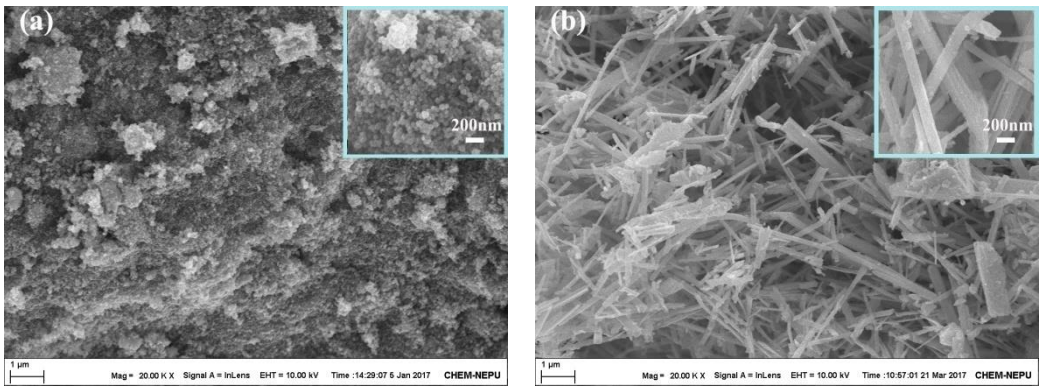

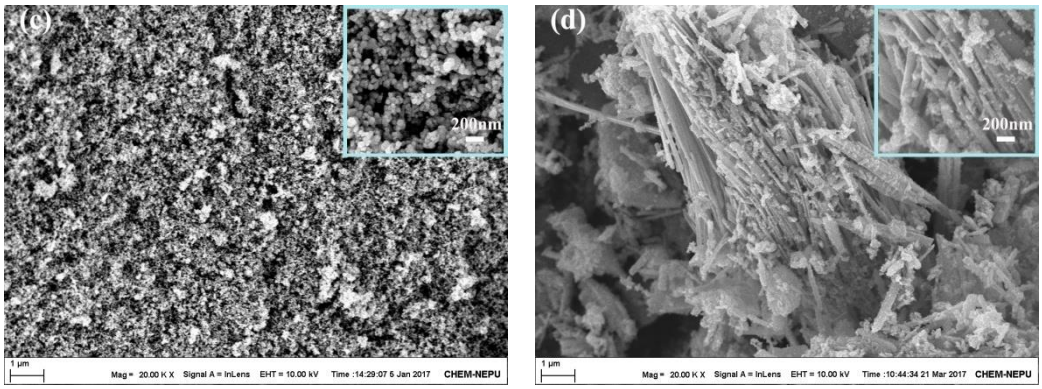

Fig 7.2: The morphology of as-prepared catalysts; (a) Co_3O_4/TiO_2-A and TiO_2-A, (b) Co_3O_4/TiO_2-W and TiO_2-W, (c) Co_3O_4/TiO_2-A-U, (d) Co_3O_4/TiO_2-W-U

Table 7.1 illustrates the BET measurement of the supports and as-prepared Co_3O_4 catalysts. It can be observed from Table 1 that as compared to TiO_2-A (70.0 $m^2 \cdot g^{-1}$), the TiO_2-W possessed higher surface area (S_{BET}) of 85.9 $m^2 \cdot g^{-1}$ with larger pore volume and pore size. Upon loading Co_3O_4, S_{BET} of both supports decreased. The Co_3O_4/TiO_2-W (77.8 $m^2 \cdot g^{-1}$) shows higher S_{BET} than that of Co_3O_4/TiO_2-A (60.9 $m^2 \cdot g^{-1}$), which is understandable, because the pore structure of TiO_2-W is better than that of TiO_2-A. Upon U treatment, the S_{BET} of Co_3O_4/TiO_2-A increased, in contrast, the S_{BET} of Co_3O_4/TiO_2-W decreased. This complies with the results of SEM, which shows that the morphology of TiO_2 whiskers damaged badly under the U treatment. Comparing with the Co_3O_4/TiO_2-A-U, the Co_3O_4/TiO_2-W-U possesses a relatively low surface, which may have a negative influence on its performance.

Table 7.1: Pore properties and Co content of catalysts

Sample	S_{BET} ($m^2 \cdot g^{-1}$)	V_p ($cm^3 \cdot g^{-1}$)	d (nm)	Surface Co content (wt%)
TiO_2-A	70.0	0.241	13.5	
TiO_2-W	85.9	0.400	18.3	
Co_3O_4/TiO_2-A	60.9	0.231	14.1	13.0

Co_3O_4/TiO_2-W	77.8	0.323	15.9	4.2
Co_3O_4/TiO_2-A-U	72.3	0.229	12.4	2.8
Co_3O_4/TiO_2-W-U	70.6	0.302	15.2	1.8

Fig. 7.3 illustrates the Co 2p3/2 spectra of Co_3O_4/TiO_2-W, Co_3O_4/TiO_2-A, Co_3O_4/TiO_2-W-U and Co_3O_4/TiO_2-A-U catalysts. The XPS patterns of all the samples show two peaks at 78.6.1 eV and 779.4 eV and the shake–up satellite. The small peak at 786.1 eV can be attributed to Co^{2+} species, while the big peak at 779.4 eV can be attributed to Co^{3+} species, showing that the Co_3O_4 is the predominant phase for all the samples. The surface mass contents of Co species are listed in Table 7.1 (Column 5). It can be seen that the surface Co contents of Co_3O_4/TiO_2-A (13.0 wt%) is much higher than the bulk theoretical Co content of 8wt%, showing most of the Co species are located on outer surface. In contrast, the Co content on surface of Co_3O_4/TiO_2-W (4.2 wt%) is much lower than the bulk theoretical Co content of 8wt%, showing most of the Co species are located in inner surface of pore. This means a better dispersion of active Co_3O_4 phase is achieved for Co_3O_4/TiO_2-W, which may have a positive influence on its performance. This can be explained with the large pore size of TiO_2-W support (18.3 nm) since large pore possesses a potential advantage of making the Co species inter into the inner pore. The higher surface area and larger pore volume as compared with TiO_2-A (Table 7.1) are another reason for the better dispersion. Upon U treatment, the surface Co contents are both decreased to a lower level, showing a better dispersion of Co_3O_4 is reached for both catalysts.

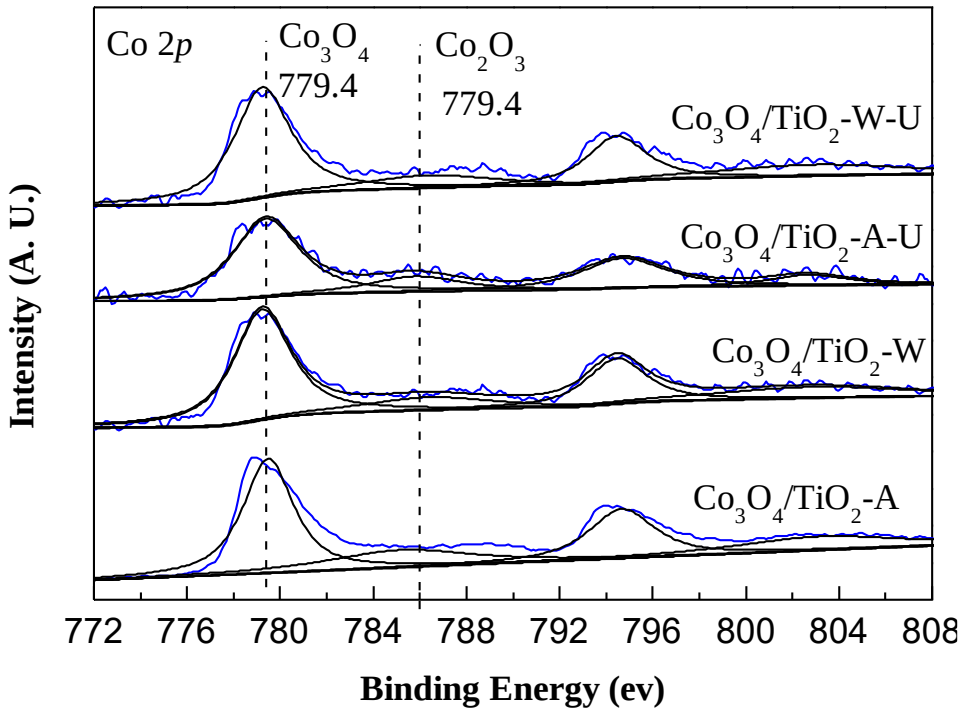

Fig. 7.3: The Co 2p3/2 spectra for as-prepared catalysts

7.2.2 Performance of Co_3O_4 catalysts with different supports

Fig. 7.4 shows the results of power density and single electrode potential measurement. The data (Fig. 7.4(up)) suggested that the Co_3O_4/TiO_2-W catalyst (101 mW/m^2) shows a higher performance than Co_3O_4/TiO_2-A catalyst (62 mW/m^2). This is possibly because a better dispersion of active Co_3O_4 phase is achieved for Co_3O_4/TiO_2-W than Co_3O_4/TiO_2-A (XPS analysis), showing that the dispersion of active Co_3O_4 phase plays an important role. The power density of MFC with Co_3O_4/TiO_2-A-U catalyst is 132 mW/m^2. Upon U treatment, the power density is increased by 70 mW/m^2. A similar phenomenon is also observed for MFC with Co_3O_4/TiO_2-W-U catalyst (135 mW/m^2). As it is described in discussion of Fig. 7.3, this is possibly because most of the Co species are located in inner surface of the supports and a better dispersion of active Co_3O_4 phase on surface of catalyst could be achieved after U treatment. It should be noted that after U treatment the power densities of Co_3O_4/TiO_2-A and Co_3O_4/TiO_2-W

have the basically same values. This is understandable, because the surface Co contents are both decreased to a very low level (Table 7.1), showing a similar better dispersion of Co_3O_4 is reached for both catalysts after U treatment. The damage of whiskers structure of TiO_2-W during U treatment is another reason for this result. It can be seen in Fig. 7.4(down) that the cathode potential of the cell descended much slower with Co_3O_4/TiO_2-W-U and Co_3O_4/TiO_2-A-U than corresponding Co_3O_4/TiO_2-W and Co_3O_4/TiO_2-A. This reveals that the performance of the cathode can be improved by U treatment during catalyst preparation because of the improvement of the dispersion of Co_3O_4 phase. However, it can be seen that the potential of the cathode still descended significantly, while the potential of anode ascended only slightly. Therefore, new forms of cathode should be further developed to improve the performance of MFC.

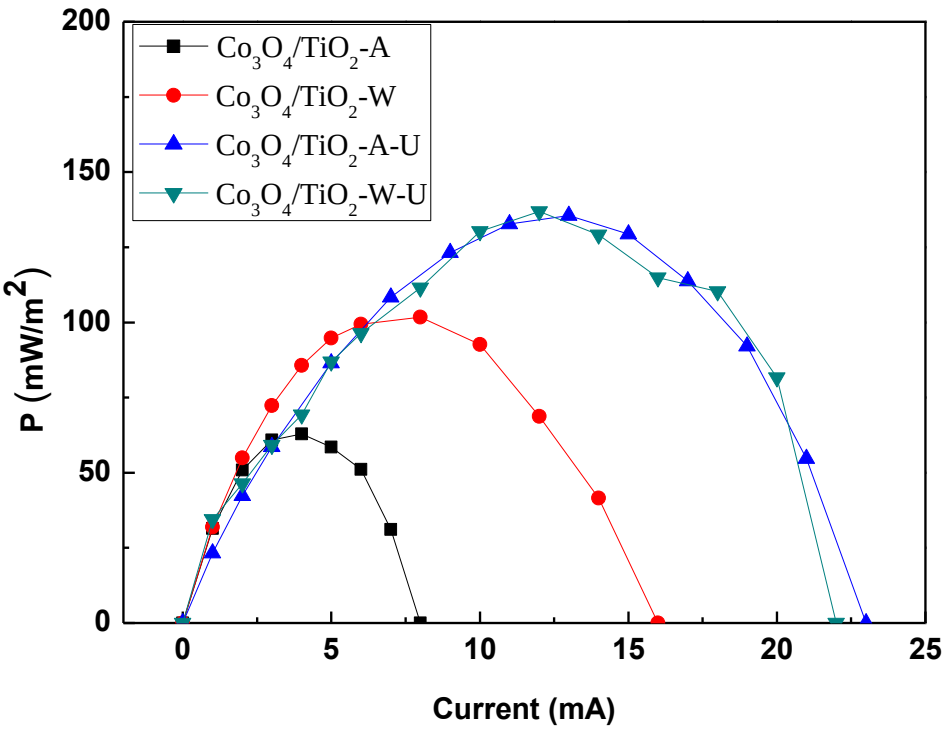

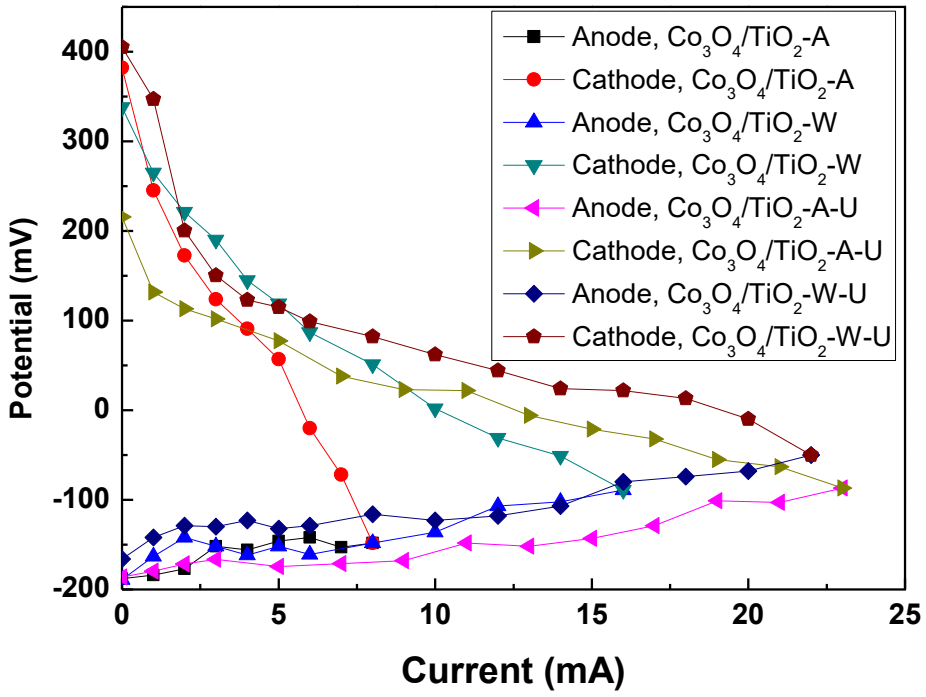

Fig. 7.4: Power densities of MFCs with cathodes based on the combination of graphite and Co_3O_4 with different supports as indicated (up) and the corresponding potential measurement (down).

7.2.3 Elemental analysis

The EDS analysis of catalyst after chemical reaction was studied. The Co_3O_4/TiO_2-A and Co_3O_4/TiO_2-A-U were taken as examples. The surface atomic elements of Co_3O_4/TiO_2-A and Co_3O_4/TiO_2-A-U by EDS analysis and the atomic compositions are listed in Table 7.2.

Table 7.2: The atomic compositions of different ACN-211 samples

Sample	C-K (%)	O-K(%)	N-K (%)	Na-K (%)	P-K (%)	Ti-K (%)
Co_3O_4/TiO_2-A	63.7	22	13.9	0.1	0.1	
Co_3O_4/TiO_2-A-U	99.9					0.1

7.3 Conclusions

The two different structures of TiO_2 (TiO_2-W and TiO_2-A) supported Co_3O_4 catalysts for cathode were synthesized and studied. The XRD results showed that the crystalline phases are remained unchanged after Co_3O_4 loading and successive U treatment. As compared to TiO_2-A (70.0 $m^2 \cdot g^{-1}$), the TiO_2-W possessed a higher surface area 85.9 $m^2 \cdot g^{-1}$ with a larger pore volume, especially a larger pore size (18 nm), which would have a potential advantage of making the Co species inter into inner pore, and thus to achieve a better dispersion of the active phase. This conclusion is further confirmed by the surface metal contents obtained from XPS analysis. The Co_3O_4/TiO_2-W possesses a higher surface area when compared to Co_3O_4/TiO_2-A. However, the whisker structure of TiO_2-W is damaged under U treatment (SEM analysis) and therefore, a decrease in surface area is observed for Co_3O_4/TiO_2-W-U. The XPS results showed that for Co_3O_4/TiO_2-A, most of the Co species are located on outer surface, showing a poor dispersion of Co_3O_4. While for Co_3O_4/TiO_2-W (supported on TiO_2-W with large pore size), most of the Co species are located on inner surface, showing a better dispersion of Co_3O_4 have achieved. As compared to Co_3O_4/TiO_2-A catalyst (62 mW/m^2), the Co_3O_4/TiO_2-W catalyst shows a higher power density of 101 mW/m^2. This can be attributed to its better dispersion of active Co_3O_4 phase, showing that dispersion of Co_3O_4 on surface of catalysts plays an important role. The power density of MFC with Co_3O_4/TiO_2-A-U catalyst is 132 mW/m^2. Upon U treatment, the power density is increased by 70 mW/m^2. A similar phenomenon is also observed for MFC with Co_3O_4/ TiO_2-W-U catalyst (135 mW/m^2). The main reason for this is that U treatment can improve the dispersion of the active Co species on catalyst surface. It is also observed that a tiny difference of power density between Co_3O_4/TiO_2-A-U and Co_3O_4/TiO_2-W-U were observed, whose main reason is a better dispersion of Co_3O_4 is reached for both catalysts after U treatment and the whiskers structure of TiO_2-W is damaged during U treatment. In conclusion, the large pore size of TiO_2-W and U treatment are both beneficial to achieve a better dispersion of active Co_3O_4, which could improve performance

of catalysts. It can be concluded that the Co_3O_4 was not better than MnO_2. Furthermore, the precursor of Co_3O_4, which is $Co(NO_3)_2$, possessed also a relatively high price. Because of this reason, we developed Co_3O_4 with nanorod structure as ORR catalyst of MFC.

8 Co_3O_4 as catalyst of MFC

For further study of Co_3O_4 catalyst performance, Co_3O_4 nanorods with different calcination temperatures (300 °C, 400 °C, 500 °C, 550 °C and 600 °C) were tried to synthesiz according to the method of Kumar et al.[79] It was planned to investigate the effect of calcination temperature on performance of catalysts. In which 3 g $CoCl_2$ and 0.15 g $CO(NH_2)_2$ were mixed in 100 mL distilled water. The mixture was then dried at 100 °C for 24 h. After drying for 24 h, the catalysts were treated with different temperatures, which are mentioned above.

8.1 Characterization of Co_3O_4 catalysts

The SEM images of Co_3O_4 nanorod catalysts with different calcination temperatures are shown in Fig. 8.1. It can be observed in Fig. 8.1 that the Co3O4 catalyst did not possess the form of nanorod as it is described in literature [79].

The Co_3O_4 catalyst with calcination temperature of 300 °C (Fig. 8.1 (a)) possesses a relatively low surface area, which can be confirmed by the dimension of particles in this image. With rising calcination temperature, this dimension became smaller, which results in a larger reaction surface (Fig. 8.1 (b) to (d)). However, agglomeration of particles with small dimensions is observed when the calcination temperature reaches 600 °C (Fig. 8.1 (e)), which may have a negative influence on the performance of the catalysts.

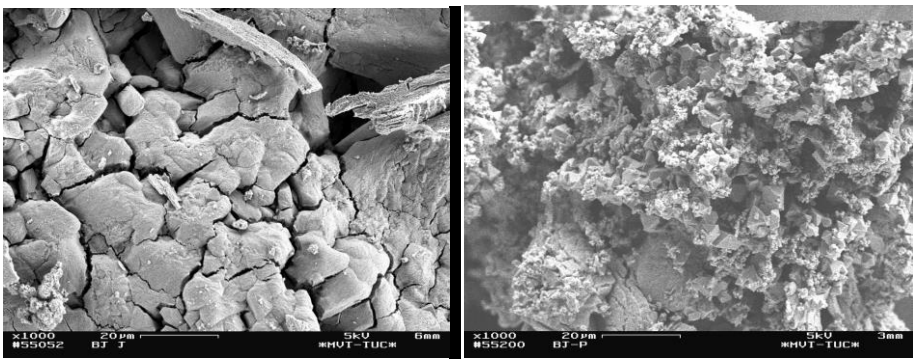

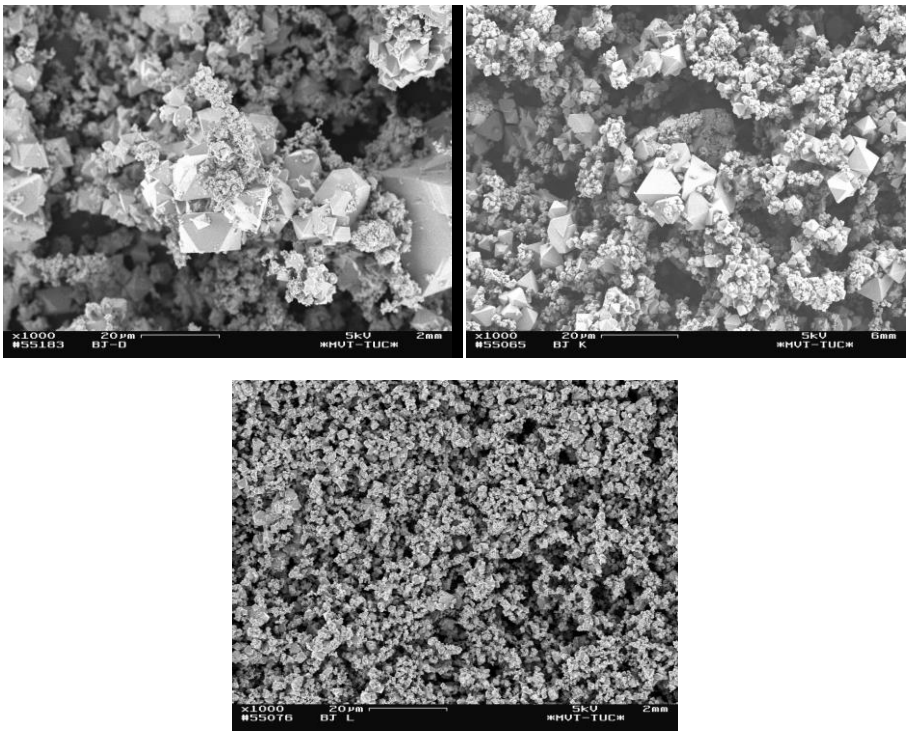

Fig. 8.1: SEM images of Co_3O_4 catalysts (a) 300 °C, (b) 400 °C, (c) 500 °C, (d)550 °C, (e) 600 °C calcination temperature

8.2 Performance of Co_3O_4 catalyst

Results in Fig. 8.2 (left) suggested that the Co_3O_4 nanorod catalyst with a calcination temperature of 550 °C shows a higher power density (128 mW/m^2) than the Co_3O_4 nanorods with a calcination temperature from 300 °C to 500 °C. Comparing with nanorods with calcination temperature of 600 °C (126 mW/m^2), the power density of the nanorod catalyst with a calcination temperature of 550 °C is also slightly higher. This reveals that 550 °C is the optimal calcination temperature for Co_3O_4 nanorods. A reversible hydrogen electrode (RHE) is also used in our experiments for measuring the potential of single electrodes. It can be seen in Fig 8.2 (right) that the cathode potential of Co_3O_4 nanorod catalyst with a calcination temperature of 550 °C descended slower than the Co_3O_4 nanorods with other calcination temperatures during the measurement. This reveals that the performance of a cathode can be improved by calcinating

Co_3O_4 nanorods with a temperature of 550 °C during catalyst preparation. However, it can be seen that the potential of the cathodes still descended significantly with increase of current, while the potential of anode ascended only slightly. Therefore, new cathode catalysts should be further developed for improving the performance of MFC.

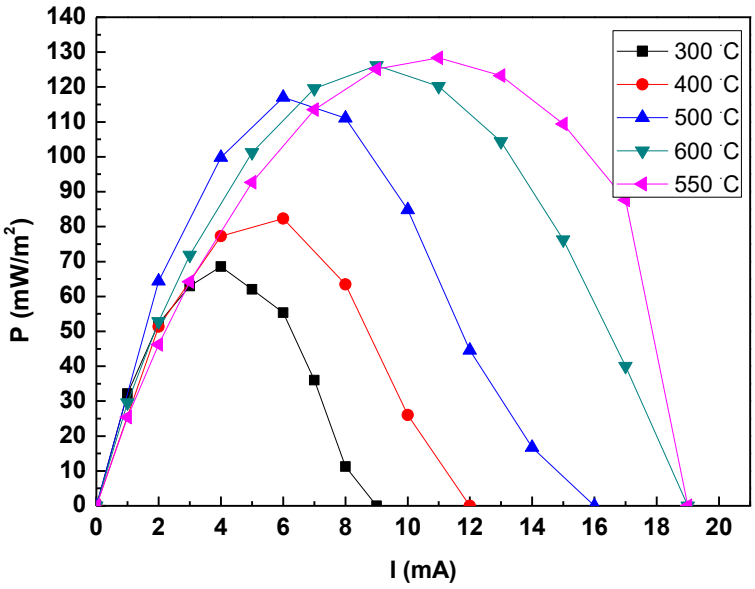

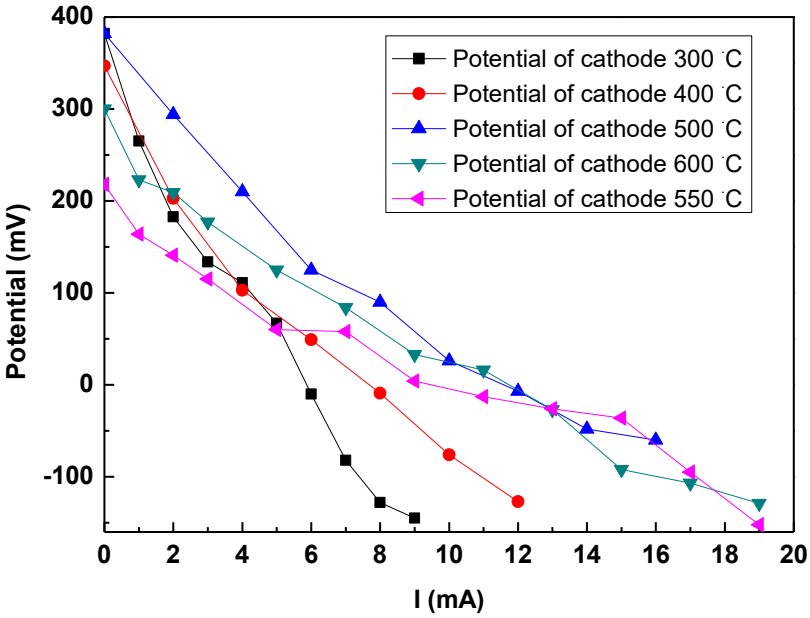

Fig. 8.2: Power densities of MFCs with cathodes based on the Co_3O_4 nanorods with different calcination temperatures as indicated (up) and the corresponding potential measurement (down) for cathode

8.3 Conclusions

Co_3O_4 catalysts on supports is a catalyst well suited for the cathode of a MFC. The power densities of the MFCs increased rapidly and reached relatively high values. For calcination temperature, 550 °C is optimal for Co_3O_4 nanorods, with which the power density reached 128 mW/m^2. Agglomeration of particles is observed when the calcination temperature reaches 600 °C, which resulted in a negative influence on the performance of the catalysts. As cobalt oxide catalysts in this study did not perform much better in MFCs and cobalt is higher in price for further studies MnO_2 MoS_2 combinations were used. Therefore, during the scaling up of MFC, the MnO_2 was used as ORR catalyst for larger MFCs.

9 Scaling up of MFC for industrial use

The final constructed MFC for industrious application possessed three anode plates with dimension of 700 mm × 150 mm× 7 mm (single anode plate), which are parallel constructed. Comparing with the electrodes that are mentioned above, the parallel constructed anode plates possessed no channels. A frame is used as anode chamber, in which three anode plates are inserted. The anode plates and cell construction are shown in Fig. 9.1. Like the MFCs which are constructed in the former phase, ion-exchange membranes and stainless steel cathodes with catalyst on the surface are built on both side of anode chamber. A wastewater treatment tank with a volume of 5 m^3 was built for industrial use.

Fig. 9.1: Parallel constructed anode plates for industrial application

9.1 Conductivity measurement of anode plates

Since the voltage of MFCs was rather low under load conditions, attempts were made to improve electrode plates' conductivity by copper inserts. Plates were provided by Eisenhuth corporation,

Osterode, Germany. For optimization of anode plate performance, different anode plates with same dimension are constructed for first version of scaled up MFCs. To improve the conductivity of anode plate, anode plates with copper are constructed, which is shown in Fig 9.2. To study the influence of copper on conductivity of anode plate, the electrical resistances of more 900 points on the anode plate is measured by a conductivity measuring apparatus which is shown in Fig 9.3.

Fig. 9.2: Anode plate with (left) and without copper (right)

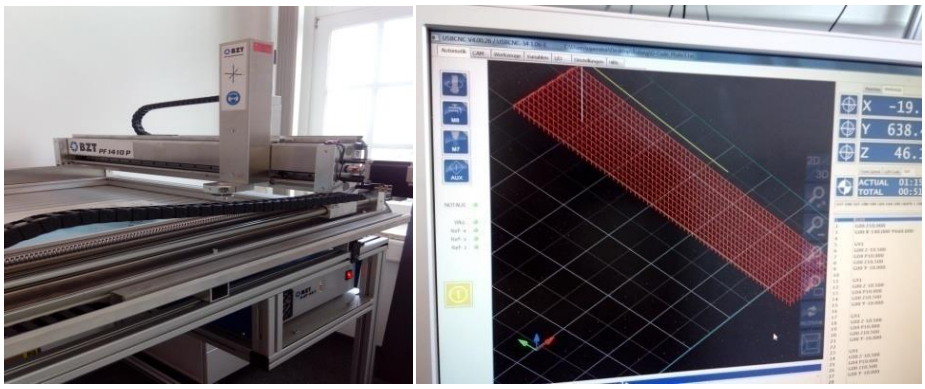

Fig. 9.3: Facility for measuring conductivity of anode plate (left) and its operation system (right)

To compare the conductivities of electrode plates in electrolyte, the saturated solution of NaCl was prepared. The anode plate and a copper plate are put into the solution simultaneously and the resistance between anode plate and copper plate is measured. The construction of the measuring system is shown as follows.

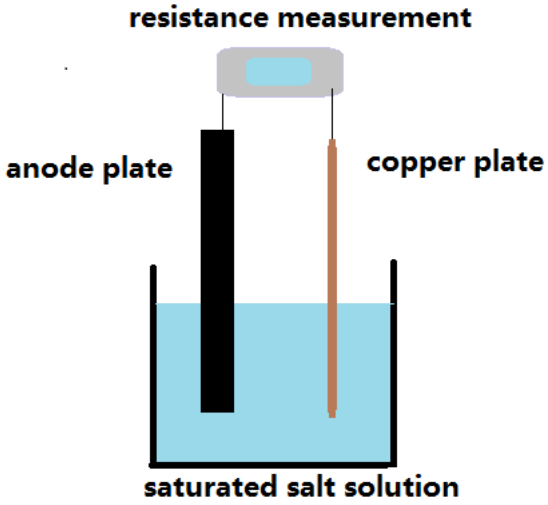

Fig. 9.4: Measurement of resistance between anode plate and copper plate in salt solution

9.2 Results of conductivity measurement

Fig. 9.5 shows the results of conductivity measurement of anode plates by adding copper inserts. A great difference of resistance can be observed in Fig. 9.5. Comparing with the value of anode plate with copper, whose resistance on surface is less than 0.06 Ω, the anode plate without copper possessed a significant higher value of resistance, some of which are more than 0.2 Ω, showing that copper has improved the conductivity of the anode plate.

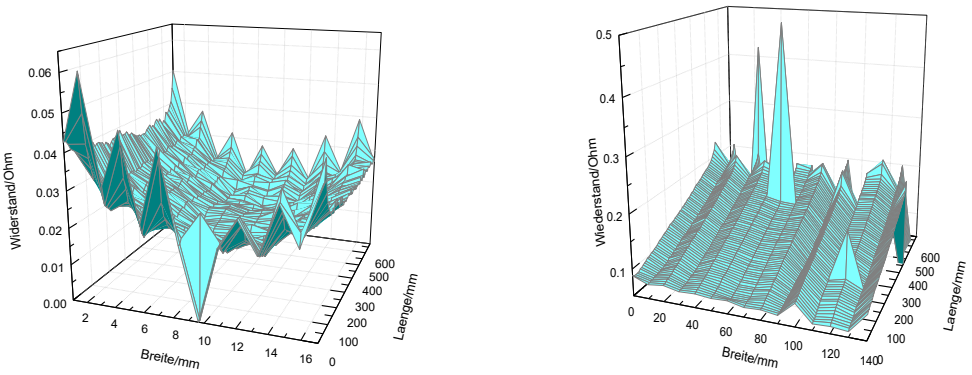

Fig. 9.5: Distribution of resistance on the surface of anode plate with copper (left) and without copper (right)

9.3 Coating process on the surface of cathode by using spray machine

Manual coating process, which is used for the cathode in former research phases, is usually slow and causes irregular distribution of catalyst on the surface of cathode, which is unbeneficial for cathodic reaction. Therefore, for coating process of cathode with larger reacting surface, it is necessary to use a certain facility to realize automation. One typical example of spray machine, which is used for coating process in the research, is shown in Fig. 9.6. The machine is operated by LabVIEW system. I wish to thank my colleague Thorben Muddemann for construction and programming the software of this machine and also for his help and the assistance of my colleague Dennis Haupt to prepare coated cathodes with this device.

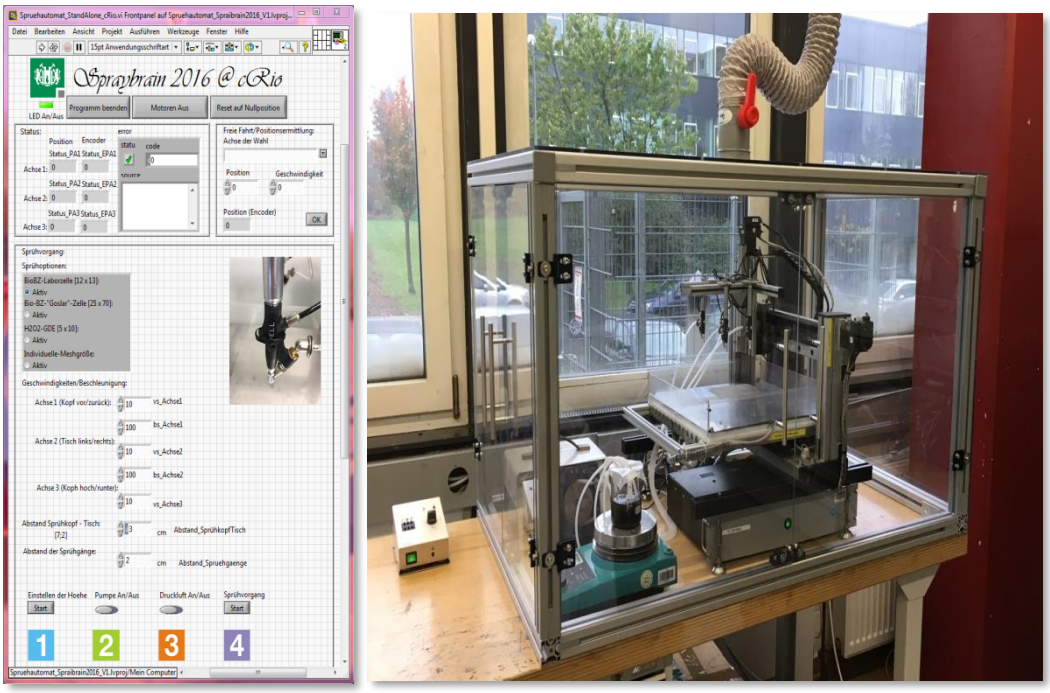

Fig. 9.6: The LabVIEW operating system of spray machine (left) and the construction of spray machine (right)

Fig. 9.7 shows the whole coating process by using the spray machine. The produced coating

material is homogenized by ball milling. Contemporarily, the stainless steel cathode is treated by spraying graphite on its surface. Instead of coating by hand, the coating material is than sprayed on the surface of the cathode. The influences of several variables on the performance of cathode are studied, which are spraying velocity, the distance between spraying jet and cathode plate, spraying pressure, flowing rate of suspension and temperature of the spraying process.

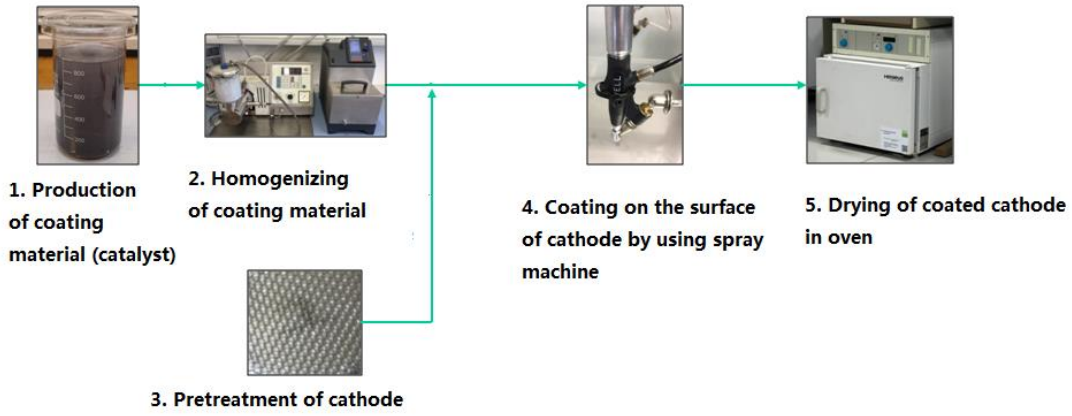

Fig.9.7: Coating process on the surface cathode by using spray machine

According to the results showed in conductivity measurement, new forms of anode plate were constructed with copper strip, which was convenient to connect with operation system. Stainless steel cathodes were coated by spray machine and built with anode together. Furthermore, different MFC constructions were also conducted at the end of our research, whose main difference is the sequence of electrodes and membranes (cathode + membrane + anode + membrane + cathode and anode + membrane + cathode + membrane + anode). The MFC with two cathodes were submerged into tap water with sparged air, while the MFC with two anodes were submerged directly into wastewater. It is planned to build 50 MFCs for commercial wastewater treatment at the end of our project. The typical example of scaled up MFC and wastewater treatment tank are shown in Fig. 9.8. However, in order to obtain a relatively high power density, these MFC need longer time to start up.

Fig. 9.8: Construction of scaled up MFCs (left) and scaled up MFCs in wastewater treatment tank (right)

10 Summary

This work focussed mainly on developing ORR catalysts to improve the performance of MFC. In the first phase of this study, different types of ORR catalysts such as carbon fiber (ACN and GFD), MnO_2, MoS_2, Co_3O_4 (with brookite, anatase and active carbon as carriers) and novel catholyte (potassium ferrocyanide) as well as scaling up of MFC was investigated.

During the long term performance measurement for $K_3Fe(CN)_6$, the power density increased with time firstly and then increased slightly after 10^{th} day. A high power density of 1020 mW/m^2 is achieved at 10^{th} day. The best performance of breaking current is achieved at 25^{th} day, whose value reached 45 mA, showing that the performance of MFC can be improved by adding $K_3Fe(CN)_6$ to cathode solution continuously.

Different carbon felts (ACN and GFD) were treated by Fenton's reagent and by thermal modification, respectively. For the Fenton's reagent treated GFD-*x*, the MFC with GFD-100 exhibited the best performance with optimal power density of 190 mW/m^2. The optimal value decreased in the order: GFD-100 > GFD-150 > GFD-50 > GFD-0. Among the ACN-211-*x*, the MFC with ACN-211-150 exhibited the best performance with optimal power density of 450 mW/m^2. The thermal modification of ACN-211, which showed better performance, at different temperatures (300 °C, 400 °C and 450 °C) and times (2 h, 5 h and 10 h) were tested and the effects of treatment conditions on the performance of MFC were also studied. The MFC with ACN-211 treated under 400°C and 2 h exhibited the best performance of power density with the maximum value of 470 mW/m^2, which is higher than that of MFC with ACN-211 treated by Fenton's reagent.

For long term performance of MFCs with MnO_2 and MoS_2 catalysts, the MFC fabricated using the catalyst prepared with graphite, ß-MnO_2 and MoS_2 in a proportion of 20:1:1 possessed a power density of 165 mW/m^2 on the 1^{st} day, which fluctuated at ~142 mW/m^2 and was the highest among all the combinations tested. When compared with the graphite, γ-MnO_2 and MoS_2 combination, the optimal power density of the MFC fabricated with a catalyst prepared using graphite, ß-MnO_2 and MoS_2 in a proportion of 20:1:1 was higher (158 mW/m^2), showing that the

performance of ß-MnO_2 with a whisker structure was much better than that of γ-MnO_2 owing to its higher surface area, larger pore diameter and great pore volume. Furthermore, the ß-MnO_2 possessed a higher oxidation state than γ-MnO_2, which is also an important reason for better performance of ß-MnO_2.

As compared to Co_3O_4/TiO_2-A catalyst (62 mW/m^2), the Co_3O_4/TiO_2-W catalyst shows a higher power density of 101 mW/m^2. This can be attributed to its better dispersion of active Co_3O_4 phase, showing that dispersion of Co_3O_4 on the surface of the catalysts plays an important role. The power density of MFC with Co_3O_4/TiO_2-A-U catalyst is 132 mW/m^2. Upon U treatment, the power density is increased by 70 mW/m^2. A similar phenomenon is also observed for MFC with Co_3O_4/ TiO_2-W-U catalyst (135 mW/m^2). The main reason for this is that U treatment can improve the dispersion of the active Co species on the catalyst surface. A tiny difference of the power density between Co_3O_4/TiO_2-A-U and Co_3O_4/TiO_2-W-U was observed, whose main reason is a better dispersion of Co_3O_4. reached for both catalysts after U treatment. But the whiskers structure of TiO_2-W is damaged during U treatment.

The power densities of the MFCs with Co_3O_4 catalysts increased rapidly and reached relatively high values. A calcination temperature of 550 °C is optimal for Co_3O_4 catalysts, with which the power density reached 128 mW/m^2. Agglomeration of particles is observed when the calcination temperature reached 600 °C, which resulted in a negative influence on the performance of the catalysts. As MnO_2 based catalysts exhibited comparable power densities and showed better performance, therefore, during the scaling up of MFC, MnO_2 was used as ORR catalyst for larger MFCs.

Different scaled up MFC constructions were also conducted at the end of our research, whose main difference is the sequence of electrodes and membranes (cathode + membrane + anode + membrane + cathode and anode + membrane + cathode + membrane + anode). The MFC with two cathodes were submerged into tap water with sparged air, while the MFC with two anodes were submerged directly into wastewater. It is planned to build 50 MFCs for commercial wastewater treatment at the end of our project. However, in order to obtain a relatively high power density, these MFCs need longer time to start up, which in addition is influenced by low water

temperatures and a high dilution of the wastewater by a lot of rain and snow during the last months in the winter season in the Harz region.

With this work an important building block towards the way to large scale MFCs was achieved. Solid catalysts, a coating procedure and electrochemical evaluation of single electrodes and whole cells were developed. First steps for scale up these methods to a municipal wastewater treatment plant were done.

It should be mentioned, that this work contributed to “BioBZ-Die bio-elektrochemische Brennstoffzelle als Baustein einer energieerzeugenden Abwasserbehandlungsanlage” was awarded by the “German Sustainability Award 2018” (Deutscher Nachhaltigkeitspreis 2018). This award is one of the most important awards in this subject in Europe.

Publications

[1] Bolong Jiang, Thorben Muddemann, Ulrich Kunz, Hinnerk Bormann, Michael Niedermeiser, Dennis Haupt, Ottmar Schläfer and Michael Sievers: Evaluation of microbial fuel cells with graphite plus MnO_2 and MoS_2 paints as oxygen reduction cathode catalysts, J. Electrochem. Soc. 2017 164(3) H3083-H3090, dx.doi.org/10.1149/2.0131703jes

[2] Bolong Jiang, Thorben Muddemann, Ulrich Kunz, Hinnerk Bormann, Michael Niedermeiser, Dennis Haupt, Ottmar Schläfer and Michael Sievers: Effect of $K_3Fe(CN)_6$ on long-term electrochemical power output of four series stack MFCs. Int. J. Current Research, 2017, www.journalcra.com/sites/default/files/20442.pdf

[3] Bolong Jiang, Thorben Muddemann, Ulrich Kunz, Hinnerk Bormann, Michael Niedermeiser, Dennis Haupt, Ottmar Schläfer and Michael Sievers: Evaluation of microbial fuel cells with graphite plus Co_3O_4 paints as oxygen reduction cathode catalyst by using different forms of TiO_2. CEMEPE, 2017

[4] Jiang, B.; Muddemann, T.; Kunz, U.; Bormann, H.; Niedermeiser, M.; Haupt, D. R.; Schläfer, O.; Sievers, M.: Evaluation of Microbial Fuel Cells with Graphite/MnO_2 and MoS_2 Composite Oxygen Reduction Cathode Catalyst with Different Supports and Producing Methods, ECS Trans. 77 (11) (2017) 1043-1051, dx.doi.org/10.1149/07711.1043ecst

[5] Jiang, B.; Muddemann, T.; Kunz, U.; Niedermeiser, M.; Bormann, H; Haupt, D. R.; Schläfer, O.;Sievers, M.: Effects of Fenton's reagent and thermal modification on the electrochemical properties of graphite felt for microbial fuel cell, Res Chem Intermed (2017) doi.org/10.1007/s11164-017-3125-y

[6] Muddemann, T.; Haupt, D. R.; Gomes Silva e Silva, L.; Jiang, B.; Kunz, U.; Bormann, H.;

Niedermeiser, M.; Schläfer, O.; Sievers, M., Integration of Upscaled Microbial Fuel Cells in Real Municipal Sewage Plants, ECS Trans. 77 (11) (2017) 1053-1077, dx.doi.org/10.1149/07711.1053ecst

[7] Jiang, B.; Muddemann, T.; Kunz, U.; Gomes Silva e Silva, L.; Bormann, H.; Niedermeiser, M.; Haupt, D.; Schläfer, O.; Sievers, M., Graphite/MnO2 and MoS2 Composites Used as Catalysts in the Oxygen Reduction Cathode of Microbial Fuel Cells, J. Electrochem. Soc. Tech. 164 (14) (2017) E519-E524 dx.doi.org/10.1149/2.0801714jes

[8] Bolong Jiang, Thorben Muddemann, Ulrich Kunz, Dennis Haupt and Michael Sievers: Continuous Electricity Generation at high Power by Using Microbial Fuel Cells with Potassium Ferricyanide, SciRev, 2018, **Under review**

[9] Ulrich Kunz, Bolong Jiang, Ottmar Schläfer, Michael Sievers: Push-pull boost converters for low voltage power sources with output power capability of several 100 mW and easy power adjustment. Eingereicht bei IEEE ENERGY CONVERSION CONGRESS & EXPO, 2018

List of abbreviations

MFC	Microbial fuel cell
RHE	Reversible hydrogen electrode
REM	Reflection electron microscopy
W	Whiskers(brookite)
A	Anatase
U	Ultrasonic
ICVT	Institut für Chemische Verfahrenstechnik
CUTEC	Clausthaler Umwelttechnik Forschungszentrum
BMBF	Bundesministerium für Bildung und Forschung
PEM	Proton exchange membrane
PDMS	Polydimethylsiloxane
AFMBR	Anaerobic fluidized bed membrane bioreactor
ML-MFC	Membrane-less microbial fuel cell
ETC	Electron transport chain
PCR	Polymerase chain reaction
DGGE	Denaturing gradient gel electrophoresis
COD	Chemical oxygen demand
FPMFC	Flat plate MFC
ABMFC	Algae biofilm microgbial fuel cell
CE	Coulombic efficiency
ORR	Oxygen reduction reaction
MOF	Metal-organic framework
AC	Activated carbon
AAPyr	Aminoantipyrine

CNT	Carbon nanotube
GO	Graphite oxide
OMS	octahedral molecular sieve
MEC	Microbial electrolysis cell
MPPT	Maximum power point tracking
SMFC	Sediment microbial fuel cell
PMS	Power management system
BMFC	Benthic microbial fuel cells
SSC	Self-stratifying urine column

List of symbols

Constants

F	FARADAY-constant	96 485 C/mol
R	Universal gas constant	8.3145 J/(mol K)

Greece script

η_C	Coulombic efficiency	
η_E	Energy efficiency	
G	Gibbs'enthalpy	J/mol

Latin script

E_{max}	Maximum voltage of MFC	mV
R_a	Arithmetic mean roughness	µm
R_z	Average rough deepness	µm

References

[1] Kim, Y., Yamanaka, S., Nakajima A. and Ogawa T. “Novel Electro Thermodynamic Power Generation”. In: *Advanced Energy Materials* **5**(2015), 6-11. DOI: 10.1002/aenm.201401942.

[2] Straub, A.P., Yip, N.Y., Lin, S. and Lee J. “Harvesting low-grade heat energy using thermo-osmotic vapour transport through nanoporous membranes”. In:*Nature Energy* **1**(2016), 16090-16095. DOI: 10.1038/NENERGY.2016.90.

[3] Carati, A., Marino, M. and Brogioli, D. “Thermodynamic study of a distiller-electrochemical cell system for energy production from low temperature heat sources”. In: *Energy* **93**(2015), 984-993. DOI: 10.1016/j.energy.2015.09.108.

[4] Niu, X., Yu, J.L. and Wang, S.Z. “Experimental study on low-temperature waste heat thermoelectric generator”. In: *Journal of Power Sources* **188**(2009), 621-626. DOI: 10.1016/j.jpowsour.2008.12.067.

[5] Jiang, B., Muddemann, T., Kunz, U., Bormann, H., Niedermeiser, M., Haupt, D. and Sievers M. “Evaluation of microbial fuel cells with graphite plus MnO_2 and MoS_2 paints as oxygen reduction cathode catalyst”. In: *Journal of Electrochemical Society* **164**(2016), H3083-H3090. DOI: 10.1149/2.0131703jes.

[6] Rathore, D., Nizami, A.S., Sing A. and Pant, D. “Key issues in estimating energy and greenhouse gas savings of biofuels: challenges and perspectives”. In: *Biofuel Research Journal* **3** (2016), 380-393. DOI: 10.18331/BRJ2016.3.2.3.

[7] Zhang, X., He, W., Ren, L., Stager, J., Evans, P.J. and Logan, B.E. “COD removal characteristics in air-cathode microbial fuel cells”. In: *Bioresource Technology* **176**(2015), 23-31. DOI: 10.1016/j.biortech.2014.11.001.

[8] Beenish, S., Christy, A.D., Yu, Z. and Anne, C. “Sustainable power generation from bacterio-algal microbial fuel cells (MFCs): An overview”. In: *Renewable and Sustainable Energy Reviews* **73**(2017), 75-84. DOI: 10.1016/j.rser.2017.01.115.

[9] Yuan, H., Hou, Y., Reesh, I.M.A., Chen, J. and He, Z. “Oxygen reduction reaction catalysts used

in microbial fuel cells for energy-efficient wastewater treatment: a review". In: *Materials Horizons* **3**(2016), 382-401. DOI: 10.1039/C6MH00093B.

[10] Zhang, L., Liu, C., Zhuang, L., Li, W., Zhou, S., and Zhang J. "Manganese dioxide as an alternative cathodic catalyst to platinum in microbial fuel cells". In: *Biosensors and Bioelectronics* **24**(2009), 2825-2829. DOI: 10.1016/j.bios.2009.02.010.

[11] Chouler, J., Bentleya, I., Vaza, F., Annabel, O.F., Cameron, P.J. and Lorenzo, M.D. "Exploring the use of cost-effective membrane materials for Microbial Fuel Cell based sensors". In: *Electrochimica Acta* **231**(2017), 319–326. DOI: 10.1016/j.electacta.2017.01.195.

[12] Liu, J., Zhang, F., He, W., Zhang, X., Feng, Y. and Logan B.E. "Intermittent contact of fluidized anode particles containing exoelectrogenic biofilms for continuous power generation in microbial fuel cells". In: *Journal of Power Sources* **261**(2014), 278–284. DOI: 10.1016/j.jpowsour.2014.03.071.

[13] Ren, L., Y. Ahn, Y., Logan, B.E. "A Two-Stage Microbial Fuel Cell and Anaerobic Fluidized Bed Membrane Bioreactor (MFC-AFMBR) System for Effective Domestic Wastewater Treatment". In: *Environmental Science & Technology* **48**(2014), 4199−4206. **DOI:** 10.1021/es500737m.

[14] Thung, W.E., Ong, S.A., Ho, L.N., Wong, Y.S., Ridwan, F., Oon, Y.L., Oon Y.S. and Lehl H.K. "Sustainable green technology on wastewater treatment: The evaluation of enhanced single chambered up-flow membrane-less microbial fuel cell". In: *Journal of Environmental Sciences* **66**(2018), 295-330. DOI: 10.1016/j.jes.2017.05.010.

[15] Logan, B.E. "Microbial Fuel Cells." Wiley-Interscience, 2008. ISBN: 0470239484.

[16] Li, Z., Tao, H., Liang, M., Li, W., Xue, A. "Dioscin Production Wastewater Treatment by Two -Chamber Microbial Fuel Cells with Different Inoculation." In: *Research of Environmental Sciences* **4**(2009), 462-467.

[17] Sun, Y., Zuo, J., Cui, L. and Dang. Y. "Analysis of microbial diversity in microbial fuel cells under different wastewater." In: *China Environmental Science*, **28**(2008), 1068-1073.

[18] Lin, C., Wu, C., Huang, W. and Tsai, S. "Evaluation of different cell-immobilization

strategies for simultaneous distillery wastewater treatment and electricity generation in microbial fuel cells". In: *Fuel* **144**(2015), 1–8. DOI: 10.1016/j.fuel.2014.12.009.

[19] Katz, E. and Willner, I. "A Biofuel Cell with Electrochemically Switchable and Tunable Power Output". In: *Journal of American Chemical Society* **125**(2003), 6803-6813. DOI:10.1021/ja034008v.

[20] Mano, N., Mao, F. and Heller, A. "Characteristics of a Miniature Compartment-less Glucose-O_2 Biofuel Cell and Its Operation in a Living Plant". In: *Journal of American Chemical Society* **124**(2012) 12962-12969. **DOI:** 10.1021/ja0346328.

[21] Min, B. and Logan, B.E. "Continuous Electricity Generation from Domestic Wastewater and Organic Substrates in a Flat Plate Microbial Fuel Cell". In: *Environmental Science & Technology* **38**(2004), 5809-5814. **DOI:** 10.1021/es0491026.

[22] Kazemi, S. and Mohseni, M. "Passive air breathing flat-plate microbial fuel cell operation". In: *Journal of Chemical Technology and Biotechnology* **90**(2015), 468–475. DOI: 10.1002/jctb.4325.

[23] Yang, Z.G., Pei H.Y., Hou Q.J., Jiang L.Q., Zhang L.J. and Nie, C.L., "Algal biofilm-assisted microbial fuel cell to enhance domestic wastewater treatment: Nutrient, organics removal and bioenergy production". In: *Chemical Engineering Journal* **332**(2018), 277-285. DOI: 10.1016/j.cej.2017.09.096.

[24] Logan, B., Cheng, S., Watson, V. and Estadt, G. "Graphite Fiber Brush Anodes for Increased Power Production in Air-Cathode Microbial Fuel Cells". In: *Environmental Science & Technology* **41**(2007), 3341-3346. **DOI:** 10.1021/es062644y.

[25] Zhang, C., Liang, P., Jiang, Y. and Huang, X. "Enhanced power generation of microbial fuel cell using manganese dioxide-coated anode in flow-through mode". In: *Journal of Power Sources* **273**(2015), 580-583. DOI: 10.1016/j.jpowsour.2014.09.129.

[26] Wang, H.Y., Wang, G.M., Ling, Y.C., Qian, F., Song, Y., Lu, X.H., Chen, S.W., Tong, Y.X. and Li, Y. "High power density microbial fuel cell with flexible 3D graphene–nickel foam as anode". In: *Nanoscale* **5**(2013), 10238-10290. DOI: 10.1039/C3NR03487A.

[27] Rismani-Yazdi, H., Carver, S.M., Christy, A.D., Tuovinen, O.H. "Cathodic limitations in

microbial fuel cells: An overview". In: *Journal of Power Sources* **180**(2008), 683-694. DOI: 10.1016/j.jpowsour.2008.02.074.

[28] He, W., Yang, W., Tian Y. and Zhu, X. "Pressurized air cathodes for enhanced stability and power generation by microbial fuel cells". In: *Journal of Power Sources* **332**(2016), 447-453.DOI: 10.1016/j.jpowsour.2016.09.112.

[29] Rossi, R., Yang, W., Setti, L. and Logan, B.E. "Assessment of a metal–organic framework catalyst in air cathode microbial fuel cells over time with different buffers and solutions". In: *Bioresource Technology* **233**(2017), 399-405. DOI: 10.1016/j.biortech.2017.02.105.

[30] Watson V.J., Delgado, C. and Logan, B.E. "Influence of Chemical and Physical Properties of Activated Carbon Powders on Oxygen Reduction and Microbial Fuel Cell Performance". In: *Environmental Science & Technology* **47**(2013), 6704-6710. **DOI:** 10.1021/es401722j.

[31] Gajda, I., Greenman, J., Santoro, C., Serov, A., Melhuish, C. " Atanassov P, Ieropoulos IA, Improved power and long term performance of microbial fuel cell with Fe-N-C catalyst in air-breathing cathode". In: *Energy* **144**(2018), 1073-1079. DOI: 10.1016/j.energy.2017.11.135.

[32] Zhang, D., Chi D., Okajima T. and Ohsaka, T. "Catalytic activity of dual catalysts system based on nano-manganese oxide and cobalt octacyanophthalocyanine toward four-electron reduction of oxygen in alkaline media". In: *Electrochimica Acta* **52**(2007), 5400-5406. DOI: 10.1016/j.electacta.2007.02.060.

[33] Antolini, E. "Composite materials for polymer electrolyte membrane microbial fuel cells". In: *Biosensors and Bioelectronics* **69**(2015), 54-70. DOI: 10.1016/j.bios.2015.02.013.

[34] Li X., Hu, B., Suib, S., Lei, Y. and Li, B. "Manganese dioxide as a new cathode catalyst in microbial fuel cells". In: *Journal of Power Sources* **195**(2010), 2586–2591. DOI: 10.1016/j.jpowsour.2009.10.084.

[35] Zhang, L., Liu, C., Zhuang, L., Li, W., Zhou, S. and Zhang, J. "Manganese dioxide as an alternative cathodic catalyst to platinum in microbial fuel cells". In: *Biosensors and Bioelectronics* **24**(2009), 2825–2829. DOI: 10.1016/j.bios.2009.02.010.

[36] Hinnemann, B., Moses, P.G., Bonde, J., Jørgensen, K.P., Nielsen, J.H., Horch, S., Chorkendorffand, I. and Nørskov, J.K. "Biomimetic Hydrogen Evolution: MoS_2 Nanoparticles

as Catalyst for Hydrogen Evolution". In: *Journal of American Chemical Society* **127** (2005), 5308-5309. **DOI:** 10.1021/ja0504690.

[37] Yuan, H., Li, J., Yuan C. and He, Z. "Facile Synthesis of MoS_2@CNT as an Effective Catalyst for Hydrogen Production in Microbial Electrolysis Cells". In *Chem Electro Chem* **1**(2014), 1828-1833. DOI:10.1002/celc.201402150.

[38] Hou, Y., Zhang, B. and Wen, Z. "A 3D hybrid of layered MoS_2/nitrogen-doped graphene nanosheet aerogels: an effective catalyst for hydrogen evolution in microbial electrolysis cells". In: *Journal of Materials Chemistry A* **2**(2014), 13795-13800. DOI: 10.1039/C4TA02254H.

[39] Tokash, J.C. and Logan, B.E. "Electrochemical evaluation of molybdenum disulfide as a catalyst for hydrogen evolution in microbial electrolysis cells". In: *International Journal of Hydrogen Energy* **36**(2011), 9439-9445. DOI: 10.1016/j.ijhydene.2011.05.080.

[40] Logan, B.E. and Rabaey, K. "Conversion of wastes into bioelectricity and chemicals by using microbial electrochemical technologies". In: *Science* **337**(2012), 686–690. DOI: 10.1126/science.1217412.

[41] Muhannad, A., Ren, Z. and Park, J. "Microbial fuel cell energy harvesting using synchronous flyback converter". In: *Journal of Power Sources* **247** (2014), 636-642. DOI: 10.1016/j.jpowsour.2013.09.017.

[42] Boghani, H.C., Papaharalabos, G., Michie, I., Fradler, K.R., Dinsdale, R.M., Guwy, A.J., Ieropoulos, I., Greenman, J. and Premier, G.C. "Controlling for peak power extraction from microbial fuel cells can increase stack voltage and avoid cell reversal". In: *Journal of Power Sources* **269**(2014), 363-369. DOI: 10.1016/j.jpowsour.2014.06.059.

[43] Donovan, C., Dewana, A., Peng, H., Heo, D. and Beyenal, H. "Power management system for a 2.5 W remote sensor powered by a sediment microbial fuel cell". In: *Journal of Power Sources* **196**(2011), 1171–1177. DOI: 10.1016/j.jpowsour.2010.08.099.

[44] Wang, H., Park, J. and Ren, Z. "Active Energy Harvesting from Microbial Fuel Cells at the Maximum Power Point without Using Resistors". In: *Environmental Science & Technology* **46**(2012), 5247−5252. **DOI:** 10.1021/es300313d.

[45] Zhang, D., Yang, F., Shimotori, T., Wang, K. and Huang, Y. "Performance evaluation of

power management systems in microbial fuel cell-based energy harvesting applications for driving small electronic devices". In: *Journal of Power Sources* **217**(2012), 65-71. DOI: 10.1016/j.jpowsour.2012.06.013.

[46] Heidrich, E.S., Dolfing, J. and Wade, M.J. "Temperature, inocula and substrate: Contrasting electroactive consortia, diversity and performance in microbial fuel cells". In: *Bioelectrochemistry* **119**(2018), 43-50. DOI: 10.1016/j.bioelechem.2017.07.006.

[47] Liu, Y., Tuo, A. and Jin, X. "Quantifying biodegradable organic matter in polluted water on the basis of coulombic yield". In: *Talanta* **176**(2018), 485–491. DOI: 10.1016/j.talanta.2017.08.029.

[48] Nikhil, G.N., Suman, P., Mohan, S. and Swamy Y.N. "Energy-positive nitrogen removal of pharmaceutical wastewater by coupling heterotrophic nitrification and electrotrophic denitrification". In: *Chemical Engineering Journal* **326**(2017), 715–720. DOI: 10.1016/j.cej.2017.05.165.

[49] Qin, M., White, C. and Zou, S. "Passive separation of recovered ammonia from catholyte for reduced energy consumption in microbial electrolysis cells". In: *Chemical Engineering Journal* **334**(2018), 2303–2307. DOI: 10.1016/j.cej.2017.11.190.

[50] Shen, J., Wang, C. and Liu, Y. "Effect of ultrasonic pretreatment of the dairy manure on the electricity generation of microbial fuel cell". In: *Biochemical Engineering Journal* **129** (2018), 44–49. DOI: 10.1016/j.bej.2017.10.013.

[51] Cerrillo, M., Vinas, M. and Bonmati, A. "Microbial fuel cells for polishing effluents of anaerobic digesters under inhibition, due to organic and nitrogen overloads". In: *Journal of Chemical Technology & Biotechnology* **92**(2017), 2912-2920. DOI: 10.1002/jctb.5308.

[52] Wei, J.C., Liang, P. and Huang, X. "Recent progress in electrodes for microbial fuel cells". In: *Bioresource Technology* **102**(2011), 9335-9344. DOI: 10.1016/j.biortech.2011.07.019.

[53] Feng, Y., Yang, Q., Wang, X. and Logan, B.E. "Treatment of carbon fiber brush anodes for improving power generation in air–cathode microbial fuel cells". In: *Journal of Power Sources* **195**(2010), 1841-1844. DOI: 10.1016/j.jpowsour.2009.10.030.

[54] Zhou, M., Chi, M., Luo, J., He, H. and Tao, J. "An overview of electrode materials in

microbial fuel cells". In: *Journal of Power Sources* **196**(2011), 4427-4435. DOI: 10.1016/j.jpowsour.2011.01.012.

[55] Dong, H., Yu, H., Wang, X., Zhou, Q. and Feng, J. "A novel structure of scalable air-cathode without Nafion and Pt by rolling activated carbon and PTFE as catalyst layer in microbial fuel cells". In: *Water Research* **46**(2012), 5777-5787. DOI: 10.1016/j.watres.2012.08.005.

[56] Dong, H., Yu, H. and Wang, X. "Catalysis Kinetics and Porous Analysis of Rolling Activated Carbon-PTFE Air-Cathode in Microbial Fuel Cells". In: *Environmental Science & Technology* **46**(2012), 13009-13015. **DOI:** 10.1021/es303619a.

[57] Liang, P. , Duan, R. , Jiang, Y., Zhang, X.Y., Qiu, Y. and Huang X. "One-year operation of 1000-L modularized microbial fuel cell for municipal wastewater treatment ". In: *Water Research* **144**(2018), 1-8. DOI: 10.1016/j.watres.2018.04.066.

[58] Babauta, J.T., Kerber, M., Hsu, L., Phipps, A. , Chadwick, D.B. and Arias-Thode Y.M. "Scaling up benthic microbial fuel cells using flyback converters". In: *Journal of Power Sources* **395**(2018), 98-105. DOI: 10.1016/j.jpowsour.2018.05.042.

[59] Zhou, M., Chi, M., Wang H., and Jin, T. "Anode modification by electrochemical oxidation: A new practical method to improve the performance of microbial fuel cells". In: *Biochemical Engineering Journal* **60**(2012), 151-155. DOI: 10.1016/j.bej.2011.10.014.

[60] Walter, X., Gajda, I., Forbes, S., Winield, J., Greenman, J. and Ieropoulos, I. "Scaling-up of a novel, simplified MFC stack based on a self-stratifying urine column". In: *Biotechnology for Biofuels* **9** (2016), 93-103. DOI: 10.1186/s13068-016-0504-3.

[61] Zhuang, L., Yuan, Y. and Wang, Y.Q. "Long-term evaluation of a 10-liter serpentine-type microbial fuel cell stack treating brewery wastewater". In: *Bioresource Technol*ogy **123**(2012), 406-412. DOI:10.1016/j.biortech.2012.07.038.

[62] Annemiek, T., Hamelers, H.V.M.C. and Buisman, C. "A bipolar membrane combined with ferric iron reduction as an efficient cathode system in microbial fuel cells". In: *Environmental Science & Technology* **40**(2006), 5200-5250. **DOI:** 10.1021/es0608545.

[63] Aelterman, P., Rabaey, K. and Pham, H.T. "Continuous electricity generation at high voltages and currents using stacked microbial fuel cells". In: *Environmental Science and*

Technology **40**(10)(2006), 3388-3394. **DOI:** 10.1021/es0525511.

[64] Ahn, Y., Ivanov, I. and Tharamani, C. "Mesoporous nitrogen-rich carbon materials as cathode catalysts in microbial fuel cells". In: *Journal of Power Sources* **269**(2014), 406-412. DOI: 10.1016/j.jpowsour.2014.06.115.

[65] Shin, S.H., Choi, Y. and Na, S. "Development of Bipolar Plate Stack Type Microbial Fuel Cells". In: *Bulletin of the Korean Chemical Society* **27**(2006), 281-285. DOI : 10.5012/bkcs.2006.27.2.281.

[66] Oh, S., Booki, M. and Logan, B.E. "Cathode Performance as a Factor in Electricity Generation in Microbial Fuel Cells". In: *Environmental Science & Technology* **38** (2004), 4900-4904. **DOI:** 10.1021/es049422p.

[67] He, W.S. and Nguyen, T.V. "Edge Effects on Reference Electrode Measurements in PEM Fuel Cells". In: *Journal of Electrochemical Society* **2**(2004), A185-A191. Doi: 10.1149/1.1634272.

[68] Rabaey, K., Boon, N., Siciliano, S.D., Verhaege, M. and Verstraete, W. "Biofuel Cells Select for Microbial Consortia That Self-Mediate Electron Transfer". In: *Applied & Environmental Microbiology* **70**(2004), 5373-5382. DOI: 10.1128/AEM.70.9.5373-5382.2004.

[69] Wei, L.L., Yuan, Z.L., Cui, M.J. Han, H.L. and Shen, J. Q. "Study on electricity-generation characteristic of two-chambered microbial fuel cell in continuous flow mode". In: *International Journal of Hydrogen Energy* **37**(2012), 1067-1073. DOI: 10.1016/j.ijhydene.2011.02.120.

[70] Skyllas-Kazacos, M. and Sun, B. "Modification of graphite electrode materials for vanadium redox flow battery application—I. Thermal treatment". In: *Electrochimica Acta* **37**(1992), 1253-1260. DOI: 10.1016/0013-4686(92)85064-R.

[71] Skyllas-Kazacos, M. and Sun, B. "Chemical modification of graphite electrode materials for vanadium redox flow battery application—part II. Acid treatments". In: *Electrochimica Acta* **37**(1992), 2459-2465. DOI: 10.1016/0013-4686(92)87084-D.

[72] Gao, C. and Wang, N. "Influence of Fenton's reagent treatment on electrochemical properties of graphite felt for all vanadium redox flow battery". In: *Electrochimica Acta* **88**(2013), 193-202. DOI: 10.1016/j.electacta.2012.10.021.

[73] www.fumatech.com/EN/Products/fumasep/

[74] Zhang, Y.P., Hua, Y.Y., Li, S.Z., Sun, J. and Hou, B. “Manganese dioxide-coated carbon nanotubes as an improved cathodic catalyst for oxygen reduction in a microbial fuel cell”. In: *Journal of Power Sources* **196**(2011), 9284-9285. DOI: 10.1016/j.jpowsour.2011.07.069.

[75] Pasupuleti, S.B., Srikanth, S., Mohan, S.V. and Pant, D. “Continuous mode operation of microbial fuel cell (MFC) stack with dual gas diffusion cathode design for the treatment of dark fermentation effluent”. In: *International Journal of Hydrogen Energy* **40**(2015), 12424-12435. DOI: 10.1016/j.ijhydene.2015.07.049.

[76] Bajracharya, S., Ter. Heijne, A., Benetton, X.D., Vanbroekhoven, K., Buisman, C.J.N., David P.B.T.B. and Pant, D. “Carbon dioxide reduction by mixed and pure cultures in microbial electrosynthesis using an assembly of graphite felt and stainless steel as a cathode”. In: *Bioresource Technology* **195**(2015), 14-24. DOI: 10.1016/j.biortech.2015.05.081.

[77] Zhang, L., Liu, C. and Zhuang, L. “Manganese dioxide as an alternative cathodic catalyst to platinum in microbial fuel cells”. In: *Biosensors & Bioelectronics* **24**(2009), 2825-2829. DOI: 10.1016/j.bios.2009.02.010.

[78] Oh, S., Yoon, J. and Gurun, A. “Evaluation of electricity generation from ultrasonic and heat/alkaline pretreatment of different sludge types using microbial fuel cells”. In: *Bioresource Technology* **165**(2014), 21-26. DOI: 10.1016/j.biortech.2014.03.018.

[79] Shen, X., Ding, Y., Liu, J., Han, Z., Budnick, J.I., Hines, W.A. and Suib, S.L. “A Magnetic Route to Measure the Average Oxidation State of Mixed-Valent Manganese in Manganese Oxide Octahedral Molecular Sieves (OMS)”. In: *Journal of American Chemical Society* **127**(2005), 6166-6167. DOI: 10.1021/ja043406a.

[80] Zhou, S., Zhuang, L., Yuan, Y. and Wang, Y. “Long-term evaluation of a 10-liter serpentine-type microbial fuel cell stack treating brewery wastewater”. In: *Bioresource & Technology* **123**(2012), 406-412. DOI: 10.1016/j.biortech.2012.07.038.

[81] Chen, S., Zhu, Y. and Li, W. “Synthesis, features, and applications of mesoporous titania with TiO_2 (B)”. In: *Chinese Journal of Catalysis* **31**(2010), 605-614. DOI: 10.1016/S1872-2067(09)60073-5.

[82] Kumar, R., Singh, L., Zularisama, A.W. and Hai, F.I. “Potential of porous Co_3O_4 nanorods as cathode catalyst for oxygen reduction reaction in microbial fuel cells”. In: *Bioresource & Technology* **220**(2016), 537-542.) DOI: 10.1016/j.biortech.2016.09.003.

.